



Title	X-RAY PHOTOELECTRON SPECTROSCOPIC STUDY ON SURFACE AND BULK STRUCTURES OF POLYMERIC SUBSTANCES
Author(s)	Takahagi, Takayuki
Citation	大阪大学, 1988, 博士論文
Version Type	VoR
URL	https://hdl.handle.net/11094/197
rights	
Note	

The University of Osaka Institutional Knowledge Archive : OUKA

<https://ir.library.osaka-u.ac.jp/>

The University of Osaka

X-RAY PHOTOELECTRON SPECTROSCOPIC STUDY ON
SURFACE AND BULK STRUCTURES OF
POLYMERIC SUBSTANCES

A Doctoral Thesis

by

Takayuki Takahagi

Submitted to the Faculty
of Science, Osaka University

October, 1987

Approvals

October, 1987

This thesis is approved
as to style and content
by

小林雅通

Member-in-chief

池田重良 (印)

Member

小高忠男 (印)

Member

勝部幸輝

Member

ACKNOWLEDGMENTS

This work was completed under direction of Professor Masamichi Kobayashi in Department of Macromolecular Science, Faculty of Science, Osaka University. This author is greatly indebted to Professor Masamichi Kobayashi, Emeritus Professor Hiroyuki Tadokoro in Osaka University and Professor Yozo Chatani in Tokyo University of Agriculture and Technology for their cordial guidance, advice and encouragement. The author wishes to express his gratitude to Dr. Akira Ishitani in Toray Research Center, Inc. for fruitful discussion, suggestion and encouragement throughout the course of this work. The author is also grateful to Dr. Kohji Tashiro in Osaka University for his suggestion and to Mr. Fusami Soeda, Mr. Ichio Shimada, Mr. Youichi Nakayama and Miss Noriko Sawada in Toray Research Center, Inc. for their contributions to this study. Thanks are extended to all the members of Material Science Laboratories of Toray Research Center, Inc. for their cooperation.

高萩隆行
Takayuki Takahagi

September, 1987

CONTENTS

Chapter 1. General Introduction	1
1-1 Introduction	1
1-2 Surface Structure	2
1-3 Bulk Structure	11
References	15
 Chapter 2. Surface Cleaning and Effect of X-ray Flux on XPS	
Study of Polymers	20
2-1 Introduction	20
2-2 Experimental	21
2-2-1 XPS Measurement	21
2-2-2 Ultrasonic Washing	22
2-2-3 X-ray Irradiation	22
2-3 Result and Discussion	22
2-3-1 Surface Cleaning	22
2-3-2 Effect of X-ray Flux	26
References	33
 Chapter 3. A Non-Empirical LCAO MO SCF and Experimental	
Investigation on the Core-Ionization Process of	
Poly(vinylidene chloride) and Poly(vinyl chloride)	34
3-1 Introduction	34
3-2 Non-Empirical LCAO MO SCF Calculation	34
3-3 Experimental	35
3-3-1 Sample	35
3-3-2 XPS Measurement	35

3-4 Result and Discussion	36
3-4-1 Surface Composition	36
3-4-2 Chemical Shift of Cls Spectra	36
References	42
Chapter 4. Monte Carlo Simulation of an Ion Sputtering Process of Fluoro Polymers	44
4-1 Introduction	44
4-2 Experimental	45
4-2-1 Sample	45
4-2-2 XPS Measurement	45
4-2-3 Ar Ion Sputtering	45
4-3 Models of Sputtering Process for Monte Carlo Simulation	46
4-4 Result and Discussion	48
4-4-1 Surface Composition of Sputtered Surface of Polymers	48
4-4-2 Monte Carlo Simulation	52
4-5 Conclusions	57
References	57
Chapter 5. XPS Study by Use of the Digital Difference Spectrum Technique of Functional Groups on the Surface of Carbon Fiber	60
5-1 Introduction	60
5-2 Experimental	61
5-2-1 XPS and FT-IR Measurement	61
5-2-2 Sample	62
5-2-3 Data Processing of XPS Spectra	62
5-3 Result and Discussion	62

5-3-1 Surface Composition	62
5-3-2 C1s Difference Spectra	67
5-3-3 FT-IR-RAS Spectrum	69
References	71

Chapter 6. XPS Study on the Surface Structure of Carbon Fibers

Using Chemical Modification and C1s Line Shape

Analysis	72
6-1 Introduction	72
6-2 Experimental	75
6-2-1 Sample	75
6-2-2 Chemical Modification Reactions	75
6-2-3 XPS Measurement	77
6-3 Result and Discussion	77
6-3-1 Chemical Modification	77
6-3-2 Line Shape Analysis of C1s Spectrum	82
References	88

Chapter 7. XPS and FT-IR Studies on the Chemical Structure of Stabilized Polyacrylonitrile Fiber and the Mechanism of Stabilization Reaction in Carbon Fiber Production

Process	91
7-1 Introduction	91
7-2 Experimental	92
7-2-1 Sample	92
7-2-2 XPS Measurement	93
7-2-3 FT-IR Measurement	93
7-2-4 Elemental Analysis	93

7-3 Result and Discussion	94
7-3-1 Elemental Composition	94
7-3-2 Molecular Structure	94
7-3-3 Reaction Mechanism	105
References	110
 Chapter 8. Molecular and Crystal Structure of Poly(vinylidene chloride)	 114
8-1 Introduction	114
8-2 Experimental	114
8-2-1 Sample	114
8-2-2 X-ray Diffraction	115
8-3 Structure Determination	116
8-3-1 Conformational Energy	116
8-3-2 Molecular Transform	120
8-3-3 Unit Cell and Space Group	122
8-3-4 Determination of Crystal Structure	122
8-4 Result and Discussion	127
8-4-1 Molecular Structure	127
8-4-2 Crystal Structure	128
References	129
 Chapter 9. Concluding Remarks	 132
 List of Publications	 136
 List of Related Papers	 137

Chapter 1

General Introduction

1-1 Introduction

Polymers are widely used in any field as specialty materials with specific properties and functions. Specialty polymers with high quality in those properties such as mechanical strength, rigidity, elasticity and heat-resistance have been replacing to metals, ceramics and other inorganic materials because of its advantage of a light weight. There are other kinds of specialty polymers with specific functions such as separability of substances, electric conductivity, photo-sensitivity or biological functions as bio-compatibility and susceptibility to living bodies.

In the past decade, it has been noticed that properties of specialty polymers and materials made from polymers depend not only on the bulk structure but also on the surface structure. For examples, such properties as adhesibility, bio-compatibility and separability of a polymer strongly depend on the surface structure, while strength, rigidity and elasticity are influenced by the bulk structure.

In general we speak of the surface of the solid material, but it would be more precise to use the term "interface", where the solid is commonly in contact with a vacuum, a gas, a liquid or another solid. The components, i.e. the atoms or the molecules, of the surface of a solid have the same neighbors in inside direction as do they in the bulk. On the contrary in the opposite direction, i.e. outside direction, they cannot find out adjacent components of the same kind of the bulk and are suddenly faced with a quite different phase. The surface must have

therefore a characteristic atomic or molecular arrangement as the result of the structural reconstruction from the bulk structure.

The author attempts to approach to a unique structural feature of the surface of polymeric substances as an extended study of the bulk structure. X-ray photoelectron spectroscopy (XPS) is mainly used to investigate the polymer surface, because XPS is highly surface-sensitive and has an ability to provide the chemical bonding information of each atoms. Furthermore, XPS is expected to be an effective technique for the analysis of the bulk chemical structure of polymeric substances because of its high capability to provide the information of the chemical state of atoms.

This thesis deals mainly with various basic problems which arise in the application of XPS to the surface studies of polymeric substances, along with its utility for the examination of the bulk chemical structure of polymers. In addition, this thesis contains the result of X-ray crystallographical analysis of poly(vinylidene chloride) (PVDC), which is performed to obtain the geometrical data of the molecule used for the non-empirical LCAO MO SCF calculation of the chemical shift of XPS.

1-2 Surface Structure

Before last decade, the surface structure of materials had attracted little attention in the industrial world. During the last decade, it has however been realized that the designation of the surface feature of materials must be taken into consideration for the development of specialty materials. The surface structure has been proved to play the important roles also in polymer materials.

Before the introduction of XPS,^{1,2} the reflection infrared spectroscopy was virtually only technique available for studying polymer surface.

This technique typically gives the information pertaining to about $1\ \mu\text{m}$ into materials. In recent years, use of Fourier transform infrared spectroscopy (FT-IR) technique has improved surface sensitivity,^{3,4} but even in the most favorable cases FT-IR cannot give us information of the outermost layer on the surface, which plays important roles in various surface phenomena.

XPS has gained widespread recognition⁵⁻⁷ as the most powerful technique for the investigation of the surface structure of polymeric substances in a solid state, because of its good surface sensitivity and capability of providing the chemical bonding information of all elements except hydrogen. The latter feature also makes XPS one of the most effective analytical techniques to study the bulk structure of polymers like IR and X-ray diffraction. It is the reason why the author tries to apply XPS for the examination of the bulk chemical structure of a condensed-ring polymer, stabilized PAN, in combination with FT-IR as described below.

The XPS experiment is accomplished by irradiating a sample with the monochromatic soft X-ray beam and analyzing the kinetic energy of the electrons emitted from the sample. The $\text{MgK}\alpha_{1,2}$ X-ray (1253.6 eV) and the $\text{AlK}\alpha_{1,2}$ X-ray (1486.6 eV) are commonly used as the incident radiation. These photon interact with the atoms in the surface region of the sample by the photoelectric effect, causing the emission of electrons. The emitted electrons have kinetic energies given by $\text{KE} = h\nu - \text{BE}$, where $h\nu$ is the energy of the photon, BE is the binding energy of the atomic orbital from which the electron originates as shown in Figure 1.1. The binding energy may be regarded as the ionization energy of a particular shell of the atom. We can assign a peak in XPS spectrum to a particular element, since the binding energy for a given core level of a given

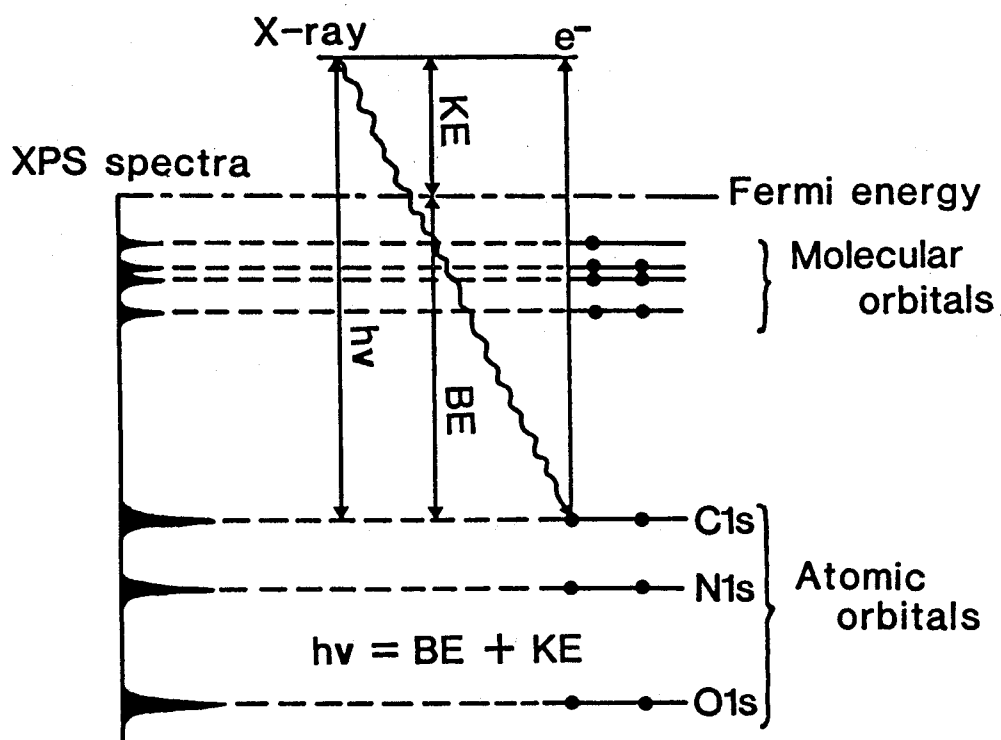


Figure 1.1 Energy diagram of the photoelectron process.

element is characteristic.

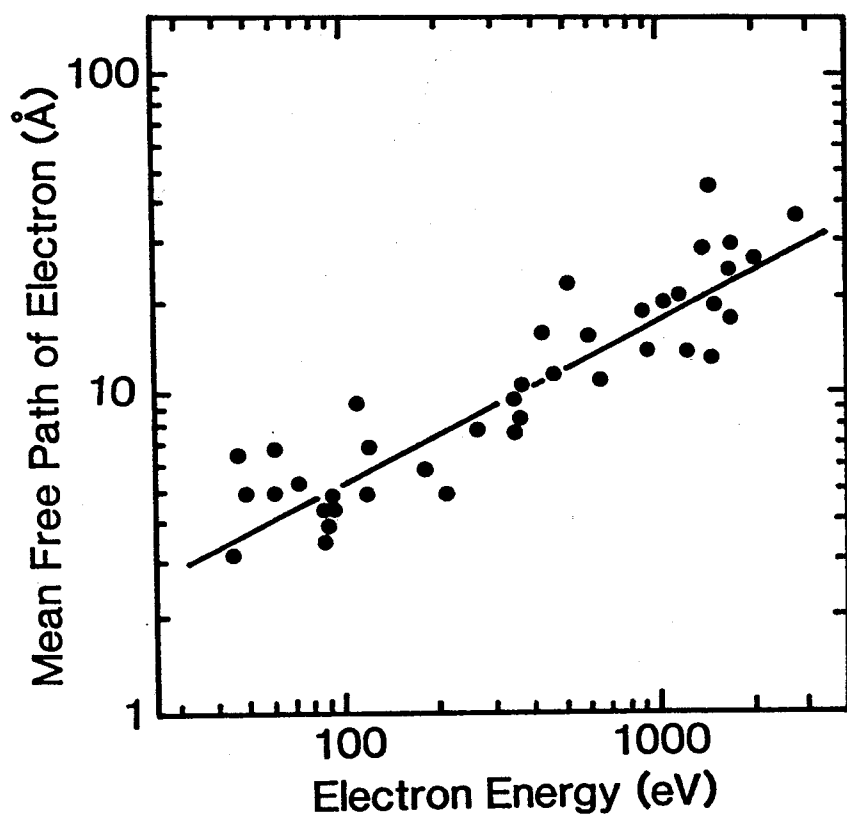
Although the energies of the core levels of an atom in molecules are sensitive to their electronic environment, the effects are short-range since the core levels are essentially localized on atoms. The chemical shift of a given core level signal is therefore dependent only on the atoms attached directly to the atom on which it resides. Thus, differences in electronic environment give rise to a small change of binding energies (i.e. chemical shifts), which is often representative of a particular structural feature. Ability to provide straightforward the chemical information gives XPS great potential as a tool for the surface science on polymeric substances. The chemical shift of an atom in the molecule can be roughly estimated by referring values of electronegativity of atoms directly attaching to the atom. For instance, the bonding of a fluorine atom with the largest electronegativity usually causes large chemical shifts of binding energies of various element atoms. But unfortunately, we cannot precisely assign the spectra to the specific chemical species by using the chemical shift estimated by referring the values of the electronegativity. Thus, in this thesis the author attempts to use the chemical shifts for the assignment of the XPS spectra by referring observed data for the model chemical compounds and by calculating binding energies by means of the non-empirical LCAO MO SCF calculation.

The measurement of the absolute values of binding energies of the core and valence level electrons in thick polymer films or powders, because of their insulating character, is not as straightforward as in the case of electrically conducting samples. The electron flux photoejected from the sample by the incident X-ray beam is generally only partly balanced by the flux of low energy secondary electrons arriving at

the sample from its surroundings. The sample usually is positively charged in the pseudo-equilibrium electronic condition. The value of the charge up of the polymer samples is usually 2 - 15 V. We must correct the value of the charge up to obtain the accurate binding energies. The author calibrates the energy scale by monitoring the C1s level of the extraneous hydrocarbon contamination and internal standards such as a hydrocarbon species in the sample.

Probabilities of interaction of the electrons with a material far exceed those of the photons, so while the path length of the photons is of the order of micrometers, that of the electrons is of the order of tens of Angstroms. Thus, while a photoelectron emission occurs to a depth of a few micrometers, only electrons that originate within tens of Angstroms below the solid surface can leave the surface without energy loss. It is these electrons which produce the peaks in the spectra. Those that undergo loss processes before emerging form the background. The energy loss is caused by inelastic scattering which involves one-electron excitations, vibrational excitations, or, in certain cases, plasmon excitations. Experimental data on mean free path of electrons in various materials in the 40 - 2000 eV range of the most interest in XPS measured by previous workers are shown in Figure 1.2. All data points lie roughly on a common curve. Mean free paths are in the range of about 5 - 30 Å and decrease with an decrease of the electron energy in the energy range usually used in XPS measurement. The extremely good surface sensitivity of XPS is a direct consequence of the short mean free path of the photoelectrons through the sample.

Applications of XPS have ranged from structural elucidation of simple homopolymers,⁸⁻¹¹ determination of copolymer composition^{8,12-16} and its morphology¹⁴⁻¹⁶ to more complicated systems like highly



crosslinked materials¹⁷⁻²⁴ and studies of surface modification reactions which take place in monolayer depth scale.²⁵⁻²⁹ However, owing to the shorter history of application of XPS to polymer materials than other conventional analytical techniques like infrared spectroscopy, nuclear magnetic resonance and X-ray diffraction, many problems have been left unclarified in the XPS measurement of polymers. Before the present work, there was no detailed and systematic study of sample preparation and measurement techniques for use of XPS on polymers such as the surface cleaning, the contamination occurring in vacuum or the degradation of a sample by X-ray flux and Ar ion sputtering.

XPS is considered to be a technique free from radiation-induced artifacts in the most of inorganic materials. On the other hand, the damage of sample surfaces by X-ray flux usually must be considered in the XPS measurement of polymers. Wheeler found a very strong effect of the X-ray flux on the surface composition of PTFE.³⁰ Chang studied the mechanism and the rate of dehydrochlorination of an oxide-free PVC film due to X-ray irradiation by using XPS.³¹ The author carries out a detailed examination of the effect of X-ray flux to various polymers and discusses the unique feature of the degradation by X-ray flux comparing with the thermal degradation.

A sample specimen surface in air is frequently contaminated by organic substances. It prevents us from obtaining the information of the real clean surface of the sample. Ar ion etching is commonly used to remove the surface contamination in the XPS measurement of inorganic materials as metals, ceramics and semiconductors. But we cannot use the technique to clean the surface of polymers, because most of polymers are extensively degraded by Ar ion sputtering. Instead, the author examines the use of an ultrasonic cleaner in organic solvents as a degradation-

free cleaning method. The surface of polymers is revealed to have the characteristic properties different from that of metals and semiconductor crystals through this examination.

The author fully investigates the XPS chemical shift of a carbon atom in poly(vinylidene chloride) (PVDC) and poly(vinyl chloride) (PVC) by means of non-empirical LCAO MO SCF calculation by the ab initio method using GAUSSIAN82 program,³² utilizing the geometrical data of the molecule of PVDC obtained by the crystal structure analysis also discussed in the following section of bulk structure. The change of binding energy of Cls the both polymers by bonding of chloride atoms is discussed in this thesis.

In inorganic materials, the mechanism of the ion sputtering was already fully examined.³³ On the other hand, no detailed study has been performed in the field of organic materials. Understanding of the sputtering mechanism of polymer materials is also far from the satisfactory level. The author examines the chemical composition on the surface of an ion sputtered poly(tetrafluoro ethylene) (PTFE) and poly(vinylidene fluoride) (PVDF) by XPS. The change in XPS spectra of the polymers on Ar ion bombardment is interpreted by a simple calculation based on a Monte Carlo simulation. The investigation of the mechanism of sputtering is particularly important in the secondary ion mass spectroscopy (SIMS) measurement of polymer materials, that has much potential for the polymer surface characterization.

The author widely and systematically applies XPS to the carbon fiber made from polyacrylonitrile which is used to make advanced composite materials combined with various polymers. The carbon fiber is a new breed among high strength materials. Although initially developed for aerospace industries, they are now finding wide use in commercial aircraft, recreational goods, and automobiles. It has low density and

thus possesses the highest specific strength in all currently available engineering materials. It is used as composites with a light weight matrix, generally epoxy resin, occasionally polyester and also polyimide, and now recently more frequently with carbon. Carbon fibers with excellent mechanical properties themselves are now available. But the efficient use of these outstanding mechanical properties in composites has not been achieved. Composites obtained from them still have poor interlaminar shear strength. This has been attributed to weak adhesion or poor bonding between the surface of carbon fibers and matrix resins.

The surface treatment of carbon fibers has been frequently used to improve the bonding property between the fibers and matrix resins in composite materials. Both of chemical and crystalline structures of the carbon fiber surface are expected to play important roles in adhesion. The characterization of the carbon fiber surface is thus much needed for the improvement of the interfacial bonding. Functional groups on the surface of carbon fibers have been studied extensively with XPS by various authors,³⁴⁻³⁸ because of its good surface sensitivity and capability of providing chemical structure informations. However, the complexity due to the asymmetric line shape of Cls spectrum³⁹ as well as small observed chemical shift of Ols prevents us from studying the surface structure in detail. The peak separation of Cls spectrum of carbon fibers with a symmetric component curve, which is usually used for the analysis of chemical species of organic materials, also has misled several authors in the estimation of concentrations of surface functional groups.

In order to circumvent these difficulties, the author develops new techniques for the characterization of the surface of carbon fibers. The digital difference subtracting technique of XPS spectrum is proved to be

useful for the analysis of functional groups on the surface of carbon fibers produced by oxidation. But the discrimination of all functional groups on the surface of carbon fibers is difficult even by this technique. The author develops a technique for surface modification coupled with XPS measurement to investigate all surface functional groups of carbon fibers.^{40,41} The purpose of the chemical modification is labeling of a specific functional group by a tag element improving abilities of detection, identification and quantification.

The surface graphitization degree of carbon materials including carbon fibers is tried to examine by XPS. The surface graphitization degree cannot be determined by conventional techniques like X-ray diffraction giving all bulk information and Raman spectroscopy with a measurement depth of a few hundred Angstroms. The line shape of XPS C1s spectrum of carbon materials is found to be indicative of its graphitization degree. Utilizing this phenomenon, the author investigates the change of the graphitization degree on the surface of carbon fibers in the carbonization and the surface oxidation processes.

1-3 Bulk Structure

In the carbon fiber production process, PAN fibers stabilized at between 200 - 300 °C in air is carbonized by the heat treatment above 1000 °C in an inactive atmosphere. The mechanical properties of the final carbon fibers are much dependent on the chemical composition and the molecular structure of the stabilized fiber as the intermediate material. By using XPS, the author tries to determine the bulk chemical structure of PAN stabilized in air and to elucidate the mechanism of the stabilization reaction.

Many workers have studied the mechanism of the stabilization process

and the chemical structure of the stabilized fibers by infrared spectroscopy and evolved gas analysis.⁴²⁻⁴⁹ But, many kinds of chemical structure models proposed so far are not decisive enough to fully understand the chemistry in the stabilization process, because of experimental difficulties due to the disturbance by the intense background absorption and also due to the insolubility to any kind of organic solvent.

XPS can reveal the chemical state of carbon, oxygen and nitrogen atoms contained in stabilized PAN fibers in solid state. But it must be noticed that XPS cannot give us the chemical information of hydrogen because of its no core electron. The author uses FT-IR and elemental analysis combining with XPS to complement its disadvantage.

In the quantitative analysis of XPS spectra by means of non-empirical LCAO MO SCF calculation, we need the geometrical data of the molecular arrangement. In the case of PVDC, however there have been no these data. Then, the author started the crystallographical analysis of PVDC before the quantum theoretical calculation, which is described in the above section about the surface structure.

Crystal structure of polymers has mainly examined by X-ray diffraction, infrared spectroscopy and Raman spectroscopy.⁵⁰ X-ray diffraction technique is the most powerful tool for the investigation of structures in the crystal region. It can give us the useful crystallographical information. But imperfection of polymer crystals prevents us to determine the complete crystal structure. In order to circumvent this difficulty, many authors successfully used the conformational energy analysis technique to determine structures of polymer chains in the crystal lattice.⁵¹⁻⁶² A conformational energy calculation method has been carried out to anticipate a molecular conformation and a molecular packing with the most stable energy.

The molecular structure of PVDC has been studied by various authors,⁶³⁻⁷¹ who have proposed several molecular models for PVDC such as twisted zigzag, tub form, (2/1) helical and glide model. However, the crystal structure has not yet been completely determined. The molecular and crystal structures of PVDC are examined by X-ray structure analysis together with the conformational energy calculation.

This thesis consists of the following chapters.

Chapter 2 describes surface cleaning methods and effects of X-ray flux on the polymer surface. Ultrasonic cleaning in organic solvents is proved to be effective to remove organic contaminations on the surface of polymers. The surface chemical activities of polymer substances are revealed to be less than that of metals and semiconductor crystals. Polymers are roughly classified to three levels in the stability for X-ray flux in XPS measurement. The degradation reactions of polymers induced by the X-ray irradiation are clarified to be difference from that in the thermal degradation processes.

In chapter 3, the chemical shift of a carbon atom in poly(vinylidene chloride) and poly(vinyl chloride) is investigated by means of a non-empirical LCAO MO SCF calculation. The chemical shift of Cls in these polymers by bonding of a chlorine atom is mainly discussed. The chemical shift of Cls by bonding of a chlorine atom is resulted to be less than that by bonding of a fluorine atom.

In chapter 4, Monte Carlo simulation of an ion sputtering process of fluoro polymers is described. Sputtering processes on Ar ion bombardment of PTFE and PVDF are studied by XPS measurement of sputtered surface of the polymers and by the analysis based on the random elimination of fluorine atoms from polymer chains. In both polymer systems, fluorine

atoms are preferentially sputtered away from the polymer chains, leaving carbon atoms behind. Observed XPS spectra of both polymers are explained by the random elimination of fluorine atoms in Monte Carlo simulation.

Chapter 5 shows the result of XPS study of functional groups on the surface of carbon fibers by the digital difference spectrum technique. It is shown that the major functional groups introduced to the carbon fiber surface by surface oxidation are hydroxyl and carboxyl groups. The technique is proved to be useful for quantitative analysis of the surface chemistry on carbon fibers.

In chapter 6, advanced techniques of XPS are introduced on the surface analysis of carbon fibers. The chemical modification technique coupled with XPS is proved to be a useful tool for detailed and quantitative analysis of functional groups on the carbon fiber surface. The line shape analysis of XPS Cls spectrum is used to evaluate a degree of the graphitization on the carbon fiber surface. Major functional groups on the surface of unoxidized and oxidized carbon fibers are found to be carbonyl group and hydroxyl and carbonyl groups, respectively. It is shown that the surface oxidation reduces a degree of the graphitization on the surface of carbon fibers.

Chapter 7 shows the experimental result on the investigation of the chemical structure of stabilized PAN and the reaction mechanism of stabilization process in air by XPS, FT-IR and elemental analysis. It is shown that PAN stabilized in air has highly unsaturated ladder like structure mainly consisting acridone, naphthyridine and hydronaphthyridine rings. Addition of the second component by the copolymerization to the precursor is found to accelerate dehydrogenation reaction in the stabilization process.

In chapter 8, crystal structure of PVDC is discussed by using X-ray

diffraction and conformational energy calculation. The conformational energy calculation is carried out in a condition of fixing fiber period and varying two bond angles of the main chain. It is revealed that two PVDC molecular chains with glide conformation are packed in monoclinic unit cell in the crystal.

Finally in chapter 9, concluding remarks on the present study are described.

References

1. K. Siegbahn, C. Nordling, R. Fahlman, R. Nordberg, K. Hamrin, J. Hedman, G. Johansson, T. Bergmark, S. E. Karlsson, I. Lindgren, and B. Lindberg, "ESCA : Atomic, Molecular, and Solid State Structure Studied by Means of Electron Spectroscopy", *Nova Acta Regiae Soc. Sci., Upsaliensis, Ser.IV, Vol.20* (1967).
2. K. Siegbahn, C. Nordling, G. Johansson, P. F. Heden, K. Hamrin, U. Gelius, T. Bergmark, L. O. Werme, R. Manne, and Y. Baer, "ESCA Applied to Free Molecules", North-Holland Publishing Company, Amsterdam (1969).
3. T. Ohnishi, A. Ishitani, H. Ishida, N. Yamamoto and H. Tsubomura, J. Chem. Phys., 82, 1989 (1978).
4. G. J. Kemeny, P. R. Griffiths, *Appl. Spectrosc.*, 35, 128 (1981).
5. D. T. Clark, "Polymer Surfaces", p309-351, John Wiley & Sons, New York (1978).
6. A. Dilks, "Electron Spectroscopy: Theory, Techniques and Applications", Vol.4, p278-359, Academic Press, New York (1979).
7. D. Briggs, "Practical Surface Analysis", p359-396, John Wiley & Sons, New York (1983).
8. D. T. Clark, D. Kilcast, W. J. Feast, and W. K. R. Musgrave, J.

- Polym. Sci., Polym. Chem. Ed., 11, 389 (1973).
9. D. T. Clark and H. R. Thomas, J. Polym. Sci., Poly. Chem. Ed., 14, 1671 (1976).
 10. D. T. Clark and H. R. Thomas, J. Polym. Sci., Poly. Chem. Ed., 14, 1701 (1976).
 11. D. T. Clark and H. R. Thomas, J. Polym. Sci., Poly. Chem. Ed., 16, 791 (1978).
 12. D. T. Clark, D. Kilcast, W. J. Feast, and W. K. R. M. Musgrave, J. Polym. Sci., Poly. Chem. Ed., 10, 1673 (1972).
 13. D. T. Clark, W. J. Feast, I. Ritchie, W. K. R. Musgrave, M. Modena, and M. Rgazzini, J. Polym. Sci., Poly. Chem. Ed., 12, 1049 (1974).
 14. D. T. Clark and A. Dilks, J. Polym. Sci., Poly. Chem. Ed., 14, 533 (1976).
 15. D. T. Clark, J. Peeling, and J. M. O'Malley, J. Polym. Sci., Poly. Chem. Ed., 14, 543 (1976).
 16. H. R. Thomas and J. M. O'Malley, Macromolecules, 12, 323 (1979).
 17. A. Pavlath and K. S. Lee, J. Macromol. Sci. Chem., A10, 619 (1976).
 18. A. Dilks and E. Kay, "Plasma Polymerization", M. Shen and A. T. Bell, ed.; ACS Symposium Series 108, American Chemical Society, Washington, D. C. (1979).
 19. D. W. Rice and D. F. O'Kane, J. Electrochem. Soc., 123, 1308 (1976).
 20. D. F. O'Kane and D. W. Rice, J. Macromol. Sci. Chem., A10, 567 (1976).
 21. D. Peric, A. T. Bell, and M. Shen, J. Appl. Polym. Sci., 21, 2661 (1977).
 22. D. T. Clark and D. Shuttleworth, J. Polym. Sci., Polym. Chem. Ed., 17, 1317 (1979).
 23. R. W. Pekala and E. W. Merril, J. Colloid Interface Sci, 101, 120

(1984).

24. D. T. Clark and J. Peeling, J. Polym. Sci., Poly. Chem. Ed., 14, 2941 (1976).
25. D. T. Clark and A. Dilks, "Characterization of Metal and Polymer Surfaces", Vol.2, L. H. Lee, ed., Academic Press, New York (1977).
26. D. T. Clark and A. Dilks, J. Polym. Sci., Poly. Chem. Ed., 15, 2321 (1977).
27. D. T. Clark and A. Dilks, J. Polym. Sci., Poly. Chem. Ed., 16, 911 (1978).
28. D. T. Clark and A. Dilks, J. Electron Spectrosc., 11, 225 (1977).
29. D. T. Clark and A. Dilks, J. Polym. Sci., Poly. Chem. Ed., 17, 957 (1979).
30. D. R. Wheeler and S. V. Pepper, J. Vac. Sci. Technol., 20, 226 (1982).
31. H. P. Chang and J. H. Thomas, J. Electron Spectrosc. Relat. Phenom., 26, 203 (1982).
32. J. S. Binkley, R. A. Whiteside, K. Ragharachari, R. Seeger, D. J. DeFees, H. B. Schlegel, M. J. Frisch, J. A. Pople and L. R. Kahn, "GAUSSIAN82 Release A", Carnegie Mellon University, Pittsburgh, 1982.
33. H. Shimizu, M. Ono and K. Nakayama, Surf. Sci., 36, 817 (1973).
34. A. Ishitani, "Molecular Characterization of Composite Interfaces", p321, Plenum Publishing Corporation (1985).
35. M. Barber, P. Swift, E. L. Evans and J. M. Thomas, Nature, 227, 1131 (1970).
36. J. M. Thomas, E. M. Evans, M. Barber and P. Swift, Trans. Faraday Soc., 67, 1815 (1971).
37. J. M. Donnet, E. Papirer and H. Dauksh, Int. Conf. Carbon Fibers,

- their place in Modern Technology, Paper No. 9, London (1974).
38. F. Hopfgarten, *Fiber Science and Technology*, 11, 65 (1978).
 39. P. M. Th. M. Van Attekum and G. K. Wertheim, *Phys. Rev. Lett.*, 43, 1896 (1976).
 40. D. S. Everhart and C. N. Reilly, *Anal. Chem.*, 53, 665 (1981).
 41. R. A. Dickie, J. S. Hammond, J. E. deRies and J. W. Holubka, *Anal. Chem.*, 54, 2045 (1982).
 42. R. C. Houtz, *Textile Res. J.*, 20, 786 (1950).
 43. W. J. Burlant and J. L. Parsons, *J. Polym. Sci.*, 22, 249 (1956).
 44. L. H. Peebles, Jr. and J. Brandrup, *Macromol. Chem.*, 98, 189 (1966).
 45. A. E. Standage and R. Matkowsky, *Nature*, 224, 688 (1969).
 46. W. Watt, *Proc. Roy. Soc. Lond., A*, 319, 5 (1970).
 47. N. Grassie and R. McGuchan, *Eur. Polym. J.*, 7, 1356 (1971).
 48. J. W. Johnson, W. Potter, P. G. Rose and G. Scott, *Br. Polym. J.*, 4, 527 (1972).
 49. M. M. Coleman and R. J. Petcavich, *J. Polym. Sci. Polym. Phys. Ed.*, 15, 821 (1978).
 50. H. Tadokoro, "Koubunshi no Kouzou", Kagaku Dojin Co. Ltd., Tokyo (1976).
 51. G. Natta, P. Corradini, P. Ganis, *Makromol. Chem.*, 39, 238 (1960).
 52. A. I. Kitaigorodskii, "Organic Chemical Crystallography", Consultants Bureau, New York (1961).
 53. P. de Santis, E. Giglio, A. M. Liquori, A. Ripamonti, *J. Polym. Sci. A*, 1, 1383 (1963).
 54. A. I. Kitaigorodskii, *Acta Cryst.*, 18, 585 (1965).
 55. A. M. Liquori, *J. Polym. Sci. C*, 12, 209 (1966).
 56. R. A. Scott, H. A. Scheraga, *J. Chem. Phys.*, 44, 3054 (1966).

57. R. A. Scott, H. A. Scheraga, J. Chem. Phys., 45, 2091 (1966).
58. P. Corradini, G. Avitabile, Eur. Polym. J., 4, 385 (1968).
59. R. Hasegawa, M. Kobayasi, H. Tadokoro, Polym. J., 3, 591 (1972).
60. K. Tai, H. Tadokoro, Macromolecules, 7, 507 (1974).
61. T. Tanaka, Y. Chatani, H. Tadokoro, J. Polym. Sci., Polym, Phys. Ed., 12, 515 (1974).
62. H. Kusanagi, H. Tadokoro, Y. Chatani and K. Suehiro, Macromolecules, 10, 405 (1977).
63. C. S. Fuller, Chem. Rev., 26, 143 (1940).
64. R. C. Reinhardt, Ind. Eng. Chem., 35, 422 (1943).
65. P. De Santis, E. Giglio, A. M. Liquori, and A. Ripamonti, J. Polym. Sci., A, 1, 1383 (1963).
66. V. M. Coiro, P. De Santis, A. M. Liquori, and A. Ripamonti, Rec. Sci., 33 (II-A), 1043 (1963).
67. V. M. Coiro, P. De Santis, and A. M. Liquori, J. Polym. Sci., B, 4, 821 (1966).
68. T. Miyazawa and Y. Ideguchi, J. Polym. Sci., B, 3, 541 (1965).
69. P. J. Hendra and J. R. Mackenzie, Spectrochim. Acta, 25A, 1349 (1969).
70. M. M. Coleman, M. S. Wu, I. R. Harrison, and P. C. Painter, J. Macromol. Sci. Phys., B15(3), 463 (1978).
71. M. S. Wu, P. C. Painter, and M. M. Coleman, J. Polym. Sci., Polym. Phys. Ed., 18, 95 (1980).

Chapter 2

Surface Cleaning and Effect of X-ray Flux on XPS Study of Polymers

2-1 Introduction

Recently, X-ray photoelectron spectroscopy (XPS) is increasingly pervasive as a surface characterization technique of polymers because of wide applications of polymers in the fields requiring materials with a well defined surface. But, in XPS study of polymer substances, there are many difficulties due to the chemical instability of samples for the excitation radiation, i.e. the X-ray flux, and for the ion sputtering.^{1,2}

In the present study, the author mainly discusses about the method of the surface cleaning and the effect of the X-ray flux in the XPS measurement of polymers. A polymer sample frequently has an organic contamination on the surface, which prevents us from the detailed examination of the surface. Therefore, the surface cleaning is considered to be an essential preparation technique for the quantitative XPS study of polymers.

Most polymers are not free from a chemical degradation of the surface caused by the Ar ion bombardment which is usually used to clean the surface of inorganic materials such as metals, ceramics and semiconductors. For instance, the Ar ion bombardment induces deoxidation in the carboxyl group of poly(ethylene terephthalate) (PET) and preferentially sputters fluorine atoms from the main chains of poly-(tetrafluoro ethylene) (PTFE). Then, the author tries to remove the organic contamination from the polymer surface by washing with an ultrasonic cleaner in organic solvents, which is expected to be a

degradation-free method for the surface cleaning of polymer samples.

XPS is considered to be a relatively free technique from the radiation-induced disturbance in the examination of inorganic materials. On the other hand, in the XPS measurement of polymers we must pay attention to the damage on the sample surfaces induced by the X-ray flux. Wheeler³ found a very strong effect of the X-ray flux on the surface composition in XPS of PTFE. Chang⁴ studied the mechanism of dehydrochlorination of oxide-free poly(vinyl chloride) (PVC) film due to the X-ray irradiation used in XPS. The author performs the detailed study about the effect of the X-ray flux to various important polymers such as PET, PTFE, Nylon and others.

2-2 Experimental

2-2-1 XPS Measurement

The AEI-Kokusai Denki model ES-200 was used for the XPS study with AlK_{α1,2} X-ray source ($h\nu = 1486.6$ eV) in vacuo of 3×10^{-8} Torr. All spectra of XPS were collected and stored on 160 channels with a step of 0.1 eV using KRATOS model DS-300 data system based on PDP11/03 from Digital Equipment Corporation. The data processing of XPS spectra such as the peak area calculation, the charge up correction and the smoothing of spectra was done with the same data processor.

Polymer film samples were attached to a double sided adhesive tape on a sample holder made of copper and tightly bound with thin copper wires, which are effective to keep a constant level of the charge up of the samples. The values of the charge up of PET and PTFE were respectively 4.5 eV and 7 eV. The larger charge up level of PTFE is due to the large photoelectron yield of fluorine atoms abundantly contained

in PTFE.

2-2-2 Ultrasonic Washing

In the study of the surface cleaning method, the author used the commercial available PET and PTFE films with an organic contamination on their surface, which had been held in our laboratory with no care for a long time before this study. These polymer films was twice washed with an ultrasonic cleaner in a fresh organic solvent such as methanol, acetone or n-heptane for 15 min.

2-2-3 X-ray Irradiation

The X-ray source of ES-200 which was used to irradiate the polymer specimens and to excite the XPS spectra was operated at 10 kV and 20 mA. The normal of the specimen was about 80° to the direction of the incident X-ray. The specimen was placed at the point of about 1 cm from the X-ray anode separated with $20\text{ }\mu\text{m}$ Al foil in vacuo of 3×10^{-6} Torr. The contamination-free PET, PTFE, polyacrylonitrile (PAN), Nylon 6, polyimide (Kapton) and nitrocellulose films were used in the study of the degradation by the X-ray flux.

2-3 Results and Discussion

2-3-1 Surface Cleaning

XPS spectra of PET and PTFE washed with methanol, acetone and n-heptane are respectively shown in Figure 2.1 and 2.2. The Cls spectrum of the control PET films before washing has a noticeable hydrocarbon component and a weak ester component. Its Ols spectrum shows an asymmetric peak shape. The film is seemed to have the organic surface

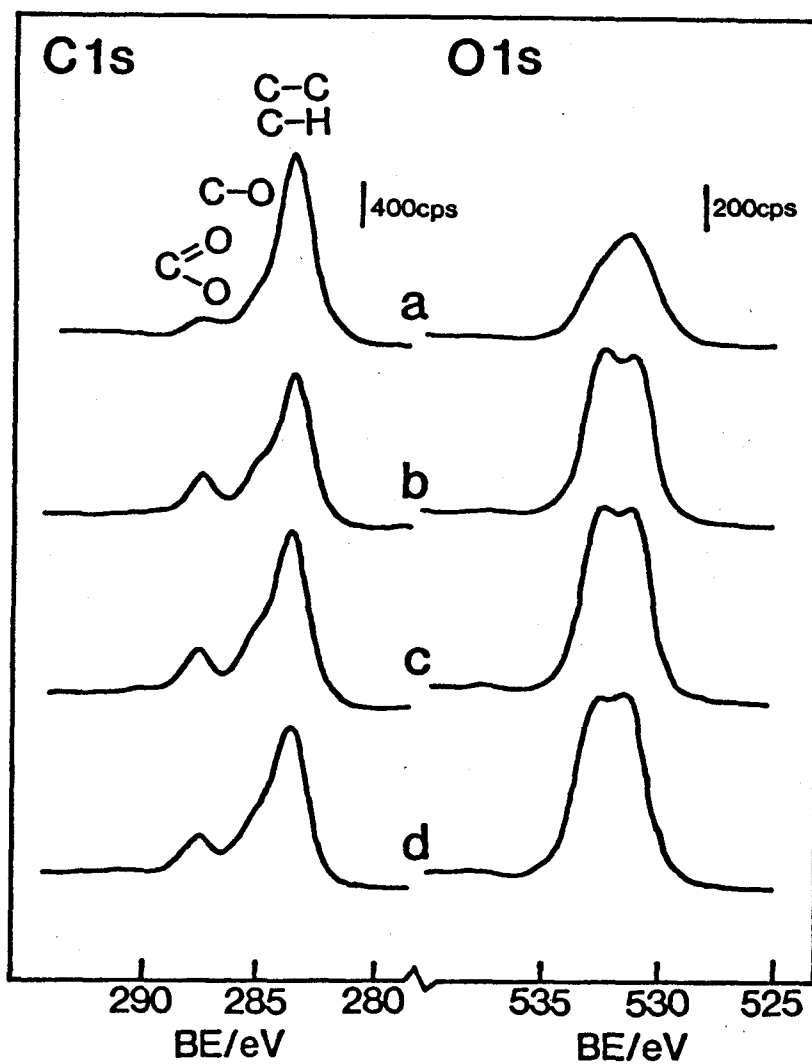


Figure 2.1 XPS spectra of PET (a) before washing, and after washing with ultrasonic cleaner in (b) methanol, (c) acetone and (d) n-heptane.

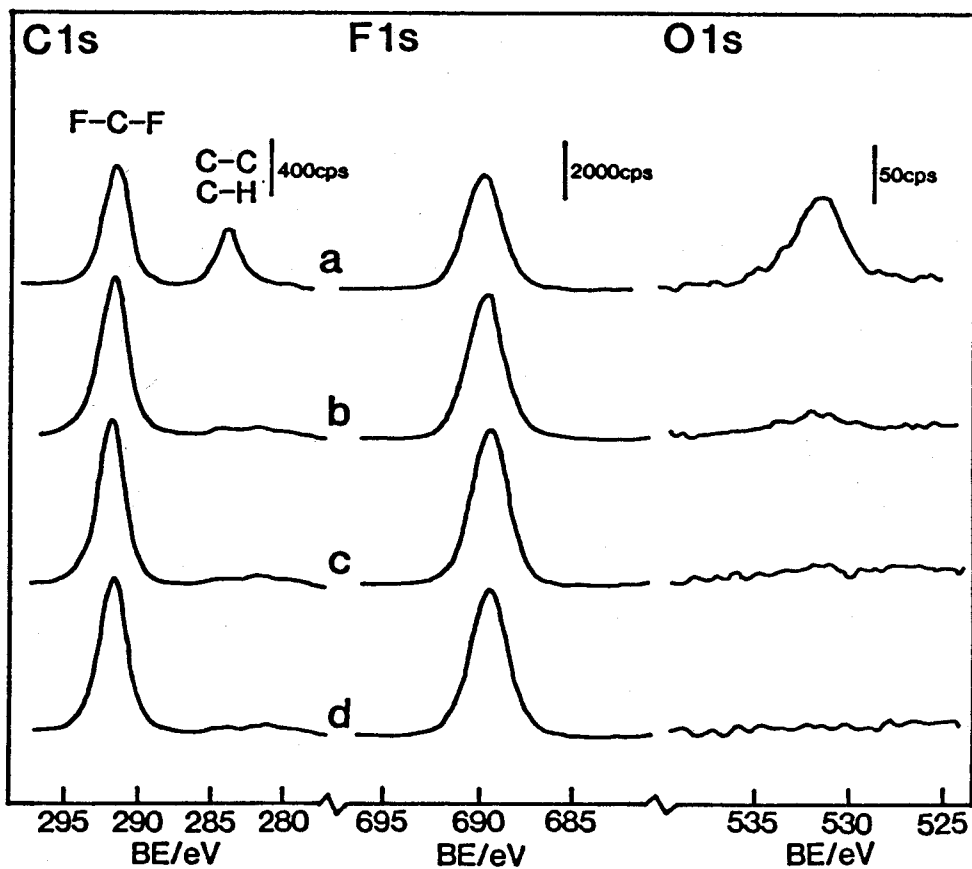


Figure 2.2 XPS spectra of PTFE (a) before washing, and after washing with ultrasonic cleaner in (b) methanol, (c) acetone and (d) n-heptane.

contamination mainly consisting with hydrocarbons. The Cls spectra of PET films washed in the organic solvents have a clear peak of the ester group and their Ols spectra show the symmetric double peaks corresponding to two oxygen atoms in the ester group. The XPS spectra corresponding to the chemical structure of PET assure the successful removal of the contamination from the surface of the PET films.⁵

The Cls spectrum of the control PTFE film before washing has two components of $\text{-CF}_2\text{-}$ and hydrocarbons, and its Ols spectrum shows a rather weak peak. This result suggests that the film also has the surface contamination mainly consisting with hydrocarbons as well as PET. The Cls spectra of PTFE films washed in acetone and n-heptane have only a $\text{-CF}_2\text{-}$ component and their Ols spectra vanish. But, the Ols spectrum of PTFE washed with methanol has a very small peak. The surface cleaning of PTFE film is also completely achieved by washing in these organic solvents excepting methanol.

It can be expected to obtain a polymer sample with contamination-free surface by the ultrasonic washing in the suitable organic solvent without the change of a composition on the surface of the sample. The surface contamination of the polymers is easily removed by the ultrasonic washing, because the polymer films have no dangling bond on the surface. On the other hand, we cannot completely remove the organic contamination on the surface of samples of metals and semiconductors with many surface dangling bonds, which are considered to form the chemisorption structure with molecules in the contamination on the surface.

The PET film held in the vacuum chamber of XPS for 24 h without X-ray flux shows no change of the surface composition. This fact indicates a lower sticking coefficient of an organic contamination to the polymer surface in the vacuum chamber of the XPS instrument compared to metals,

in the XPS measurement of which we are often prevented from quantitative analysis by the organic contamination arising in the vacuum chamber, because of the polymer surface without dangling bonds which exist on the surface of metals and semiconductor crystals. But, the surface created by cleaving of a thick polymer film is much active and quickly contaminated with organic materials as well as metals, because it has many dangling bonds generated by cutting of the polymer chains in the cleaving process.

2-3-2 Effect of X-ray Flux

XPS spectra of PET and PTFE irradiated by the X-ray flux are respectively shown on Figure 2.3 and 2.4. There is no marked change in the C1s and the O1s spectra of PET after the X-ray irradiation for several hours. The intensities of the ester component of the C1s and the O1s of PET slightly decrease without the change of the peak shape of the O1s after the X-ray irradiation for 24 h. This indicates that the ester group in main chain of PET is degraded with the decarboxylic acid reaction by the X-ray irradiation. The C1s of PTFE remarkably lost the $-CF_2-$ component along with the increase of other components during the X-ray irradiation. This spectral change indicates the elimination of fluorine atoms from the polymer chains by the X-ray irradiation.¹

The changes of O1s/C1s of PET and F1s/C1s of PTFE by the X-ray flux are shown in Figure 2.5. The oxygen concentration on the surface of PET after the irradiation of the X-ray flux for 24 h is about 90 % of that of the control PET before the X-ray irradiation. The fluorine concentration on the surface of PTFE after the irradiation of the X-ray flux for 24 h is to 50 % of that of the control PTFE. The cooling of the sample at 5 °C reduces the rate of the degradation of PTFE induced by the X-ray flux to

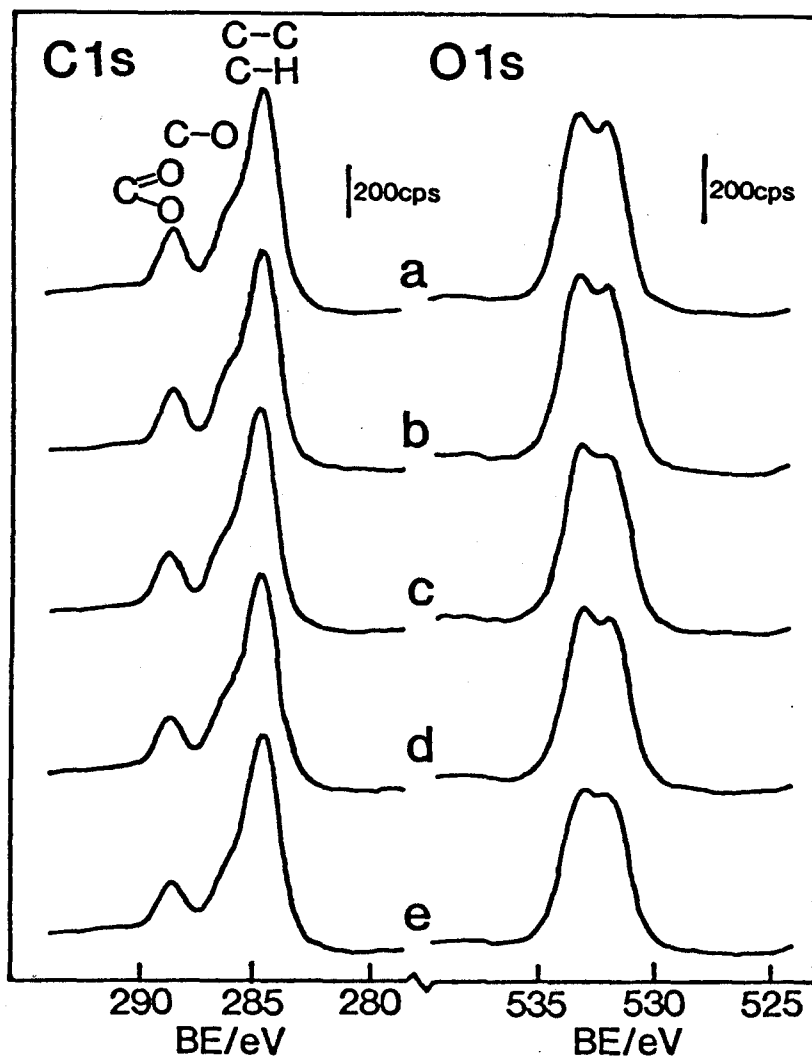


Figure 2.3 XPS spectra of PET irradiated by X-ray flux with power of 10 kV and 20 mA at 20 °C. Times of irradiation are (a) 0 h, (b) 2 h, (c) 5 h, (d) 9 h and (e) 23 h.

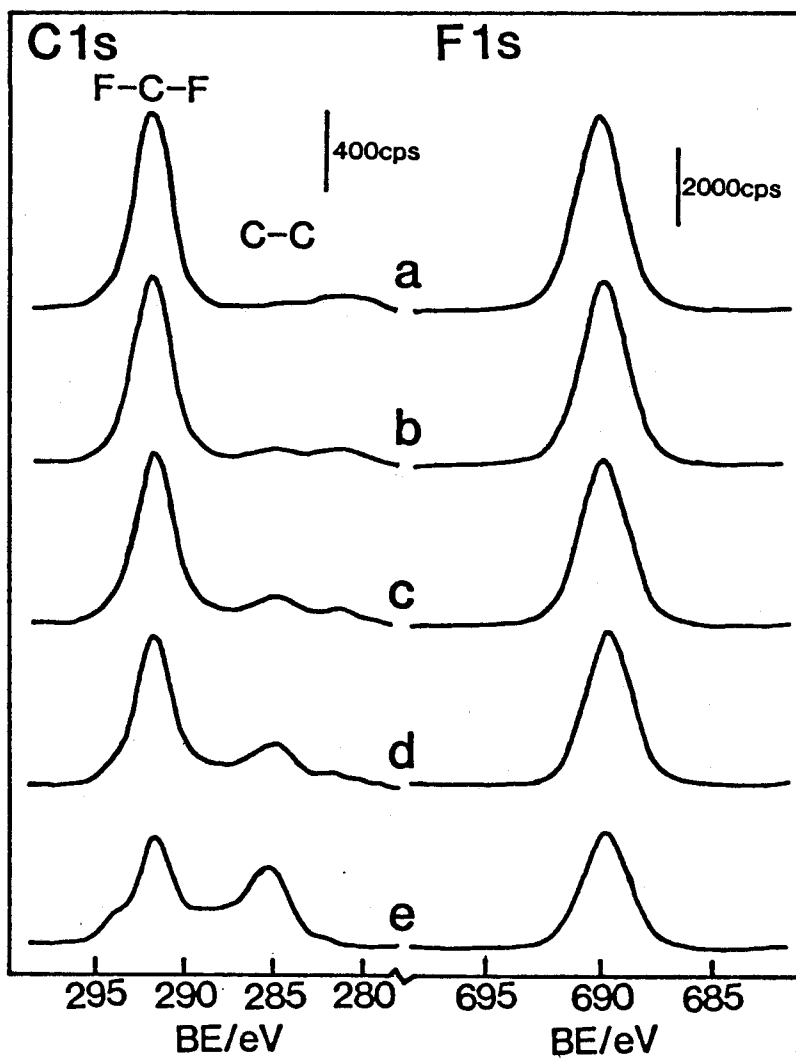


Figure 2.4 XPS spectra of PTFE irradiated by X-ray flux with power of 10 kV and 20 mA at 20 °C. Times of irradiation are (a) 0 h, (b) 2 h, (c) 5 h, (d) 9 h and (e) 23 h.

70 % of that at 20 °C. Then, the cooling of the sample is considered to be one of effective methods to reduce the X-ray damage of the sample surface. The author has the experimental result that the rate of the degradation of PTFE by the X-ray flux is directly proportional to the X-ray power. The down of the X-ray power also reduces the rate of the degradation, but taking the longer measurement time to collect XPS data. Therefore, the down of the X-ray power is not a useful method to reduce the damage of the sample surface by the X-ray flux in the XPS measurement.

The degradation behavior of several important polymers by the X-ray flux are compared in Figure 2.5. Polyimide and PAN have the high stability for the X-ray flux as well as PET. Nylon 6 has the low stability close to that of PTFE. Nitrocellulose has the extremely low stability for the X-ray flux, 50 % of the nitroester group in nitrocellulose is degraded by the X-ray flux only for an hour. Thus, it is feared that the low stability of the nitroester group misleads us in the XPS study. As an example case of the XPS study of materials containing nitrocellulose, N1s spectra of a magnetic tape are shown in Figure 2.6. The N1s spectrum in the first stage has two components of nitroester and urethane with almost even intensities. The intensity of the nitroester component rapidly diminishes and vanishes for 120 min in the XPS measurement. We probably perform the under-estimation of the amount of the nitroester in the magnetic tape.

PET, polyimide and PAN in the condition of usual XPS measurement are quite stable. PTFE and Nylon need the attention to the degradation induced by the X-ray flux in the measurement over an hour. It is extremely difficult to obtain the proper composition on the surface of materials containing nitrocellulose component using the usual XPS

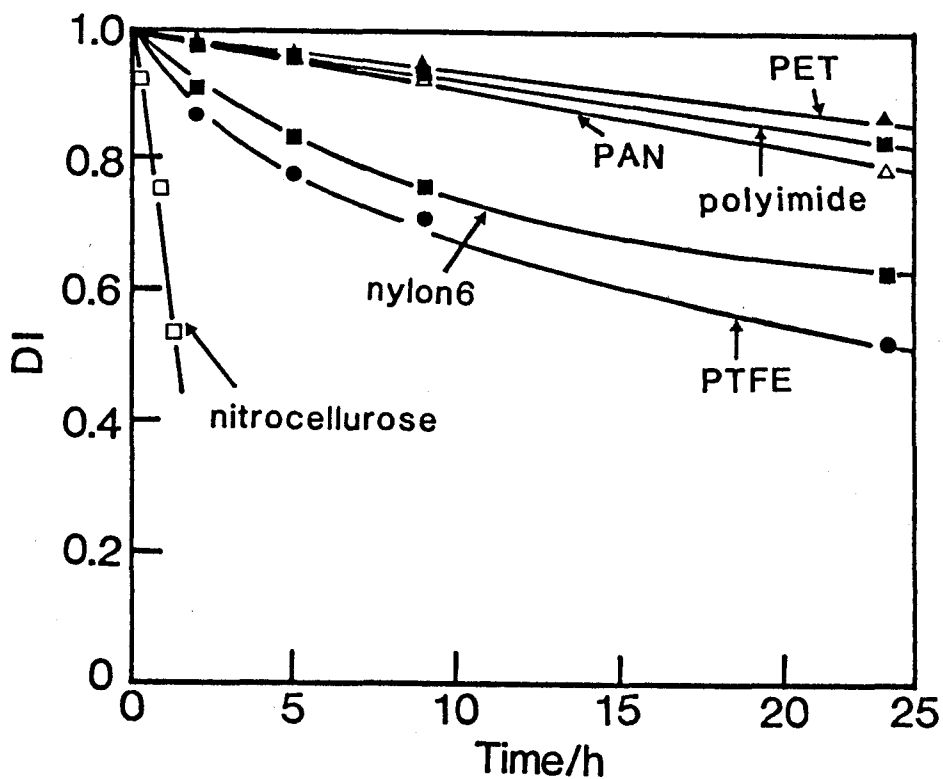


Figure 2.5 Change of surface composition of polymers in irradiation by X-ray flux with power of 10 kV and 20 mA in vacuo of 3×10^{-8} Torr at 20°C . Degradation indexes, DI are O1s/C1s for PET, F1s/C1s for PTFE, N1s/C1s for Nylon 6, polyimide, PAN and nitrocellulose. These values are normalized by that of each control sample before irradiation.

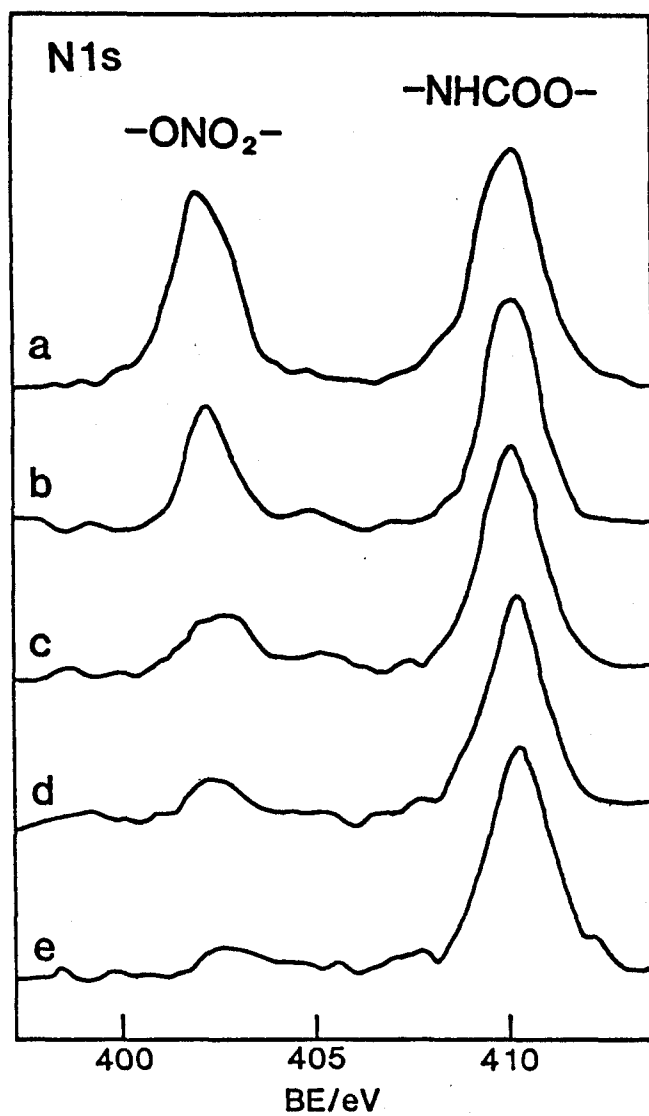


Figure 2.6 Change of N1s spectra of a magnetic tape containing nitrocellulose component in XPS measurement. Times of irradiation by X-ray flux with power of 10 kV and 20 mA in vacuo of 3×10^{-8} Torr at 20 °C are (a) 0 min, (b) 30 min, (c) 60 min, (d) 90 min and (e) 120 min.

instrument. For the quantitative XPS study of the materials, measurement techniques to enhance the sensitivity of the XPS instrument must be introduced by using such as the multi-channel detector instead of the conventional electron multiplier as the single-channel detector.

The brief consideration about the change of the chemical structures of these polymers induced by the X-ray flux was performed based on the detailed analysis of the XPS spectra. Nitrocellulose which is extremely low stable to the thermal and the mechanical shock also rapidly loses nitroester groups by the X-ray irradiation. Polymer chains of Nylon 6 and polyimide are cut with the elimination of amide and imide groups respectively in the main chains by the X-ray flux.

PTFE is known to have the high thermal stability, but its fluorine atoms are easily eliminated away from polymer chains leaving carbon atoms behind by the X-ray flux. PAN is presumed to lose the cyano groups from the main chains by the X-ray flux because of the decrease of the intensity of the N1s spectrum without the change of its peak position along with the decrease of the component assigned to cyano group of the C1s spectrum. The degradation behavior of PAN induced by the X-ray irradiation is fairly different from that in the thermal treatment in air discussed in chapter 7 of this thesis. In the thermal treatment in air, PAN forms the conjugated aromatic ladder structure through the cyclization reaction of the cyano groups.

The difference between the degradation behaviors by the X-ray flux and by the thermal treatment is considered to arise from the extreme difference of energies of activated species in these processes. The activated species with a high energy yielded by the X-ray may be able to initiate the reactions which cannot occur in the thermal process.

References

1. T. Takahagi and A. Ishitani, *Macromolecules*, 20, 404 (1987).
2. S. Storp, *Spectrochimica*, 40B, 745 (1985).
3. D. R. Wheeler and S. V. Pepper, *J. Vac. Sci. Technol.*, 20, 226 (1982).
4. H. P. Chang and J. H. Thomas III, *J. Electron Spectrosc. Relat. Phenom.*, 26, 203 (1982).
5. Y. Nakayama, T. Takahagi, F. Soeda and A. Ishitani, to be published.

Chapter 3

A Non-Empirical LCAO MO SCF and Experimental Investigation on the Core-Ionization Process of Poly(vinylidene chloride) and Poly(vinyl chloride)

3-1 Introduction

There are many previous studies on the XPS chemical shift of a carbon atom by a fluorine atom bonding in polymer materials.¹⁻⁸ But, the influence of a chlorine atom bonding on the core-ionization energy of the carbon atom in polymers has been studied no in detail. In this study, the XPS chemical shift of a carbon atom in poly(vinylidene chloride) (PVDC) and poly(vinyl chloride) (PVC) is investigated by using a non-empirical LCAO MO SCF calculation. The change of binding energy of Cls of the both polymers by bonding of chlorine atoms is mainly discussed.

3-2 Non-Empirical LCAO MO SCF Calculation

The non-empirical LCAO MO SCF calculation was carried out on the ground state of the model structures of the both polymers and polyethylene (PE) by the ab initio method using GAUSSIAN82 program¹⁰ executed on an DEC VAX8600 computer. The molecular models, which is subsequently described, need much computational time because of their large number of molecular orbitals, i.e. 30, 46, 62 orbitals for respectively PE, PVC and PVDC. The basis set used in all cases was STO-3G, which is the most simplest but has a high precision enough to calculate core orbital energy, in order to save the computational time. The binding energies were obtained directly from energy values of each

electron orbitals in ground state in the Koopmans' theorem.¹¹

The molecular model used in the calculation of PVDC is a cluster molecule consisting with two monomeric units set up based on the precise geometrical data of the molecule, the bond length, bond angles and torsional angles, obtained in the crystallographical structure analysis fully discussed in the chapter 8 of this thesis, and also both of two terminal bonds of the cluster molecule are filled with hydrogen atoms. The molecular models of PVC and PE was assumed to be cluster molecules with planer zigzag conformations.¹²⁻¹⁵

3-3 Experimental

3-3-1 Sample

Films of PVDC and PVC were cast on a clean surface of a silicon wafer from dilute solutions of o-dichlorobenzene. The film of PVC had smooth surface, but the film of PVDC had a fairly rough surface because of its high crystallinity. These films were also cleaned with an ultrasonic bath in n-heptane before the XPS measurement based on the result of the study in the previous chapter.

3-3-2 XPS Measurement

The XPS system using for the investigation in the previous chapter was also used for the XPS measurement in this study. A strip of 15 mm long and 10 mm wide cut from the silicon wafer with the sample polymer was bound to a copper slab sample holder by using a thin copper wire. Samples were cooled to 5 °C by a nitrogen gas vaporized from a liquid nitrogen during the X-ray irradiation in the XPS measurement. All spectra of XPS were collected at the takeoff angle of photoelectrons of

80°.

3-4 Result and Discussion

3-4-1 Surface Composition

The XPS wide scan spectra of PVDC and PVC are shown in Figure 3.1. Both spectra only have peaks from carbon and chlorine atoms making up these polymers and no peak of any other element. Then, the both polymer film samples are considered to have the clean surfaces enough to the quantitative XPS study.

XPS Cls, Cl2p and valence spectra of PVDC and PVC are shown in Figure 3.2. The Cls spectrum of PVDC has two marked components separating by about 2 eV. The Cls spectrum of PVC has a broad single peak. The Cl2p spectra of the both polymers show the asymmetric peak shape consisting of two components due to 2p_{1/2} and 2p_{3/2}. The both valence spectra of PVDC and PVC have two intense peaks due to chlorine atoms.

3-4-2 Chemical Shift of Cls Spectra

The binding energies of Cls obtained by the ab initio calculation of PVDC, PVC and PE are listed in Table 3.1. These values are larger by about 20 eV compared with the observed ones, about 285 eV. This difference is considered to be due to leaving the relaxation energies accompanying the core ionization in Koopmans' theorem. The calculated binding energies were corrected using the same relaxation energy of 17.8 eV, which was obtained assuming the binding energy of the Cls of PE to be 284.6 eV. The corrected binding energies are shown in Table 3.2. The result of the ab initio calculation suggests that Cls of the carbon atoms

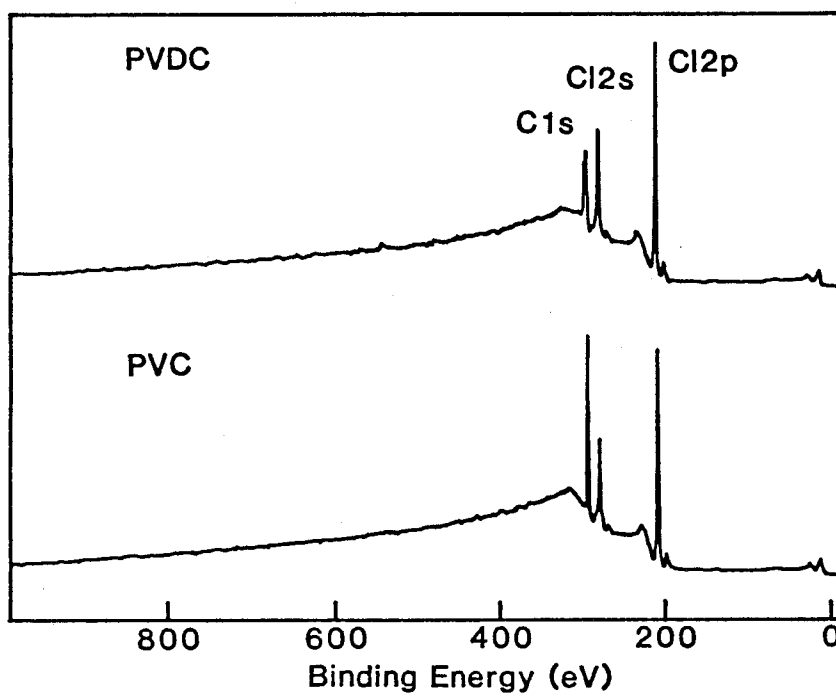


Figure 3.1 XPS wide scan spectra of PVDC and PVC.

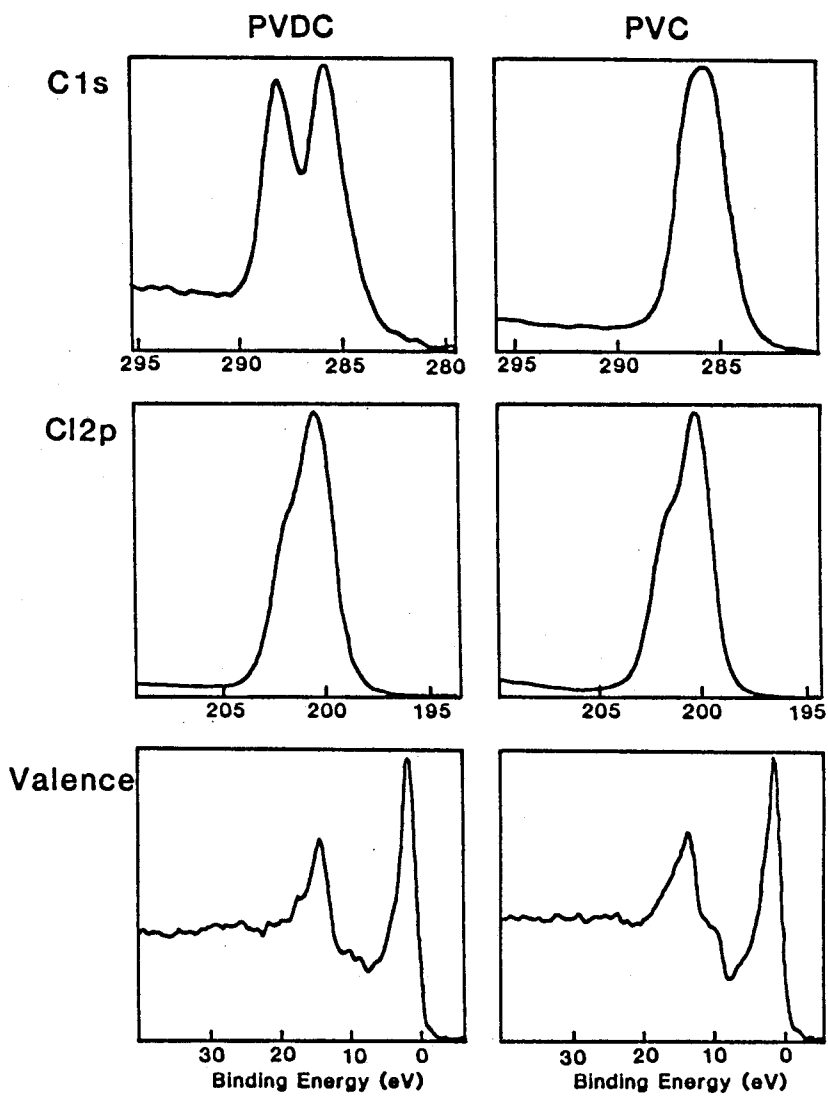


Figure 3.2 XPS C1s, Cl2p and valence spectra of PVDC and PVC.

Table 3.1 Cls binding energy (eV) obtained by ab initio calculation of PVDC, PVC and PE using GAUSSIAN82.

polymer	-CCl ₂ -	-CHCl-	-CH ₂ -
PVDC	307.6	----	305.3
PVC	----	305.4	303.9
PE	----	----	302.4

Table 3.2 Calculated and observed Cls binding energy (eV) of PVDC and PVC, the former was obtained by correction of the relaxation energy of 17.8 eV from the data shown in Table 3.1.

polymer	-CCl ₂ -		-CHCl-		-CH ₂ -	
	calc.	obs.	calc.	obs.	calc.	obs.
PVDC	289.8	288.0	----	----	287.5	285.8
PVC	----	----	287.6	286.5	286.1	285.3

of $\text{-CCl}_2\text{-}$ in PVDC and -CHCl- in PVC have lower binding energies by 2.3 eV and 1.5 eV, respectively, compared to $\text{-CH}_2\text{-}$ in each polymers, which have also lower binding energies compared to $\text{-CH}_2\text{-}$ in PE.

The curve resolving of Cls spectra was carried out consulting with the result of the ab initio calculation. The result of curve resolving of the Cls of PVDC and PVC are shown in Figure 3.3. Two intense peaks of the Cls of PVDC with almost even intensity are assigned to $\text{-CCl}_2\text{-}$ and $\text{-CH}_2\text{-}$. The Cls of PVC consists of two components assigned to -CHCl- and $\text{-CH}_2\text{-}$. Further, the Cls spectra of both polymers have small peaks at the lowest binding energy, which are considered to be due to hydrocarbons of the surface contaminations. The Cls peaks of these hydrocarbon components was used as the reference for the chemical shift of observed XPS spectra, assuming their binding energies to be 284.6 eV. The observed binding energies of the Cls components are compared with the calculated binding energies in Table 3.2.

There are a little differences between observed and calculated binding energies, 1.7 - 1.8 eV for PVDC and 0.8 - 1.1 eV for PVC. Probably because, the relaxation energies of these polymers are different from that of PE. The observed values of the chemical shift of $\text{-CCl}_2\text{-}$ in PVDC and -CHCl- in PVC from $\text{-CH}_2\text{-}$ in each polymers are 2.2 eV and 1.2 eV respectively, well corresponding to the calculated values, 2.3 eV for PVDC and 1.5 eV for PVC. This result indicates that the carbon atoms in $\text{-CCl}_2\text{-}$ and -CHCl- have large positive charges due to the bonding of chlorine atoms with higher electronegativity. The carbon atoms in $\text{-CH}_2\text{-}$ lying between two $\text{-CCl}_2\text{-}$ or -CHCl- also have some positive charge because of the electron accepting effect of the chlorine atom through the carbon atom in $\text{-CCl}_2\text{-}$ or -CHCl- . Through the consideration of chemical shift of the carbon atoms due to the chlorine atom bonding, it is concluded that

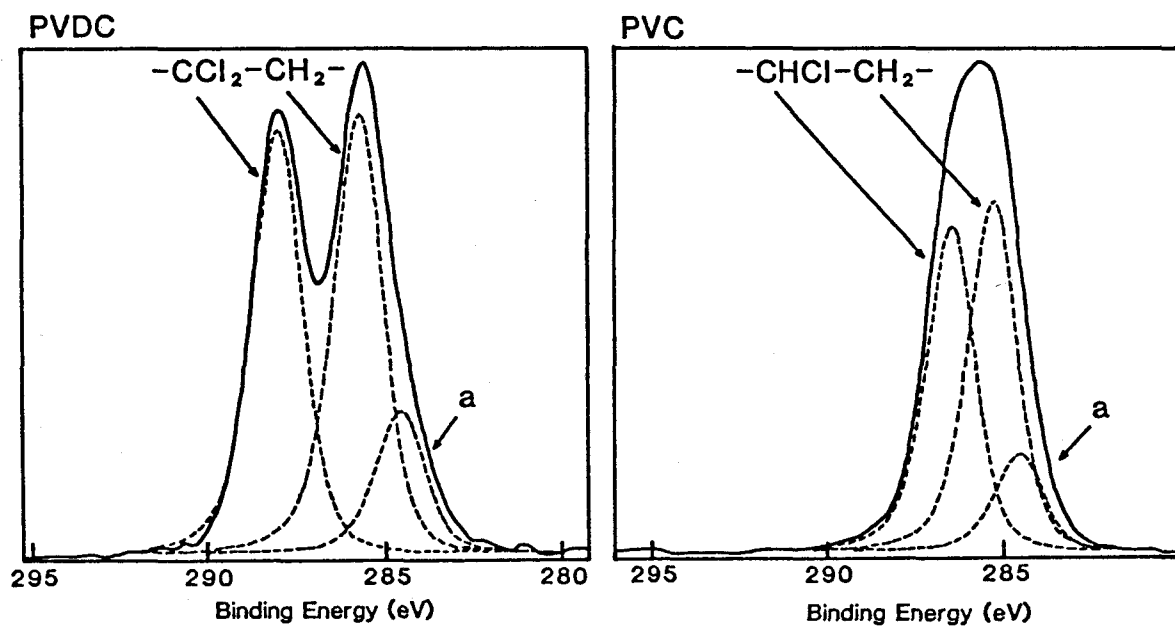


Figure 3.3 The result of curve resolving of Cls spectra of PVDC and PVC, where letter "a" indicates a component of hydrocarbon surface contamination.

replacing a chlorine atom to a hydrogen atom bonding to a carbon atom gives rise to the chemical shift of 1.8 eV to binding energy of Cls of the carbon atom and the chemical shift of 0.3 eV to one of Cls of the adjacent carbon atom. These substituent effects of a chlorine atom are smaller than the effects of a fluorine atom, that are 2.9 eV and 0.35 eV respectively,¹ because of the lower electronegativity of a chlorine atom comparing to that of a fluorine atom.

References

1. D. T. Clark, W. J. Feast, D. Kileast and W. K. R. Musgrave, J. Polym. Sci., Polym. Chem. Ed., 11, 389 (1973).
2. D. T. Clark, W. J. Feast, I. Ritchie, W. K. R. Musgrave, M. Modena, M. Ragazzini, J. Polym. Sci. Polym., Chem. Ed., 12, 1049 (1974).
3. D. T. Clark and J. Peeling, J. Polym. Sci., Polym. Chem. Ed., 14, 2941 (1976).
4. D. T. Clark and H. R. Thomas, J. Polym. Sci., Polym. Chem. Ed., 16, 791 (1978).
5. D. T. Clark and A. Dilks, J. Polym. Sci., Polym. Chem. Ed., 16, 911 (1978).
6. D. T. Clark and D. Shuttleworth, J. Polym. Sci., Polym. Chem. Ed., 17, 1317 (1979).
7. D. T. Clark, W. J. Feast and P. J. Tweedale, J. Polym. Sci., Polym. Chem. Ed., 18, 1651 (1980).
8. E. Sacher, J. Electron Spectrosc. Relat. Phenom., 33, 369 (1984).
9. H. P. Chang and J. N. Thomas III, J. Electron Spectrosc. Relat. Phenom., 26, 213 (1982).
10. J. S. Binkley, R. A. Whiteside, K. Ragharachari, R. Seeger, D. J. DeFees, H. B. Schlegel, M. J. Frisch, J. A. Pople and L. R. Kahn,

"GAUSSIAN82 Release A", Carnegie Mellon University, Pittsburgh,
1982.

11. T. A. Koopmans, *Physica*, 1, 104 (1933).
12. G. Natta and P. Corradini, *J. Polym. Sci.*, 20, 251 (1956).
13. C. E. Wilkes, V. L. Folt and S. Krimm, *Macromolecules*, 6, 235
(1973).
14. C. W. Bunn, *Trans. Faraday Soc.*, 35, 482 (1939).
15. P. R. Swan, *J Polym. Sci.*, 56, 409 (1962).

Chapter 4

Monte Carlo Simulation of an Ion Sputtering

Process of Fluoro Polymers

4-1 Introduction

Ion sputtering is frequently used in surface analysis. It is used to obtain signals in secondary ion mass spectroscopy (SIMS) and also for surface cleaning and depth profiling in X-ray photoelectron spectroscopy (XPS), Auger electron spectroscopy (AES) and ultraviolet photoelectron spectroscopy (UPS). It is important to obtain new information for better understanding of the sputtering mechanism in SIMS, especially for organic polymers. It is also desirable to have detailed knowledge of the change of surface composition in depth profiling or in cleaning by sputtering, especially in quantitative analysis.

XPS is expected to be a useful tool for investigation of the change of surface composition induced by the ion sputtering process because of its good surface sensitivity and capability of providing chemical bonding information. The effects on inorganic materials induced by ion sputtering have already been studied in detail by XPS by many authors.¹⁻¹⁰ On the other hand, not many studies have concerned ion sputtering on organic materials.^{5,11-13} An understanding of the mechanism of sputtering is particularly important for SIMS measurement of polymer materials,¹³⁻¹⁷ however, it is far from satisfactory.

In this paper, the author examines the change of chemical composition on the surface of poly(tetrafluoro ethylene) (PTFE) and poly(vinylidene fluoride) (PVDF) by Ar ion bombardment with XPS because these fluoro polymers have already been extensively studied by XPS¹⁸⁻²² and

SIMS.^{13,15,17} Thickness of a damaged layer on the sputtered polymer surface is estimated by the photoelectron takeoff angle variation measurement of XPS. Change of XPS spectra of the polymers by Ar ion bombardment is interpreted by a simple calculation based on Monte Carlo simulation.

4-2 Experimental

4-2-1 Sample

PTFE and PVDF used in this study are commercially available as 50 μm thick sheets. These sheets were well washed with an ultrasonic cleaner in n-heptane to remove organic contamination from the surface before use.²³

4-2-2 XPS Measurement

XPS measurement was performed by using the same instrument, ES-200, as one used in previous chapters. A sample was attached by double sided adhesive tape and tightly bound with thin copper wires to copper sample holder. XPS spectra were recorded at the takeoff angle of photoelectrons of 90° in ordinary measurement, and at takeoff angles of 90°, 60°, 40°, 30° and 20° in the angle-resolved measurement. The takeoff angle here is the angle of observation of photoelectrons relative to the sample surface. The observed depth is directly proportional to a sine of the takeoff angle of photoelectrons in angle-resolved measurement, which gives us the depth information in the surface region of a sample. In all XPS measurements, samples were cooled at 5 °C to reduce the degradation induced by X-ray flux.

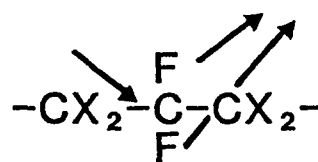
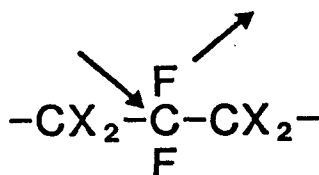
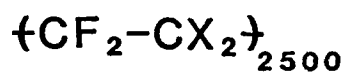
4-2-3 Ar Ion Sputtering

Sputtering was done using an ion beam with a 500 nA/cm^2 density and a 1 keV energy at 2×10^{-4} Torr of Ar pressure in the preparation chamber of ES-200. The back side of sample holder faced to Ar beam during adjustment of the acceleration voltage and the beam current, and the sample side was turned to the direction of the beam after its stabilization achieved in order to accurately control Ar sputtering time. The author observed the beam current to a copper sample holder in spite of that to the sample polymer, since the beam current was unsteady at sputtering process.

4-3 Models of Sputtering Process for Monte Carlo Simulation

The simulation is executed on a cyclic polymer chain containing 2500 monomeric units which is safely considered to be large enough for statistical calculation. It is assumed that only fluorine atoms are sputtered away, whereas all carbon atoms are left intact because of the great difference in their sputtering rates. Another model based on simultaneous elimination of both fluorine and carbon with different rates is also tried but showed little difference from the simpler one. Sputtering of hydrogen atoms in the PVDF system is also neglected since hydrogen cannot be detected in XPS measurement and its elimination brings about very little chemical shift on a carbon atom.²⁴

Ar ion sputtering is simulated with two models shown in Figure 4.1. In model A, elimination of only a single fluorine atom by one encounter with an activated particle is assumed; that is, any fluorine atom in a polymer chain is independently sputtered away in complete randomness. On the other hand, in model B, it is assumed that the both single and double fluorine atom elimination concurrently occur, where the second process happens in a probability of $r \%$. The double elimination here means that



Model A 100 %

0 %

Model B 100 - r %

r %

Figure 4.1 Models of sputtering process of polymer chains for Monte Carlo simulation, where X represents a fluorine atom in PTFE and a hydrogen atom in PVDF respectively.

two fluorine atoms bonding to a carbon atom are broken off together from a polymer chain by one encounter with a single activated particle. An activated particle can be an Ar ion itself, an electron, or another ion generated in the sputtering process.

Actual calculation of the Monte Carlo simulation is carried out by using two models explained above with the following procedure. A segment of the polymer is picked up by a random integer of uniform distribution over the range from 1 to 2500. The integer is generated with a random number function and it corresponds to one encounter by an activated particle. In model A, one fluorine atom leaves from the segment. In model B, two fluorine atoms leave with probability of r %, and one fluorine atom elimination takes place with probability of $100 - r$ %. A series of calculations is repeated until the atomic ratio F/C reaches the value that corresponds to the one determined by the XPS experiment.

C1s chemical shift values of all possible chemical structures after partial and complete removal of fluorine atoms from a polymer chain in both simulation models are shown in Table 4.1. These chemical shift values are estimated on the basis of experimental data of a fluorine polymer series¹⁸ taking the diad effect of the fluorine atom into account. The author determined the distribution of residual structures from those chemical shifts at each stage of the simulated sputtering process.

4-4 Result and Discussion

4-4-1 Surface Composition of Sputtered Polymers.

Variation of the XPS wide scan spectra of PTFE and PVDF by sputtering is shown in Figure 4.2 and 4.3. The rapid decrease of fluorine peaks in both spectra indicates that fluorine atoms are

Table 4.1 Cls chemical shifts of all possible chemical structures of sputtered PTFE and PVDF, where a hydrogen atom in PVDF is neglected because of its very small effect on Cls chemical shift.

Chemical structures	$\Delta E(\text{eV})$
$\text{C}-\text{C}^*-\text{C}$	0.00
$\text{C}-\text{C}^*-\text{CF}$	0.35
$\text{C}-\text{C}^*-\text{CF}_2$, $\text{CF}-\text{C}^*-\text{CF}$	0.70
$\text{CF}-\text{C}^*-\text{CF}_2$	1.05
$\text{CF}_2-\text{C}^*-\text{CF}_2$	1.40
$\text{C}-\text{C}^*\text{F}-\text{C}$	2.90
$\text{C}-\text{C}^*\text{F}-\text{CF}$	3.25
$\text{C}-\text{C}^*\text{F}-\text{CF}_2$, $\text{CF}-\text{C}^*\text{F}-\text{CF}$	3.60
$\text{CF}-\text{C}^*\text{F}-\text{CF}_2$	3.95
$\text{CF}_2-\text{C}^*\text{F}-\text{CF}_2$	4.30
$\text{C}-\text{C}^*\text{F}_2-\text{C}$	5.80
$\text{C}-\text{C}^*\text{F}_2-\text{CF}$	6.15
$\text{C}-\text{C}^*\text{F}_2-\text{CF}_2$, $\text{CF}-\text{C}^*\text{F}_2-\text{CF}$	6.50
$\text{CF}-\text{C}^*\text{F}_2-\text{CF}_2$	6.85
$\text{CF}_2-\text{C}^*\text{F}_2-\text{CF}_2$	7.20

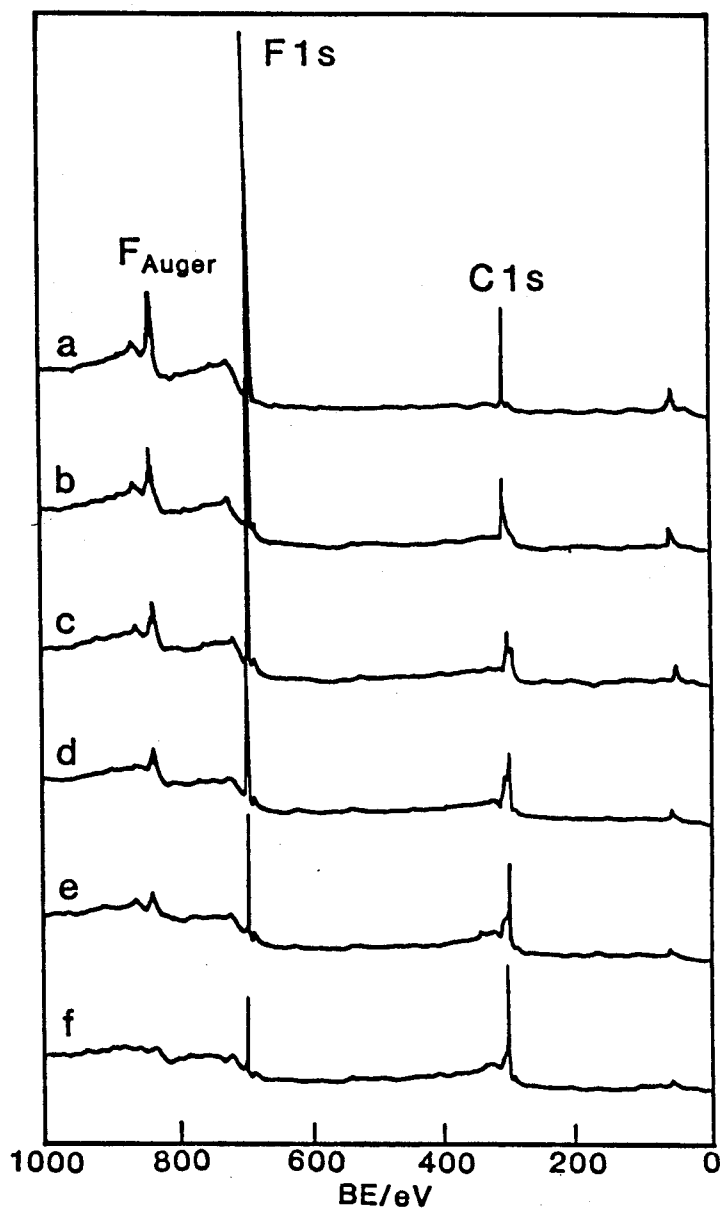


Figure 4.2 XPS wide scan spectra of PTFE sputtered by Ar ions. Sputtering times are (a) 0 s, (b) 10 s, (c) 30 s, (d) 60 s, (e) 120 s, (f) 300 s.

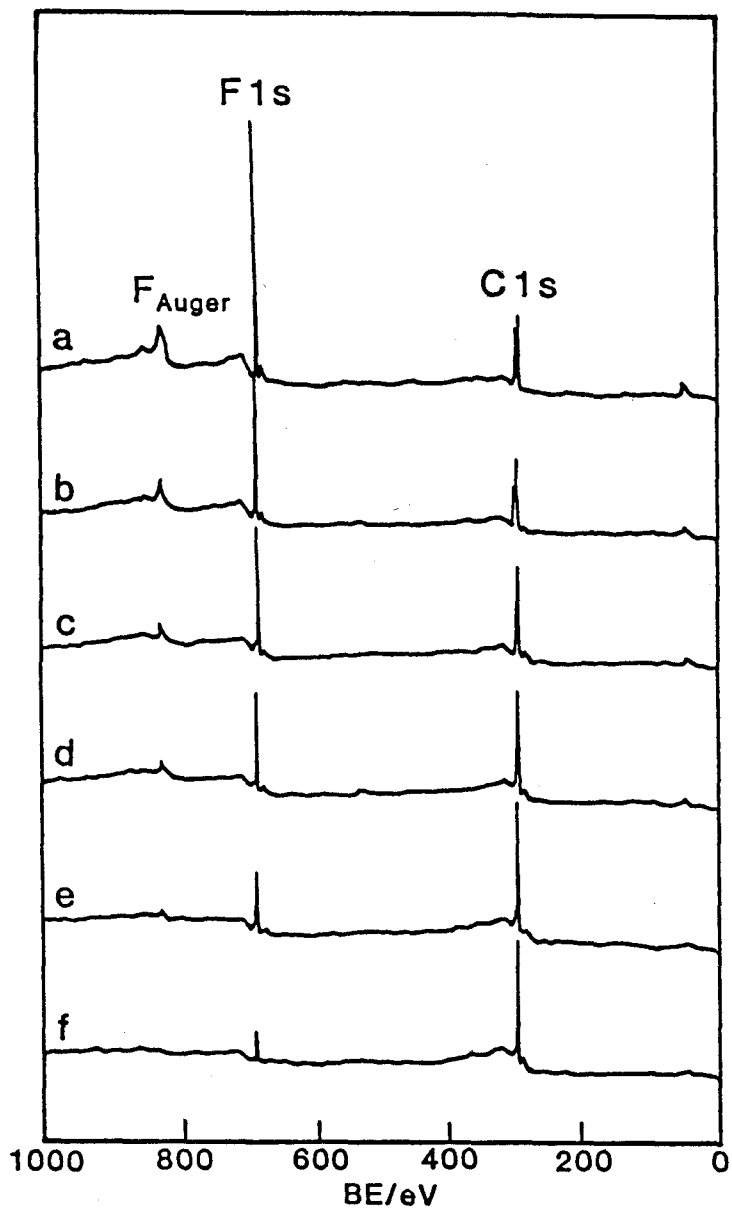


Figure 4.3 XPS wide scan spectra of PVDF sputtered by Ar ions. Sputtering times are (a) 0 s, (b) 2 s, (c) 5 s, (d) 10 s, (e) 20 s, (f) 30 s.

preferentially sputtered away from polymer chains, leaving carbon atoms behind in both polymer systems.

The result of the angle resolved XPS measurement of sputtered PTFE is indicated in Figure 4.4. The photoelectron mean free path is estimated to be a few score Å in an XPS measurement of polymer materials.²⁵ The sampling depth on the surface is proportional to $\sin\theta$ where θ is a takeoff angle of photoelectrons.²⁶ The chemical composition represented by F1s/C1s is independent of $\sin\theta$ at any sputtering stage. The result suggests that the damaged layer of the bombarded PTFE has homogeneous composition within a sampling depth of XPS. This ensures that XPS is seeing a homogeneous layer produced by Ar ion sputtering.

The C1s spectra of sputtered PTFE and PVDF are shown by solid lines in Figure 4.5 and 4.6. Surfaces of both polymers show broad C1s spectra because of many overlapping peaks of different chemical shifts which depend on the number of fluorine atoms bonding to the carbon atom. The shift of C1s by elimination of fluorine atoms is significant because of the large electronegativity of fluorine. A major component of C1s spectra comes from $-\text{CF}_2-$ species in earlier stages of the sputtering process of PTFE, while in later stages it comes from $-\text{C}-$ species after removal of all fluorine atoms. The $-\text{CF}_2-$ species also gradually decrease in sputtering of PVDF. These C1s spectra are expected to provide information about the mechanism of sputtering of fluorine atoms from the polymer chains.

4-4-2 Monte Carlo Simulation.

The simulated and observed C1s spectra of sputtered PTFE are compared in Figure 4.5. Bar graphs and solid lines show simulated and observed C1s spectra respectively. The simulated spectra by model A are

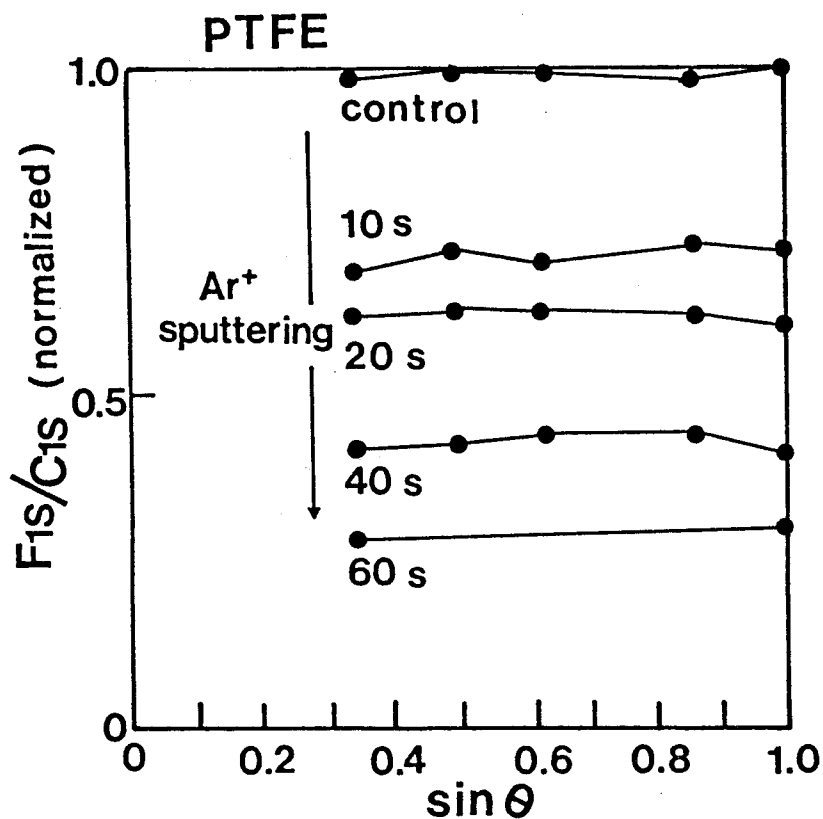


Figure 4.4 Result of angle-resolved XPS of Ar ion sputtered PTFE, where θ represents takeoff angle of photoelectrons.

F1s/C1s(normalized) in the vertical axis means a peak area ratio of F1s to C1s normalized by that of the control sample before Ar ion sputtering.

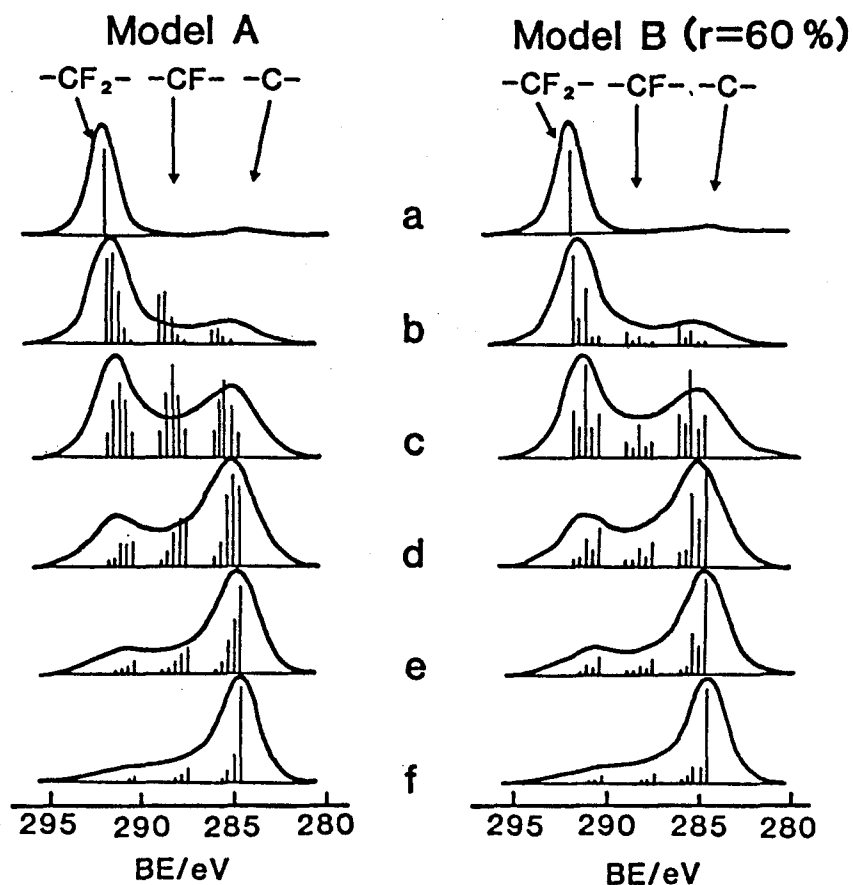


Figure 4.5 The observed (solid line) and simulated (bar graph) XPS C1s spectra of PTFE after Ar ion sputtering. Sputtering times, fractions of sputtered fluorine and atomic ratios (F/C) are (a) 0 s, 0 % and 2.00, (b) 10 s, 25 %, and 1.50, (c) 30 s, 50 % and 1.00, (d) 60 s, 70 % and 0.60, (e) 120 s, 80 % and 0.40, (f) 300 s, 90 % and 0.20.

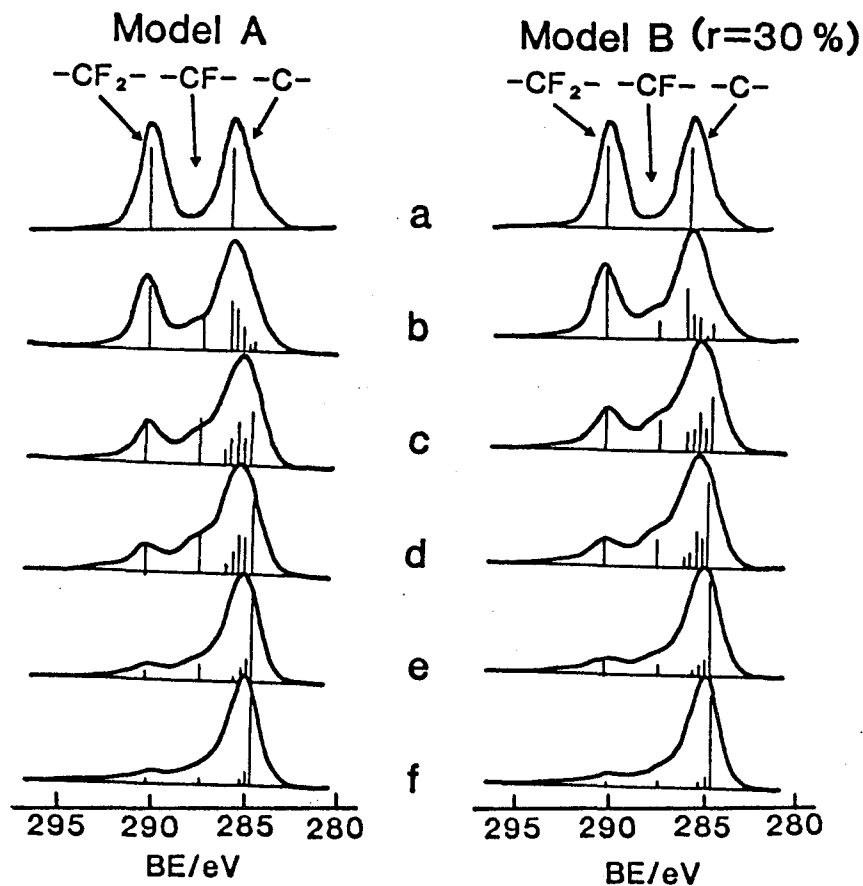


Figure 4.6 The observed (solid line) and simulated (bar graph) XPS C1s spectra of PVDF after Ar ion sputtering. Sputtering times, fractions of sputtered fluorine and atomic ratios (F/C) are (a) 0 s, 0 % and 1.00, (b) 2 s, 22 % and 0.78, (c) 5 s, 50 % and 0.50, (d) 10 s, 63 % and 0.37, (e) 20 s, 82 % and 0.18, (f) 30 s, 90 % and 0.10.

in good agreement with the observed spectra after more than 80 % of the fluorine is sputtered away, but they are in poor agreement for the earlier stages before 50 % of the fluorine leaves, especially in the chemical shift region of the -CF- group. In order to improve the fitting, model B with the double elimination of fluorine is added stepwise with increasing probability, r , in 10 % intervals from 10 % to 100 %. Model B with an r value of 60 % presents the best fitting for every stage. This simulation reveals that broadening of Cls spectra in the earlier stages of sputtering is due to generation of various kinds of chemical species, and renarrowing in the later stages is due to a decrease in the variety of species.

The result of a similar procedure on PVDF is indicated in Figure 4.6. The Cls spectra simulated by model A are in better agreement with the observed spectra for all stages than they are with PTFE. Model B with an r value of 30 % best explains the observed Cls spectra of sputtered PVDF. The presence of a methylene group in the vicinity seems to work in favor of single elimination of fluorine. The electron donating effect of a methylene group possibly stabilizes -CF- species produced in single elimination of a fluorine atom.

The residual chemical structure left behind in polymer chains after elimination of fluorine atoms by sputtering may have unsaturated bonds, cross-links, and also radicals and ions that are composed of carbon atoms. Evidence for the existence of such chemical species is gathered from the following observations. Surface oxygen concentration of PTFE bombarded by Ar ion for 300 s and then exposed to air for a day is found to be 0.11 in O1s/C1s parameter, probably because of radical or ion quenching by oxygen and water in air. In the Cls spectrum of PTFE sputtered for 300 s, a tailing component is observed in the higher binding energy region

between 290 eV and 295 eV. It can be assigned as a $\pi - \pi^*$ shake-up satellite from the linear and cyclic unsaturated systems.²⁷

4-5 Conclusions

XPS is found to be useful for examining the residual composition of ion sputtered surfaces of polymers. Sputtered PTFE has a damaged layer with a homogeneous composition within sampling depth of XPS. Monte Carlo simulation has proved to be helpful in understanding the sputtering process of polymer materials. Observed XPS spectra are well explained by random elimination of fluorine atoms from polymer chains of PTFE and PVDF, and even better fitting is achieved by assuming a double fluorine atom elimination mechanism.

References

1. S. Hofmann and J. M. Sanz, *Fresenius Z. Anal. Chem.*, 314, 215 (1983).
2. H. J. Mathieu and D. Landolt, *Appl. Surf. Sci.*, 10, 100 (1982).
3. R. Kelly, *Nucl. Instr. a. Meth.*, 149, 553 (1978).
4. R. Holm and S. Storp., *Appl. Phys.*, 9, 217 (1976).
5. S. Storp and R. Holm., *J. Electron Spectrosc. Relat. Phenom.*, 16, 183 (1979).
6. A. Katrib, *J. Electron Spectrosc. Relat. Phenom.*, 18, 275 (1980).
7. K. S. Kim and N. Winograd. *Surf. Sci.*, 43, 625 (1974).
8. S. Hufner, R. L. Cohen and G. K. Wertherim, *Physica Scripta*, 5, 91 (1972).
9. T. Tsanz, G. J. Coyle, I. Adler and L. Yin, *J. Electron Spectrosc. Relat. Phenom.*, 16, 389 (1979).
10. H. Shimizu, M. Ono and K. Nakayama, *Surf. Sci.*, 36, 817 (1973).

11. A. Toth, I. Bertoti, T. Szekely and M. Mohai, Surf. Interface Anal., 7, 282 (1985).
12. D. M. Ulleving and J. F. Evans, Anal. Chem. 52, 1467 (1982).
13. D. Briggs and A. B. Wootton, Surf. Interface Anal., 4, 109 (1982).
14. J. A. Gardella, Jr. and D. M. Hercules, Anal. Chem., 52, 226 (1980).
15. J. A. Gardella, Jr. and D. M. Hercules, Anal. Chem., 53, 1879 (1981).
16. D. Briggs, Surf. Interface Anal., 4, 151 (1982).
17. D. Briggs, Surf. Interface Anal., 5, 113 (1983).
18. D. T. Clark, W. J. Feast, D. Kilcast and W. K. R. Musgrave, J. Polym. Sci. Polym. Chem. Ed., 11, 389 (1973).
19. D. W. Dwight and W. M. Riggs, J. Colloid Interface Sci., 47, 650 (1974).
20. J. Delhalle, S. Delhalle, J. M. Andre, J. J. Pireaux, J. Riga, R. Caudano and J. J. Verbist, J. Electron Spectrosc. Relat. Phenom., 12, 293 (1977).
21. D. T. Clark, W. J. Feast, P. J. Tweedale, H. R. Thomas, J. Polym. Sci. Polym. Chem. Ed., 18, 1651 (1980).
22. S. Nagarajan, Z. H. Stachurski, M. E. Hughes and F. P. Larkins, J. Polym. Sci. Polym. Phys. Ed., 20, 1001 (1982).
23. T. Takahagi, Y. Nakayama, F. Soeda and A. Ishitani, to be published.
24. K. Siegbahn, C. Nordling, G. Johansson, J. Hedman, P. F. Heden, K. Hamrin, U. Gelius, T. Bergmark, L. O. Werme, R. Manne, Y. Baer, "ESCA Applied to Free Molecules", pp113-120, North-Holland Publishing Company, Amsterdam, 1969.
25. D. T. Clark and H. R. Thomas, J. Polym. Sci. Polym. Chem. Ed., 15, 2843 (1977).

26. C. S. Fadley, "Electron Spectroscopy : Theory, Techniques and Applications", Vol.2, p124-131, Academic Press, New York, 1978.
27. J. A. Gardella, Jr., R. L. Chin, S. A. Ferguson and M. M. Farrow, J. Electron Spectrosc. Relat. Phenom., 34, 97 (1984).

Chapter 5

XPS Study by Use of the Digital Difference Spectrum Technique of Functional Groups on the Surface of Carbon Fiber

5-1 Introduction

Surface treatment of carbon fiber (CF) is frequently done to improve adhesion between the fiber and the matrix resin. Functional groups on surface of carbon fiber have been studied mainly with X-ray photoelectron spectroscopy (XPS) by various authors¹⁻⁸ because of its surface sensitivity and its capability of providing chemical information.

Ishitani also has examined the CF surface by XPS in the preceding paper.⁹ Chemical shift analysis of the Cls peak has proved to be important in elucidating the functional groups generated on the surface of CF. A problem noticed there was asymmetry of the original Cls peak of the untreated carbon fiber. This asymmetry was noticed by Thomas³ for graphite single crystals and explained to be due to the multi-electron excitation from the analogy to similar asymmetric line shapes observed in metals. When curve resolving is carried out using symmetric Gaussians to identify Cls component of oxidized carbon species, the asymmetry of the original carbon peak produces superficially a second component at 1.4 eV higher binding energy than the main component. It is difficult to distinguish a component due to real chemical change from one due to the asymmetry.

In order to circumvent this problem the digital difference spectrum technique is used in the present work. Difference spectra are calculated for the samples before and after the surface treatment, thereby eliminating

the influence of the asymmetry. An additional advantage of the technique is that variation in spectral features produced by the surface oxidation is more clearly seen because a small difference in the original spectrum is isolated and expanded in the difference spectrum as suggested by Clark.¹⁰ The FT-IR reflection absorption spectroscopy (FT-IR-RAS) measurement¹¹ is also tried to confirm the functional groups on the CF surface observed by the XPS measurement.

5-2 Experimental

5-2-1 XPS and FT-IR Measurement

XPS model ES-200 was also used in this study. For XPS measurement, CF samples were aligned on well cleaned copper sample holder using methanol and held by a thin copper plate with a hole for the XPS observation. The author carefully set bundles of carbon fibers completely covering the sample holder, because the sample setting is essential for the quantitative XPS analysis in this study. Methanol used in this preparation is considered not to disturb the XPS observation because of its immediate vaporization in the vacuum chamber of XPS. CF sample has no charge up owing to its complete electrical contact to XPS apparatus.

Reflection-absorption spectra were observed with a Digilab model FTS-20B/D FT-IR spectrometer with an attachment for RAS measurement at a resolution of 4 cm^{-1} with accumulation of 1000 scans using. Five CF bundles severally containing 3000 filaments aligned on a double sided adhesive tape of 20 mm x 40 mm size on aluminum plate were used in FT-IR RAS observation.

5-2-2 Sample

Carbon fiber (CF) and graphite fiber (GF) used in this study are TORAYCA T300 and M40 commercially available from Toray Ind. Inc. They were sampled from the production line with special care to avoid any sizing agents sticking on surface for convenience in surface analysis. Surface oxidation of CF and GF was carried out in a laboratory scale specially for the present measurement. Thermal treatment of CF and GF was done at 1000 °C in vacuo of ca. 0.1 Torr.

5-2-3 Data Processing of XPS Spectra

The C1s peak of carbon and graphite is used as a reference for the chemical shift, assuming its binding energy (B.E.) to be 284.6 eV. In XPS, spectra collecting and data processing containing digital difference spectrum calculation were performed by using the same data processor as preceding chapters. Curve resolving of difference spectra of C1s was done with du Pont "Curve Resolver" assuming a Gaussian peak shape and a width of the C1s of polyethylene measured under the same condition as a standard compound.

5-3 Results and Discussion

5-3-1 Surface Composition

The XPS spectra of surface-oxidized and of heated CF and GF are compared with the corresponding controls in Figure 5.1 and 5.2. The O1s/C1s ratios and FWHM (full width at half maximum) are summarized in Table 5.1. The C1s spectra of the control CF and GF have asymmetric peak shapes showing long tails at the higher binding energy sides of the main peaks. The C1s spectrum of the control CF is broader than that of the control GF

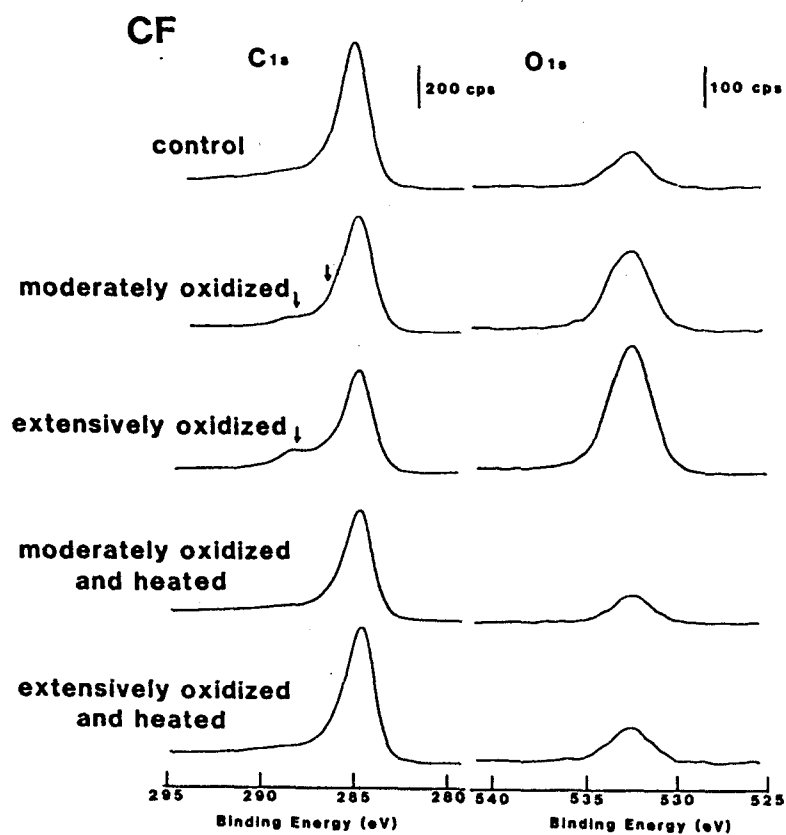


Figure 5.1 Change of the XPS spectrum of CF by surface oxidation and by thermal treatment.

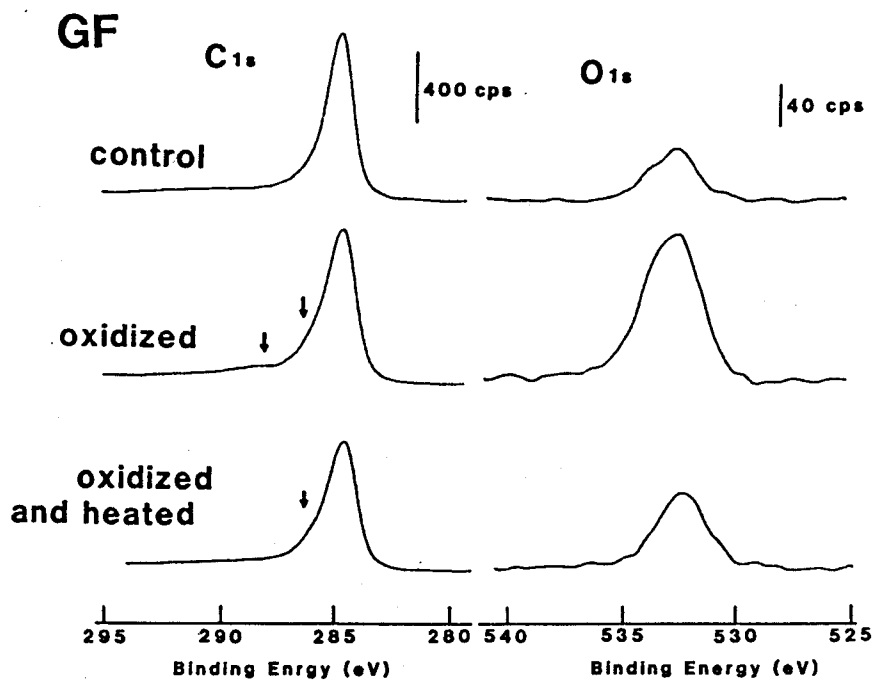


Figure 5.2 Change of the XPS spectrum of GF by surface oxidation and by thermal treatment.

Table 5.1 The XPS parameters of control, surface-oxidized and heated CF and GF.

Fiber	Treatment	O1s/C1s	FWHM(eV)	
			C1s	O1s
CF	control	0.16	1.8	2.6
CF	moderate oxidation	0.40	2.1	2.8
CF	extensive oxidation	0.66	1.9	2.8
CF	moderate oxidation and thermal treatment	0.15	1.8	2.5
CF	extensive oxidation and thermal treatment	0.16	1.8	2.7

CF	control	0.09	1.3	2.5
CF	oxidation	0.24	1.6	2.9
CF	oxidation and thermal treatment	0.12	1.5	2.5

Table 5.2 The increment of surface oxygen concentration, Δ (O1s/C1s), by surface oxidation of CF and GF.

Fiber	Treatment	Δ (O1s/C1s) ^{*1}	
		from measured O1s/C1s	calculated from C1s difference spectrum
CF	moderate oxidation	0.24	0.19
CF	extensive oxidation	0.50	0.47

CF	oxidation	0.15	0.16 ^{*2}

*1: Difference of O1s/C1s calculated between before and after oxidation.

*2: Δ (O1s/C1s) estimated from the carboxyl group component of C1s difference spectrum.

probably due to more disordered lattice structure on the surface.

The O1s/C1s ratios increase with the surface oxidation both for CF and GF. The surface oxygen concentration of CF seems to saturate at an O1s/C1s value of ca. 0.7, since the extensively oxidized CF which was treated with 4.1 times more intensity than the moderate oxidation has an O1s/C1s value of merely 0.66 compared with 0.40 of the moderately oxidized one. The oxidized GF has the surface oxygen concentration (O1s/C1s) of about 30 % of the extensively oxidized CF of the same oxidation intensity owing to higher resistance of GF against surface oxidation compared to CF. The surface oxygen concentrations of CF and GF decrease by thermal treatment to a similar level as in the controls, indicating complete decomposition of the surface functional groups produced by the surface oxidation.

The C1s spectrum of moderately oxidized CF has a shoulder at 286 eV and an additional small peak at 288-289 eV, which are not observed in the C1s spectrum of the control CF. The C1s spectrum of extensively oxidized CF has a noticeable peak at 288-289 eV but no shoulder at 286 eV. The surface oxidation of GF adds two additional components at 288-289 eV and 286 eV to the C1s spectrum.

The peak shape of the C1s spectra of both moderately and extensively oxidized CF, is reduces to that of the control CF after thermal treatment, indicating that the chemical and physical states of the surface of oxidized CF return to that of the control. On the other hand, the peak shape of the C1s spectrum of oxidized GF does not completely reduce to that of the control; the component at 288-289 eV disappears, but the component at 286 eV remains and also the line width of the main peak remains broadened.

The components in the regions at 286 eV and at 288-289 eV of the C1s

spectra of oxidized CF are assigned to the hydroxyl group (-C-OH) and carboxyl or carbonyl groups (-COOH , >C=O) respectively by reference to the reported Cls chemical shift data on various organic compounds.¹² However, the curve resolving technique used here can not be directly applied to the carbon materials because of the asymmetric peak shape.

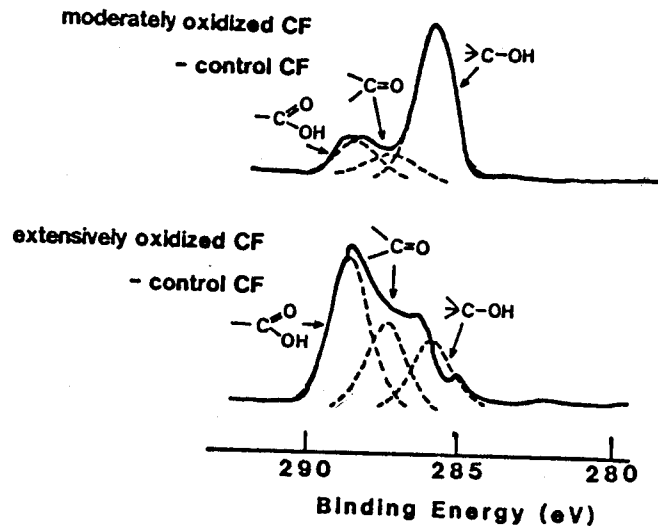
5-3-2 Cls Difference Spectra

The digital difference spectrum technique is used for qualitative analysis of surface functional groups to circumvent the problem. The difference spectra were obtained by subtraction of the Cls spectrum of control CF and GF from those of oxidized CF and GF, respectively, using appropriate weight factors leading to an elimination of the component of the main peaks of the lowest B.E. values. The obtained Cls difference spectra of CF has three components with chemical shifts corresponding to hydroxyl groups (-C-OH ; 286 eV), carbonyl groups (>C=O ; 287 eV) and also carboxyl groups (-COOH ; 288.6 eV) as indicated in Figure 5.3.

The following information is obtained as the result of the curve resolving of Cls difference spectra of CF. The composition of the functional groups introduced by the moderate oxidation of CF is 73 % of hydroxyl groups (-C-OH), 17 % of carboxyl groups (-COOH) and 10 % of carbonyl groups (>C=O). On the other hand, the composition produced by the extensive oxidation consists of 24 % of hydroxyl groups, 22 % of carbonyl groups and 54 % of carboxyl groups.

The difference spectrum of GF in Figure 5.3 has two components. The higher binding energy component which disappears after thermal treatment is assigned to carboxyl groups (-COOH), and the lower binding energy one, which is left after the thermal treatment is attributed to disordering of graphite crystal lattice brought by the surface oxidation. Such a change

C1s difference spectra



C1s difference spectrum

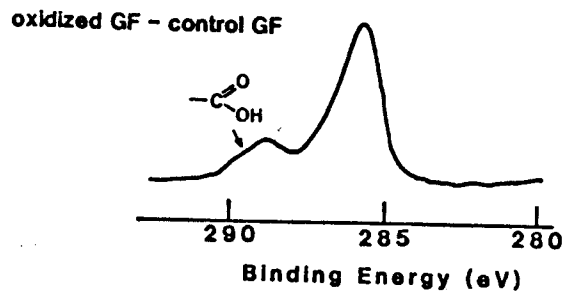


Figure 5.3 C1s digital difference spectra for CF and GF before and after surface oxidation.

of Cls peak shape due to a non-chemical perturbation of the surface is frequently seen in carbon materials. For an example, the line width (FWHM) of graphite single crystal is very small, 1.2 to 1.3 eV with the same measuring condition as in this work. The width is observed to broaden remarkably with Ar ion bombardment on the surface although no oxygen is taken up. The width of the Cls peak of carbon black, which has a more disordered structure than graphite single crystals, is also much broader, 1.6 to 1.8 eV, indicating dependence of the width on the degree of disorder of the lattice structure.

The increments of the O1s/C1s ratios during the surface oxidation of CF and GF, $\Delta(\text{O1s/C1s})$, are compared in Table 5.2 with the values calculated from the Cls difference spectrum. The sensitivity factor of O1s vs C1s is determined to be 1.74 from a measurement on poly(ethylene terephthalate). The values obtained with both methods agree fairly well as seen in Table 5.2.

5-3-3 FT-IR-RAS Spectrum

The FT-IR-RAS spectrum of the extensively oxidized CF is shown in Figure 5.4. It has a sharply tilting background because of the intense electronic absorption of carbon materials, and also a rather poor signal-to-noise level because of insufficient surface sensitivity of the technique. However, a band at 1680 cm^{-1} is identified above the background. This band can be safely assigned to the carbonyl stretching vibration of carboxyl groups directly combined to an aromatic ring. This assignment agrees well and reinforces the result from XPS measurements.

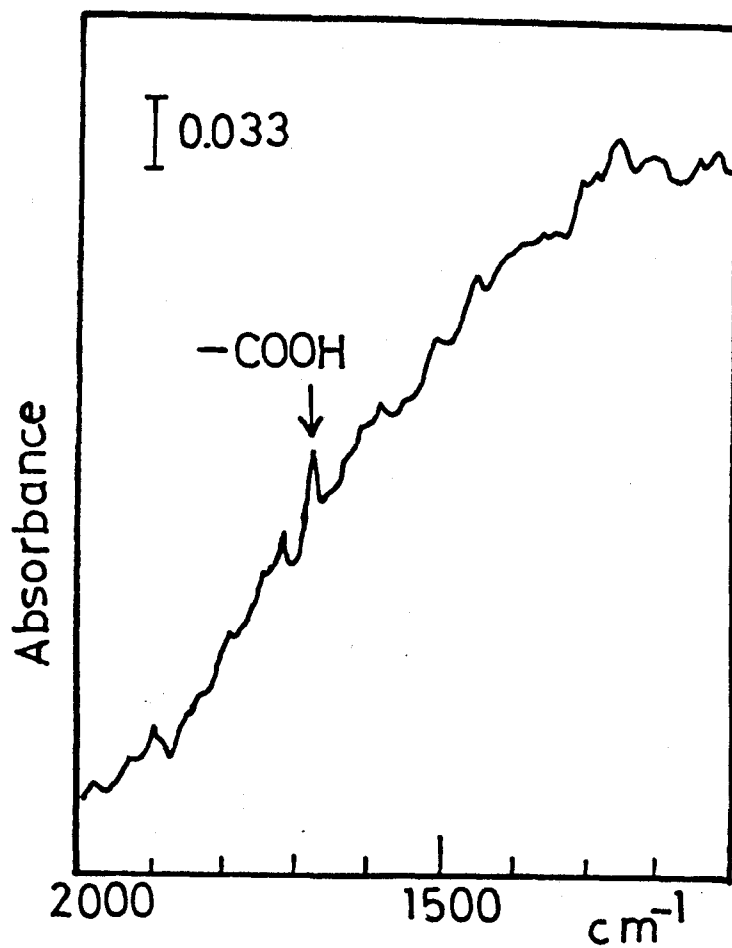


Figure 5.4 FT-IR-RAS spectrum for CF after the extensive oxidation.

References

1. J. M. Thomas, E. L. Evans, M. Barber and P. Swift, 3rd Int. Conf. on Industrial Carbon and Graphite, p441, Industrial Chemical Society, London (1970).
2. M. Barber, P. Swift, E. L. Evans and J. M. Thomas, *Nature*, 227, 1131 (1970).
3. J. M. Thomas, E. M. Evans, M. Barber and P. Swift, *Trans. Faraday Soc.*, 67, 1815 (1971).
4. E. L. Evans, J. M. Thomas, H. P. Boehm and H. Marsh, Int. Carbon Conf. (Baden-Baden), p49 (1972).
5. J. M. Donnet, E. Papirer and H. Dauksh, Int. Conf. Carbon Fibers, Their Place in Modern Technology, Paper No.9, London (1974).
6. H. Hiraoka and W. Lee, *Macromolecules*, 11, 622 (1978).
7. F. Hopfgarten, *Fiber Science and Technology*, 11, 65 (1978).
8. D. M. Brewis, J. Comyn and J. R. Fowler, *Fiber Science and Technology*, 12, 41 (1979).
9. A. Ishitani, *Carbon*, 19, 269 (1981).
10. D. T. Clark and A. Dilks, *J. Electron Spectrosc. Relat. Phenom.*, 11, 225 (1977).
11. A. Ishitani, H. Ishida, F. Soeda and Y. Nagasawa, *Anal. Chem.*, 54, 6821 (1982).
12. K. Siegbahn, C. Nordling, G. Johansson, J. Hedman, P. F. Heden, K. Hamrin, U. Gelius, T. Bergmark, L. O. Werme, R. Manne and Y. Baer, "ESCA Applied to Free Molecules", North-Holland Publishing Company, Amsterdam, 1969.

Chapter 6

XPS Study on the Surface Structure of Carbon Fibers Using Chemical Modification and C1s Line Shape Analysis

6-1 Introduction

The surface treatment of carbon fiber (CF) has been frequently used to improve the bonding property between the fiber and a matrix such as epoxy or polyimide resin in composite materials. The chemical and crystalline structure of the carbon fiber surface are expected to play important roles in the adhesion. The functional groups on the surface of CF have been studied extensively with X-ray photoelectron spectroscopy (XPS) by various authors,¹⁻¹⁶ because of its good surface sensitivity and capability of providing chemical structure information.

However, complexity due to the asymmetric line shape of the C1s XPS spectrum^{3,9} as well as small observed chemical shift of O1s in CF prevents us from studying the surface structure in full detail. In order to circumvent these difficulties, the author has been developing new techniques for the characterization of CF the surface. In the preceding study¹⁶ (in chapter 5 of this thesis), the digital difference spectrum technique of XPS has proved to be useful for analysis of functional groups on CF surfaces. Two additional techniques, surface chemical modification and C1s line shape analysis are proposed in the present study as extensions of the previous ones.

The purpose of chemical modification is a conversion of a specific functional group into a residue which is easier to identify and to quantify by XPS. The idea of this technique is shown in Figure 6.1. The

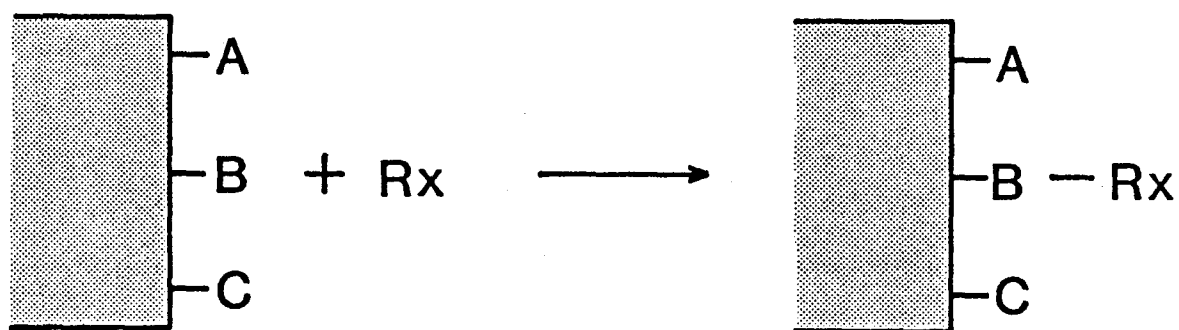


Figure 6.1 Concept of identification of a specific surface functional group by chemical modification coupled with XPS.

surface with various functional groups is treated with a reagent Rx with a tag element x which selectively reacts with a functional group B. An element like fluorine with good sensitivity in the XPS measurement is selected as a tag element. The chemical modification is expected to improve the selectivity, the sensitivity and the ease of quantification in the XPS measurement.

Similar techniques have been successfully used to analyze polymers surfaces. Everhart¹⁷ carried out detailed XPS studies on surface treated polyethylene with chemical modification reagents containing fluorine atoms like trifluoroethanol and trifluoroacetic anhydride. Dickie¹⁸ studied surface hydroxyl groups of a series of (methyl methacrylate)-(hydroxylpropyl methacrylate) copolymers using the modification with trifluoroacetic anhydride vapor. In this study, the author tries to apply the same technique for surface functional group analysis of CF utilizing the reaction condition proposed by Everhart.¹⁷

Any carbon materials with graphite structure have the characteristic asymmetric XPS C1s peak shape with a long tailing component in the higher binding energy side.^{3,9} The C1s line shape of the graphite is explained by the many body screening effect based on the joint density of states of electron-hole pair excitation explained by van Attekum.¹⁹ The sensitivity of the XPS C1s line to structure disorder in carbon materials was shown in the experiment by Evans.²⁰ Cheung^{21, 22} discussed in detail the asymmetric line shape of C1s spectrum of carbons and tried in polynuclear aromatic rings in coal by the asymmetry of C1s line. The author tries to apply the line shape analysis to evaluation of the graphitization degree of surface of CF.

6-2 Experimental

6-2-1 Samples

CF used in this study are TORAYCA T300 and M40 commercially available from Toray Ind. Inc. T300 is the high tensile strength fiber and M40 is the high modulus fiber made from polyacrylonitrile. The carbon fiber (CF) and the graphite fiber (GF) respectively indicate T300 and M40 in the Cls line shape analysis. They were sampled from production lines with special care to avoid contamination by sizing agents on the surface for a convenience in the surface analysis. The surface oxidation of CF was carried out on a laboratory scale especially for the present measurement.

In the Cls line shape analysis, CF carbonized at different temperatures between 1350 C and 2500 C in a laboratory scale were used. A highly-oriented pyrolytic graphite (HOPG), and a pyrolytic graphite (PG) from Union Carbide Corp. cleaved in (001) crystal plane were used in the Cls line shape analysis. A thin film of evaporated carbon (EC) was prepared on a gold plate cleaned with Ar ion etching. Ar ion bombardment of HOPG was done with a pressure of 2×10^{-4} Torr, an emission current of 20 mA, an ion beam energy of 1 kV and a beam current of 20 μ A.

6-2-2 Chemical Modification Reactions

Functional groups on the surface of the oxidized CF are known to consist mainly of carbonyl, carboxyl and hydroxyl groups by the previous studies.¹⁶ Three kinds of chemical modification reactions shown in Figure 6.2, which were successfully used in analysis of the surface functional groups of Ar plasma treated polyethylene by Everhart,¹⁷ were chosen to differentiate functional groups on CF (T300) surface. They are

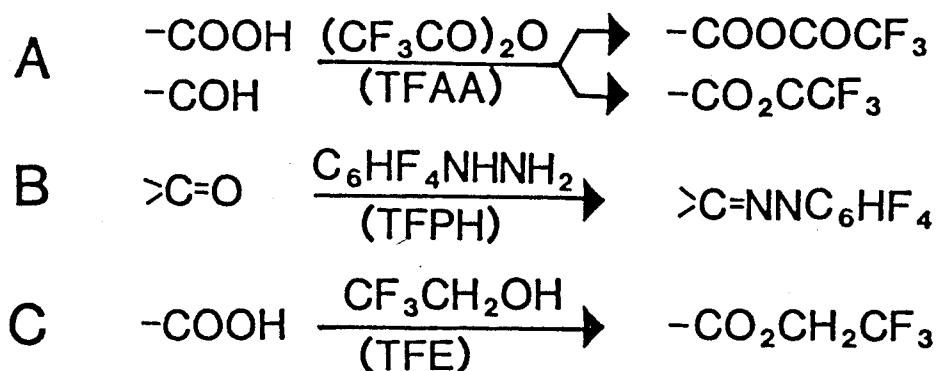


Figure 6.2 Chemical modification reactions used for examining surface functional groups of carbon fibers, where A, B and C are surface functional groups, and Rx is the chemical modification reagent selectively reacts with a specific functional group B.

trifluoroacetic anhydride (TFAA), tetrafluorophenylhydrazine (TFPH) and trifluoroethanol (TFE). TFAA reacts with both of carboxyl and hydroxyl groups. TFPH and TFE selectively reacts with carbonyl and carboxyl groups respectively.

A 10 cm long bundle containing 6000 filaments was bound at both ends with thin copper wires to avoid disassembling during the treatment. Solutions, 1 ml of TFAA and pyridine in 15 ml of benzene, 150 mg TFPH and a drop of concentrated HCl in 15 ml ethanol, and also 0.5 ml of TFE, 1 ml pyridine and 200 mg of dicyclohexyl carbodiimide in 15 ml of CH_2Cl_2 were used for chemical modification reactions. The treated CF were well washed with the solvent used in the reaction to remove residual reagents from the surface before the XPS measurement.

6-2-3 XPS Measurement

All XPS spectra were collected by using ES-200 XPS apparatus at 0°C to reduce X-ray degradation of fluoro species chemisorbing to CF surface. CF samples were set up by the same method as in chapter 5 for the XPS measurement. Savitzky's 9-points smooth method²³ considered to hardly distort line shape of XPS spectra was used to smooth all XPS spectra.

6-3 Results and Discussion

6-3-1 Chemical Modification

XPS wide scan spectra of CF (T300) after chemical modification reactions are shown in Figure 6.3. The control CF was unoxidized CF picked up at a point after the carbonization process and before surface oxidation occurred. Oxidized CF was prepared using a laboratory scale oxidation process with same method as the production line. The spectra

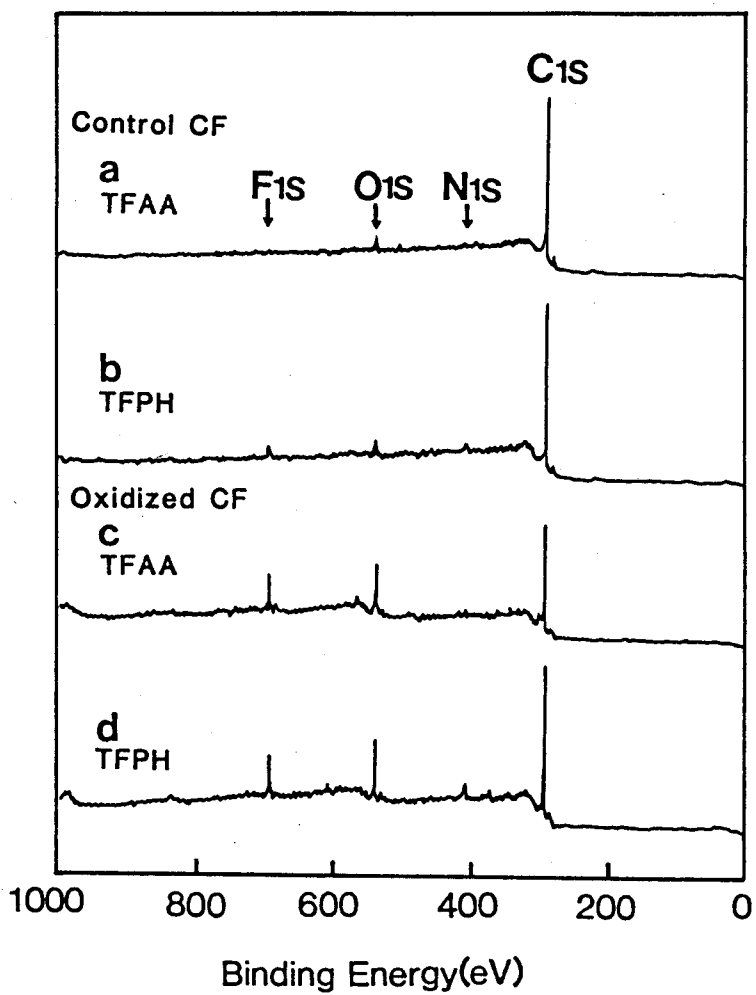


Figure 6.3 XPS wide scan spectra of carbon fibers (T300) after the chemical modification reactions.

of control CF have small F1s peaks, while the spectra of oxidized CF have more intense F1s peaks at 689 eV. This confirms successful labeling of surface functional groups of CF as in organic polymers.¹⁷ Increase of fluorine concentration (F1s/C1s) by the chemical modification reactions both at room temperature and at boiling temperatures of the used solvents for 3 h is shown in Figure 6.4. Fluorine concentrations on an oxidized CF surface treated with TFAA and TFPH at room temperature reach saturation in 200 h. The concentration reaches the same value when CF is treated with TFAA at boiling temperature within 3 h. However TFPH shows a lower saturation value when treated at boiling temperature, probably because of decomposition of the reagent at higher temperature.

The increase in fluorine concentrations from control to oxidized CF treated with TFAA and TFPH is plotted in Figure 6.5.a. Figure 6.5.b shows the concentration change of each functional group on the CF surface obtained from the data of Figure 6.5.a. The carbonyl group concentration is calculated from the fluorine concentration of CF treated with TFPH, carboxyl group from CF treated with TFE, and that of hydroxyl group is obtained from difference between CF treated with TFAA and TFE. The carbonyl group is found to be a major functional group, while carboxyl and hydroxyl groups are minor components on the control CF surface. Surface oxidation causes a remarkable increase in the hydroxyl and carbonyl groups intensity and a smaller increase in the carboxyl group intensity. This suggests that major functional groups on the oxidized CF are hydroxyl and carbonyl groups.

Oxygen concentrations of the CF surface estimated from the amounts of three functional groups determined by the surface modification reaction are compared with those from a direct measurement of O1s spectra in Figure 6.5.c. The relative amounts of oxygen, O1s/C1s calculated from

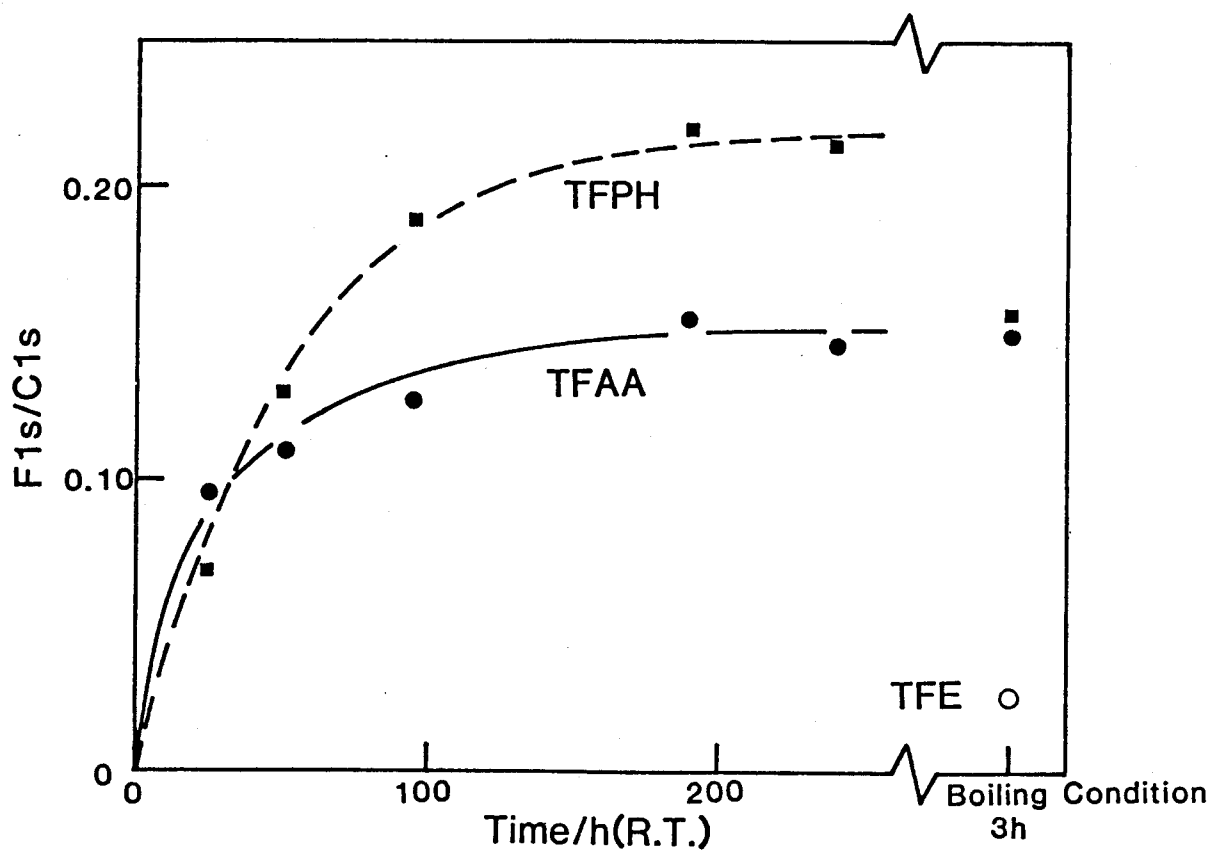


Figure 6.4 Relative fluorine concentration variation of oxidized carbon fiber (T300) by the chemical modification reactions.

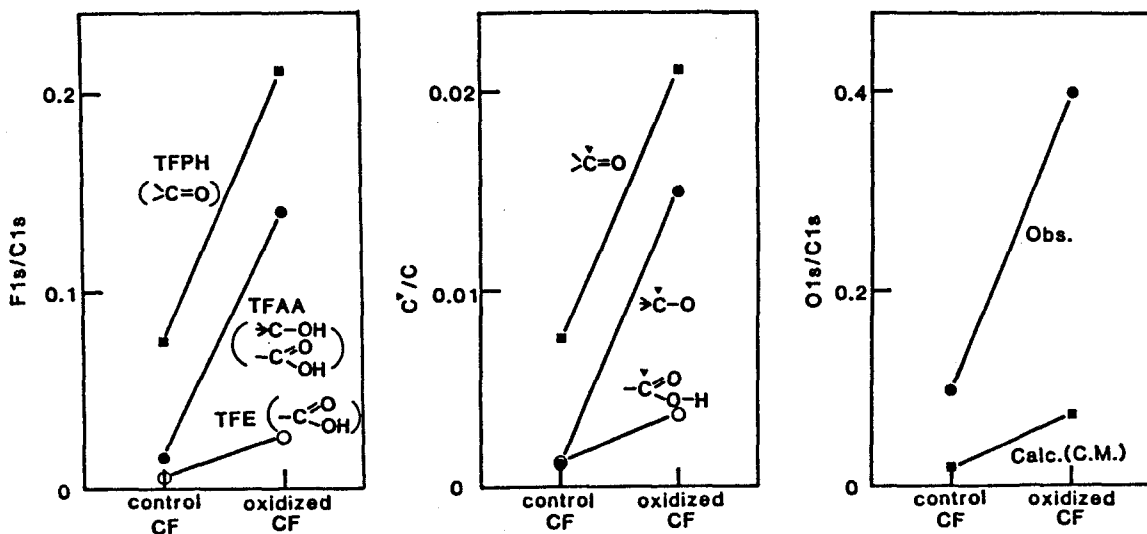


Figure 6.5 a: Change of relative fluorine concentration of chemically modified carbon fibers (T300) by surface oxidation. b: Concentrations of surface functional groups calculated from the data in a. c: Oxygen concentrations on surface of carbon fibers (T300). Calc.(C.M.) indicates the values estimated from the result of the chemical modification study shown in b, and Obs. indicates those directly obtained from area of measured O1s spectra.

the surface modification reaction are about 20 % of the observed values in both the control CF and the oxidized CF. Possibility of the existence of other functional groups such as ester and ether that are neglected in the above discussion may explain this discrepancy. However, in the previous study¹⁶, the author concluded that hydroxyl, carbonyl and carboxyl groups are major functional groups produced in the surface oxidation process, whereas the amount of ester and ether groups is negligible.

This discrepancy may be explained as follows. The chemical modification reagents may react only with the functional groups in the extremely outermost layer ($5 - 10 \text{ \AA}$) on the CF surface, because of the poor permeability of the reagent into CF. If there are more functional groups in a greater depth within the detection depth of XPS ($30 - 50 \text{ \AA}$),²⁴ the direct $\text{O}1\text{s}$ measurement will give a higher relative intensity. Thus, the chemical modification technique here may have a higher surface sensitivity than a direct XPS measurement. This may be important, because the only extremely outermost surface functional groups can react with reagents and thus contribute to the adhesion between the CF and a matrix resin in composite materials.

6-3-2 Line Shape Analysis of $\text{C}1\text{s}$ Spectrum

Spectral shapes of $\text{C}1\text{s}$ spectrum of XPS for various carbon materials were compared in Figure 6.6. They all have a characteristic $\text{C}1\text{s}$ spectra with the asymmetric line shape and the long tailing component toward a higher binding energy as observed in the XPS spectra of metals. The asymmetry is explained by the many body screening effect based on the joint density of states of electron-hole pair excitation suggested by van Attekum.¹⁹ Alteration of the density of states near the Fermi level by the variation of the completeness of the graphite crystal lattice is

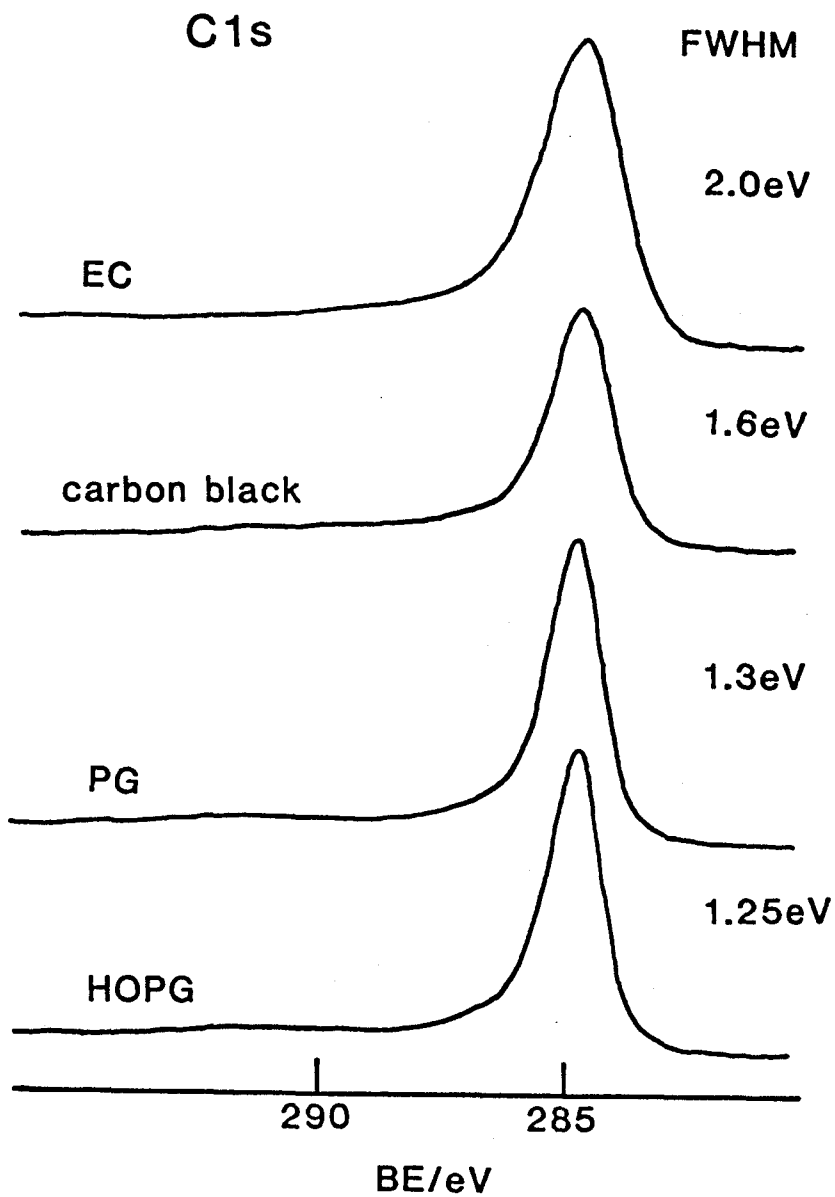


Figure 6.6 XPS C1s spectra of various carbon materials with different graphitization degree. EC : Evaporated carbon, PG : Pyrolytic graphite, HOPG : Highly-oriented graphite.

expected to change the C1s line shape of carbon materials. HOPG with the most complete graphite structure shows the narrowest peak with FWHM (full width at half maximum) of 1.25 eV, and the highest asymmetry, PG with less complete structure than HOPG shows a broader peak with FWHM of 1.3 eV. Carbon black and EC(evaporated carbon) with further more disordered structure have a very broad peak and a more symmetric line shape than HOPG and PG.

Another example of this tendency is the C1s spectral variation of HOPG by Ar ion bombardment shown in Figure 6.7. The C1s peak of HOPG rapidly broadens and loses asymmetry upon the ion bombardment.⁹ The C1s spectrum of HOPG bombarded for 30 s has a FWHM of 2.0 eV, for example, which is the same as EC as indicated in Figure 6.6. The disordering of the graphite crystal lattice on the HOPG surface caused by Ar ion bombardment was also confirmed by Raman measurement.²⁵

The C1s line shape can be specified by defining an asymmetric factor α as illustrated in Figure 6.8. C1s line shape parameters, FWHM and α of C1s are obtained after the background correction using a straight base line. The two parameters are plotted for various carbon materials, Ar ion bombarded HOPG, carbon fibers carbonized at various temperature, and commercial carbon fiber (T300) and graphite fiber (M40) in Figure 6.9. All plotted data points in the Figure 6.9 fall on a line. This indicates that a carbon material with a more complete graphite structure shows a narrower and more asymmetric C1s spectrum. Then, we can evaluate the completeness of the graphite structure on the outermost surface of a carbon material sample to point its C1s line shape parameters (FWHM, α) on Figure 6.9. For example, it is seen that the graphite lattice on the surface of the carbon fiber (T300) has same order to that of Ar ion bombarded HOPG and EC with the disordered structure. The graphite fiber

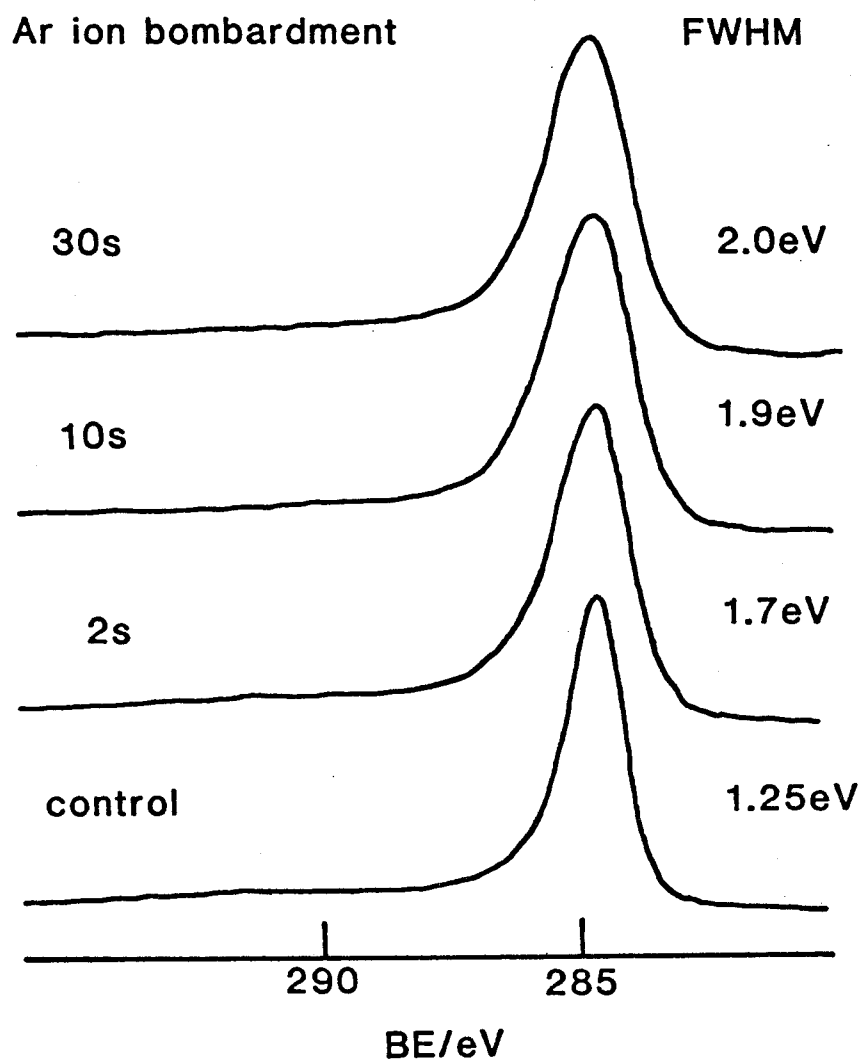


Figure 6.7 XPS Cls spectral change of HOPG by Ar ion bombardment.

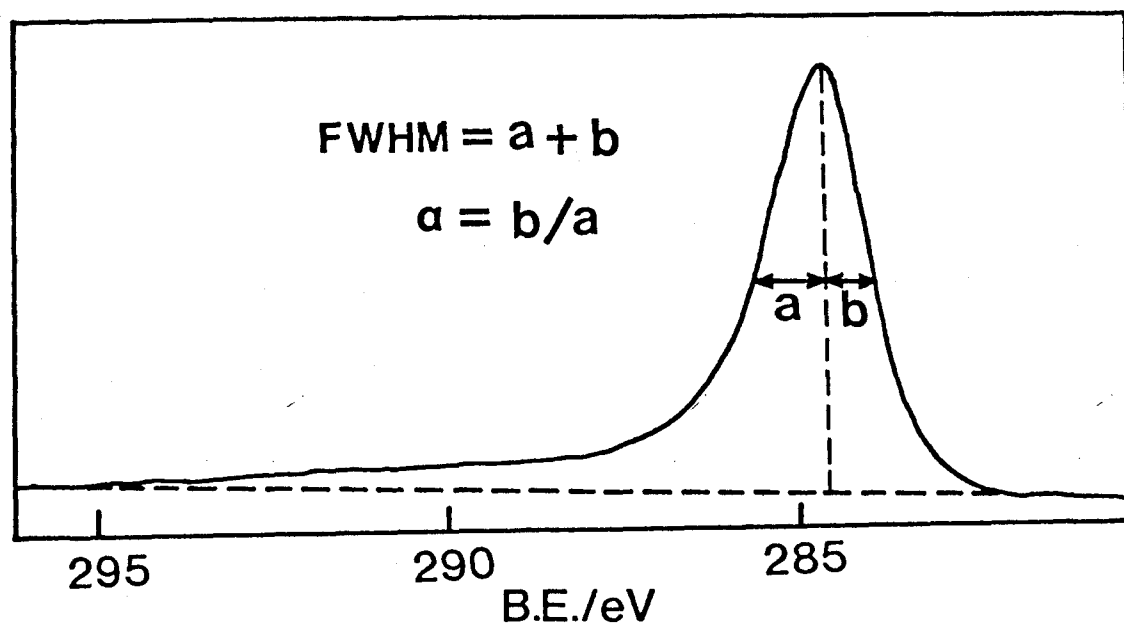


Figure 6.8 Definition of line shape parameters of XPS C1s spectrum of carbon materials.

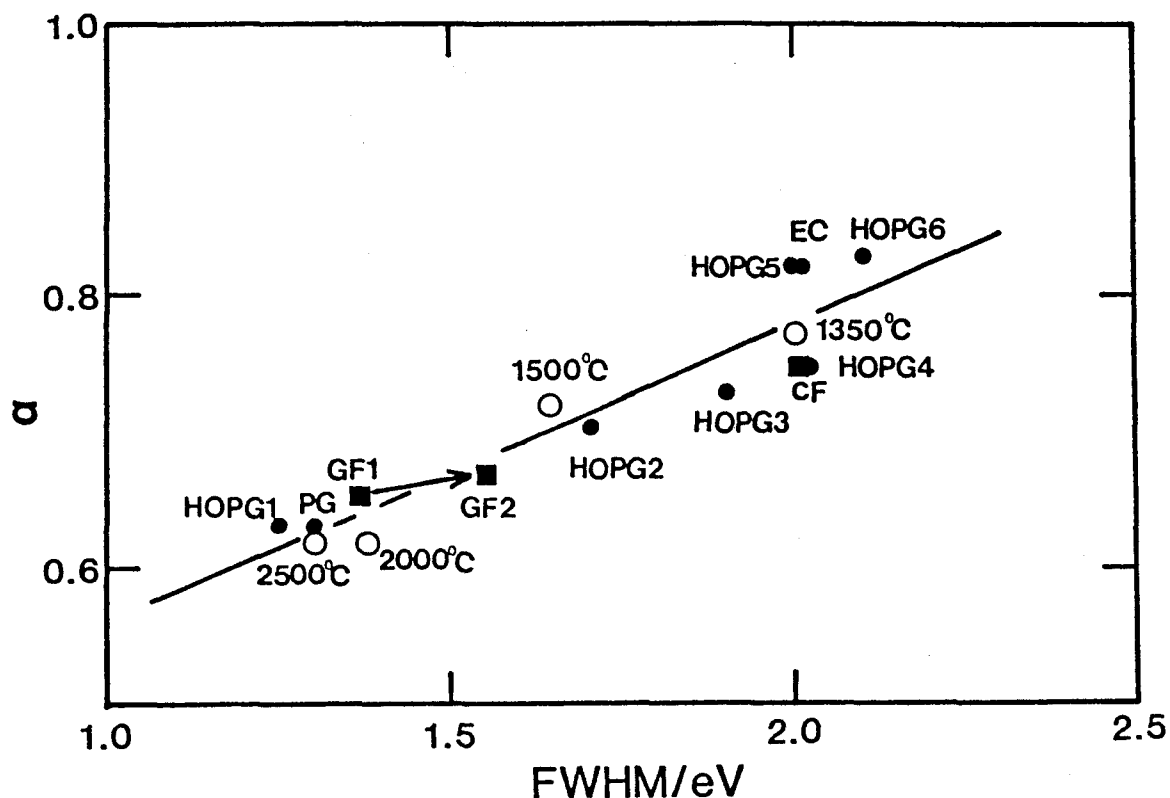


Figure 6.9 Correlation found between FWHM and the asymmetric parameter of C1s peaks of various samples. HOPG 1, 2, 3, 4, 5, 6: Control highly-oriented pyrolytic graphite (HOPG) and Ar ion bombarded HOPG for 2 s, 10 s, 30 s, 1 min and 5 min respectively, PG: Pyrolytic graphite, EC: Evapolated carbon, GF1: M40 before surface oxidation, GF2: M40 after surface oxidation and heat treatment at 1000°C in vacuo, CF: T300 before surface oxidation, Open circles: PAN based carbon fibers prepared at various temperatures indicated.

(M40) has a surface structure close to that of PG which has a nearly complete crystal lattice.

A change of the completeness of the graphite structure on the surface of GF in the surface oxidation process is evaluated by using these parameters. In the preceding paper,¹⁶ the author pointed out a broadening of Cls spectrum of GF in the surface oxidation process, suggesting disordering of the graphite structure on the surface. In the present study, the surface oxidized GF (GF2) also corresponds to a more disordered structure than GF before the surface oxidation (GF1). GF2 was heated at 1000°C in a vacuum to remove the generated the surface functional groups to avoid their disturbance the Cls line shape analysis. There was no increase in the degree of graphitization caused by the heating because GF had experienced much higher temperature in the manufacturing process. Disordering brought about in the surface oxidation process is not restored by the thermal treatment at 1000°C. The oxidized graphite fiber has the similar parameter values to carbon fiber carbonized at 1700°C. The disordered surface structure is considered to improve the adhesion between a graphite fiber and a matrix resin in composite materials. The parameters defined here enable comparison of the surface lattice structure of a wide variety of carbon materials.

References

1. J. M. Thomas, E. L. Evans, M. Barber and P. Swift, 3rd Int. Conf. on Industrial Carbon and Graphite, p411, Society of Chemical Industry, London (1970).
2. M. Barber, P. Swift, E. L. Evans and J. M. Thomas, *Nature*, 227, 1131 (1970).
3. J. M. Thomas, E. M. Evans, M. Barber and P. Swift, *Trans. Faraday*

- Soc., 67, 1875 (1971).
4. E. L. Evans, J. M. Thomas, H. P. Boehm and H. Marsh, Preprint, Int. Carbon Conf. (Baden-Baden), p49 (1972).
 5. J. M. Donnet, E. Papirer and H. Dauksh, Int. Conf. Carbon Fibers, Their Place in Modern Technology, Paper No. 9, London (1974).
 6. H. Hiraoka and W. Lee, Macromolecules, 11, 622 (1978).
 7. F. Hopfgarten, Fiber Science and Technology, 11, 65 (1978).
 8. D. M. Brewis, J. Comyn and J. R. Fowler, Fiber Science and Technology, 12, 41 (1979).
 9. A. Ishitani, Carbon, 19, 269 (1981).
 10. K. Waltersson, Fiber Science and Technology, 17, 289 (1982).
 11. A. Proctor and P. M. A. Sherwood, J. Electron Spectrosc. Relat. Phenom., 27, 39 (1982).
 12. A. Proctor and P. M. A. Sherwood, Surf. Interface Anal., 4, 212 (1982).
 13. A. Proctor and P. M. A. Sherwood, Carbon, 21, 53 (1983).
 14. R. Schlogl and H. P. Boehm, Carbon, 21, 345 (1983).
 15. A. Proctor and P. M. A. Sherwood, J. Chem. Soc., Faraday Trans., 1, 80, 2099 (1984).
 16. T. Takahagi and A. Ishitani, Carbon, 22, 43 (1984).
 17. D. S. Everhart and C. N. Reilly, Anal. Chem., 53, 665 (1981).
 18. R. A. Dickie, J. S. Hammond, J. E. deRries and J. W. Holubka, Anal. Chem., 54, 2045 (1982).
 19. P. M. Th. M. Van Attekum and G. K. Wertheim, Phys. Rev. Lett., 43, 1896 (1976).
 20. S. Evans and J. M. Thomas Proc. Roy. Soc. London, A, 353, 103 (1977).
 21. T. T. P. Cheung, J. Appl. Phys., 53, 6857 (1982).

22. T. T. P. Cheung, J. Appl. Phys., 55, 1388 (1984).
23. A. Savitzky and M. J. E. Golay, Anal. Chem., 36, 1627 (1964).
24. V. Young, Carbon, 20, 35 (1982).
25. H. Ishida, H. Fukuda, G. Katagiri and A. Ishitani, Appl. Spectros., 40, 322 (1986).

Chapter 7

XPS and FT-IR Studies on the Chemical Structure of the Stabilized Polyacrylonitrile Fiber and the Mechanism of Stabilization in the Carbon Fiber Production Process

7-1 Introduction

In recent years, high modulus carbon fiber produced from polyacrylonitrile (PAN) has become increasingly used in various fields including aircraft and space industries. The PAN precursor is first heated at between 200 and 300°C in air to stabilize it for the succeeding carbonization process, where the fiber is heated above 1000°C in an inert atmosphere. It is recognized that the mechanical properties of the final carbon fiber depend much on the chemical composition and the molecular structure of the stabilized fiber as an intermediate.

The mechanism of the stabilization process and the chemical structure of stabilized fiber have been studied using spectroscopic techniques such as infrared spectroscopy and evolved gas analysis by various authors.¹⁻⁸ Many chemical structure models for stabilized PAN have been proposed, but these models are not sufficiently precise to elucidate the chemistry involved in the stabilization process, because of experimental difficulties due to disturbance by the intense photon absorption and also due to the insolubility of the stabilized fiber to any kinds of organic solvents.

In the previous paper,⁹ Ishitani reported the preliminary study of the chemical structure change during the process of the carbon fiber production from PAN by X-ray photoelectron spectroscopy (XPS), which was found to be effective for the analysis of chemical states of each component

atom in any stage of the production of the carbon fiber. Fourier transform infrared spectrometry (FT-IR) is expected to be a powerful tool for the detailed study of a dark sample like thermally stabilized PAN because of high sensitivity due to its multiplex and throughput advantages. In recent years, the mechanism of thermal degradation of PAN under reduced pressure by FT-IR was studied.^{8,10-12} In the present work, the author tries to determine the chemical structure of the stabilized PAN in air and to investigate the reaction mechanism of the stabilization process in air by more detailed study of XPS combined with FT-IR and elemental analysis.

7-2 Experimental

7-2-1 Sample

The precursors used in this work are fibers of a PAN homopolymer and a PAN copolymer with 0.5 mol% hydroxyethylacrylonitrile. They were heated at 240 °C in air in a laboratory scale. It is necessary to prepare the sample surface with an average composition of whole of the sample in order to obtain the average bulk information using XPS, because it gives us preferentially the top of about 50 Å of a sample surface. Then, thermally prepared fibers was pulverized on cooling by liquid nitrogen to the fine powder of size of about 1 - 2 μm, that is considered to have the surface with the average composition of its bulk structure because of very small size of the powder compared with starting stabilized fiber with a diameter of about 10 μm. Nitrogen used to cool the sample is also expected to protect the fresh surface from thermal degradation in air during this preparation process.

7-2-2 XPS Measurement

The powdered samples were mounted on double sided adhesive tape on a sample holder pressing without wiping-stroke across the powder surface by a stainless steel spatula with a clean surface. This sampling technique was conformed to be contamination-free method by the examination using a clean surface polymer film as the model sample.

XPS measurement and data processing were performed by using the same apparatus and the same computer system as ones used in previous chapters. The Cls peak of hydrocarbons such as the methylene carbon within the polymers was used as a reference for the chemical shift determination assuming its binding energy to be 284.6 eV. Spectra were curve-resolved by using the non-linear least square technique after smoothing operation with Savitzky's method.

7-2-3 FT-IR Measurement

Digilab model FTS-20B/D FT-IR spectrometer was used with a resolution of 4 cm^{-1} and accumulation of 400 scans. The transmission mode was used on finely powdered samples prepared as KBr disks.

7-2-4 Elemental Analysis

Elemental analysis was carried out by Yanagimoto CHN Corder on samples kept under controlled humidity and temperature (22°C , 68 %RH) for a long time. The elemental composition was corrected taking account of the amount of adsorbed water determined with thermogravimetry by raising temperature from 20 to 120°C , because stabilized PAN has a large amount of adsorbed water preventing us to obtain its exact elemental composition. Amounts of the adsorbed water were 0.5 and 4 %, respectively in PAN and final stabilized PAN.

7-3 Result and Discussion

7-3-1 Elemental Composition

The elemental composition change of PAN and the copolymer during the stabilization process at 240 °C in air are indicated in Figure 7.1.

Decrease of hydrogen and uptake of oxygen are observed, while no change is seen for the nitrogen content. The hydrogen content of the stabilized fibers is 43 % of that of the precursors. Dehydrogenation is accompanied by introduction of unsaturated bonds and oxygen atoms into the polymer chains. The reaction rate of the dehydrogenation of the copolymer is larger than that of PAN. Oxygen content increases to 0.5 atom per repeat unit of the polymers in the final stage of the stabilization process for both precursors. The ladderlike structure formed by successive reaction between neighboring nitrile groups within a polymer chain seems to be major reaction, since the nitrogen content shows little change in the stabilization process for both precursors.

7-3-2 Molecular Structure

Figure 7.2 shows the change of the IR spectrum (4000 cm^{-1} - 450 cm^{-1}) of PAN during air stabilization process at 240 °C. The major observed variations are the decrease of intensity of the nitrile band at 2240 cm^{-1} and the methylene band at 2940 cm^{-1} , and growth of three new bands (at 1725 cm^{-1} , 1660 cm^{-1} and 1595 cm^{-1}) in the carbonyl stretch frequency region. The final product in the stabilization process after heating for 310 min has no nitrile band left in the spectrum (E in Figure 7.2). This indicates that structural changes involving the whole molecular chain of PAN takes place in the stabilization process.

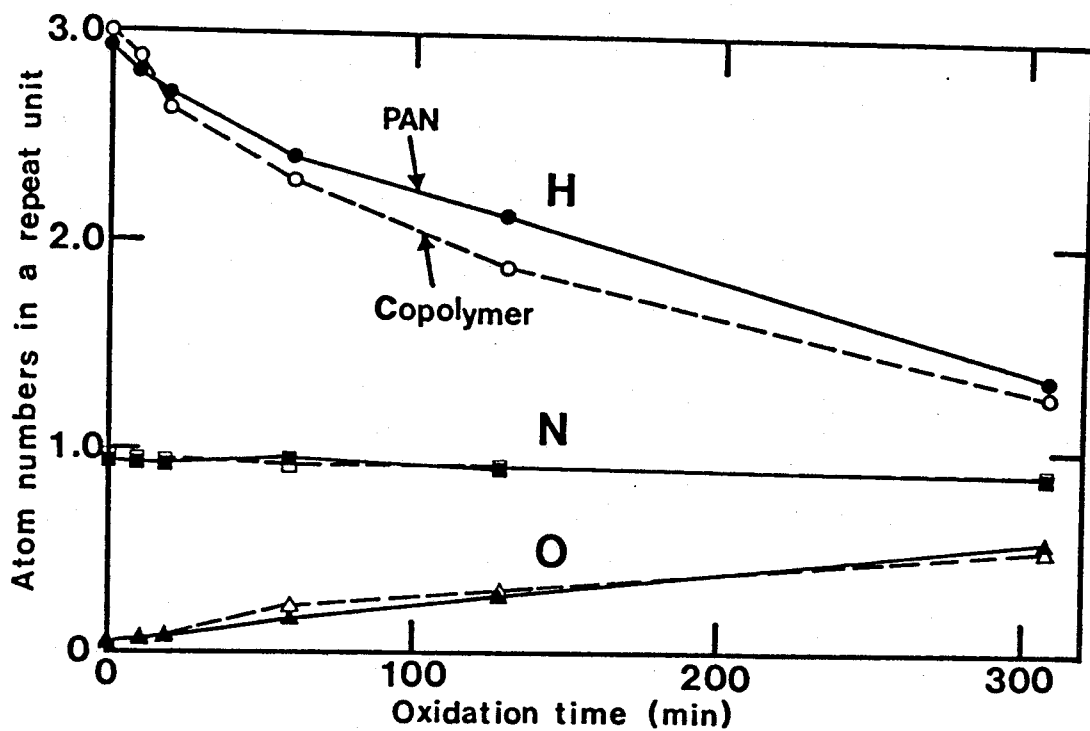


Figure 7.1 The change of elemental composition of PAN fiber and copolymer fiber during the stabilization process at 240 °C in air.

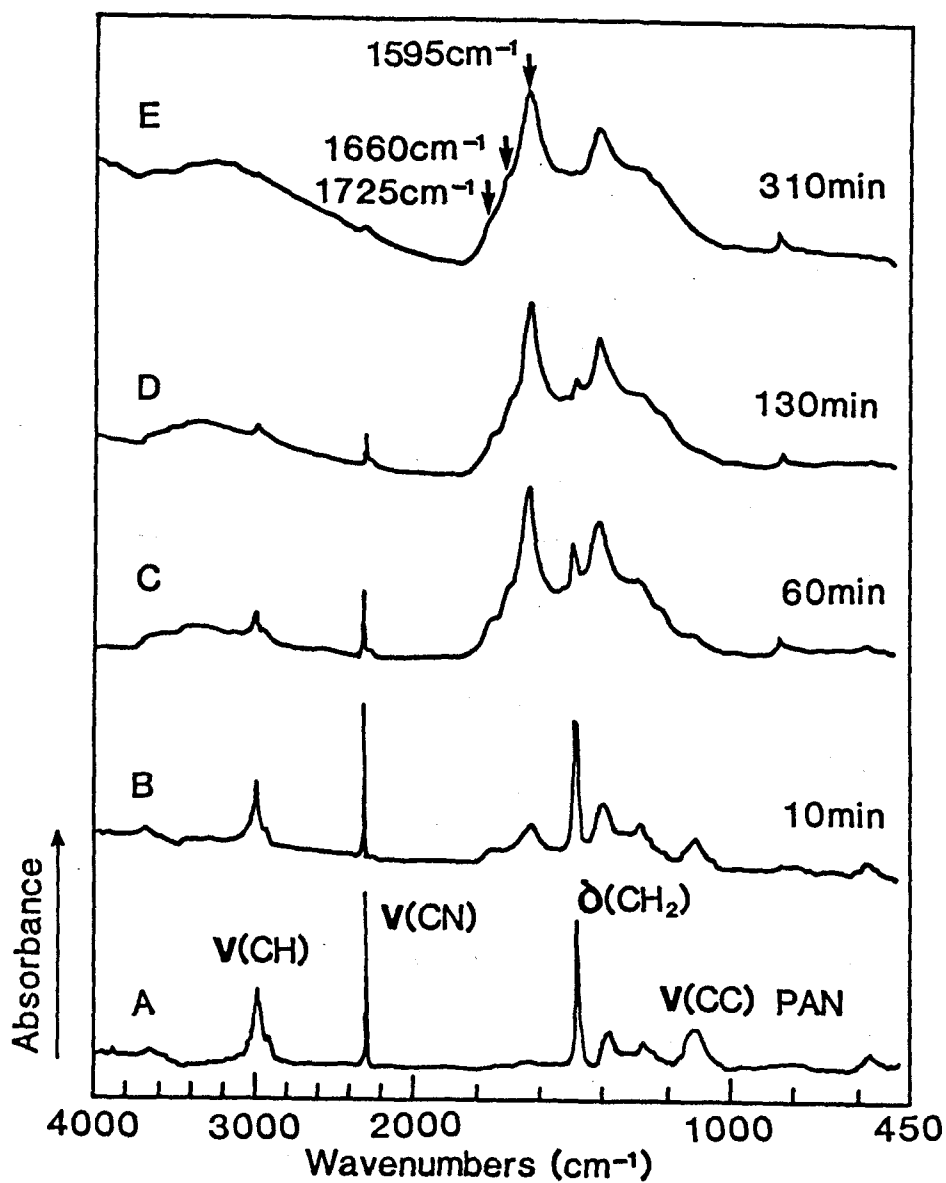


Figure 7.2 FT-IR spectra of PAN fiber during the stabilization process at 240 °C in air.

These observations agree well with those of previous workers,³ and suggest formation of ladderlike structure with conjugated unsaturated bonds formed by polymerization of cyano groups and release of hydrogen, and also with carbonyl groups incorporated by the thermal oxidation. The copolymer indicates exactly the same spectral change as the homopolymer under the same stabilization condition. The presence of hydroxyethylacrylonitrile does not change the course of the chemical reaction in the stabilization process, and the copolymer gives the same final product.

There are three bands observed in the carbonyl stretch region at 1725, 1660 and 1595 cm^{-1} for the stabilized PAN in air. In order to assign these bands, stabilized PAN at 0.1 Torr in the presence of an inert gas was prepared by heating the precursor at 200°C for 24 h under 0.1 Torr for comparison. PAN stabilized under reduced pressure condition consists of three carbon atoms, 2.97 hydrogen atom, 0.96 nitrogen atom and 0.15 oxygen atom in a repeat unit of PAN. The major difference between the elemental compositions of stabilized PAN fibers in air (see Figure 7.1) and in reduced pressure is that the latter neither loses hydrogen at all nor takes up much oxygen.

The spectrum of the stabilized PAN under reduced pressure is shown in Figure 7.3. It has two bands at 1610 and 1575 cm^{-1} in the carbonyl stretch region, but there is no measurable intensity in the area where 1725 and 1660 cm^{-1} bands appear in PAN stabilized in air. Both of 1610 and 1575 cm^{-1} bands probably correspond to the broad 1595 cm^{-1} band of the stabilized PAN in air. The author proposes to assign 1725 and 1660 cm^{-1} bands of the stabilized PAN in air as due to C=O stretch vibrations of an aliphatic ketone and that of a conjugated ketone respectively, and 1595 cm^{-1} bands as one due to combination vibrations

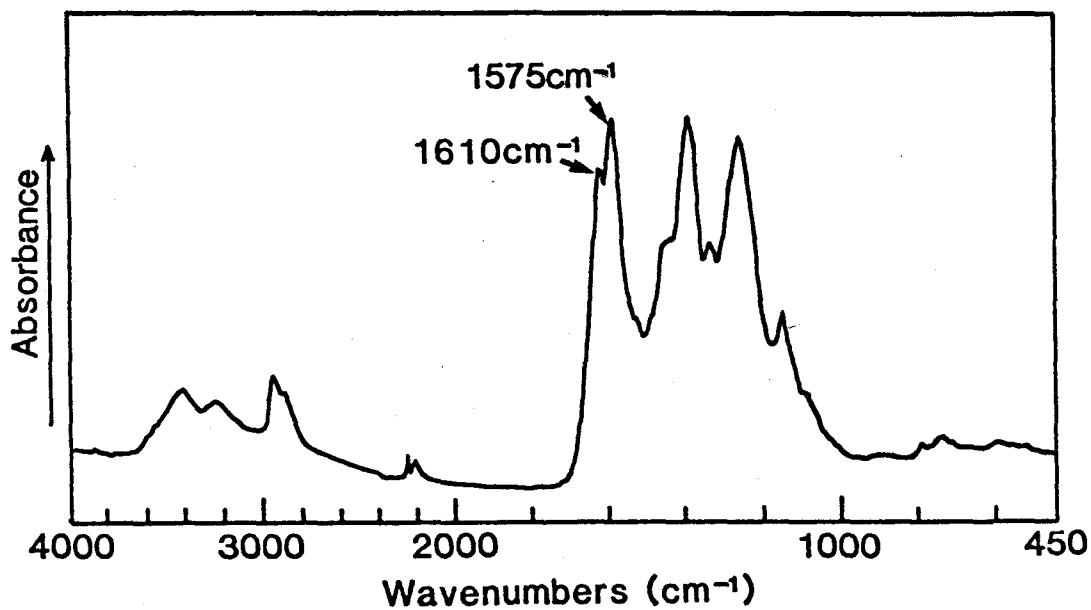


Figure 7.3 FT-IR spectrum of the stabilized PAN under reduced pressure at 200 °C for 24 h.

of C=N and C=C stretching, and NH in-plane bending of the ladder-frame structure of the stabilized PAN.

The bands at 1610 and 1575 cm^{-1} of the stabilized PAN in reduced pressure are considered to come from the ladder structure. The assignment by Coleman⁸ is partly different from the present one. He considered 1610 and 1575 cm^{-1} bands to come from ketone and the ladder structure, respectively for the stabilized fiber under reduced pressure. The present assignment is based on the assumption that no ketone are generated in the stabilization process under reduced pressure. This is verified from the elemental analysis data. First, the amount of oxygen uptaken in the process is small, close to one quarter of the process in air. Second, reduction of hydrogen content should be accompanied with generation of ketones, whereas there is no change in hydrogen content. A small amount of oxygen is probably used to produce hydroxyl groups.

Accordingly, in the case of the stabilized PAN in air, the band at 1595 cm^{-1} comes from the ladder frame, the band at 1660 cm^{-1} from the conjugated ketone in acridone ring and the 1725 cm^{-1} band from free ketones generated in hydronaphthridine rings. Presence of conjugated aromatic heterocyclic ladder structure containing acridone, naphthyridine and hydronaphthyridine rings suggested by successive XPS work.

XPS spectral changes in the stabilization process of PAN are shown in Figure 7.4. The increase observed in O1s corresponds well with the elemental analysis. Both of Cls and N1s peaks broaden in the process, indicating formation of various new chemical species. The long tails of the main peaks of Cls and N1s of the stabilized fiber in the higher binding energy sides due to shake up satellites suggest formation of extended conjugated unsaturated bonds incorporated into the polymer chains. The valence band of the precursor shows distinct peaks at 8, 15

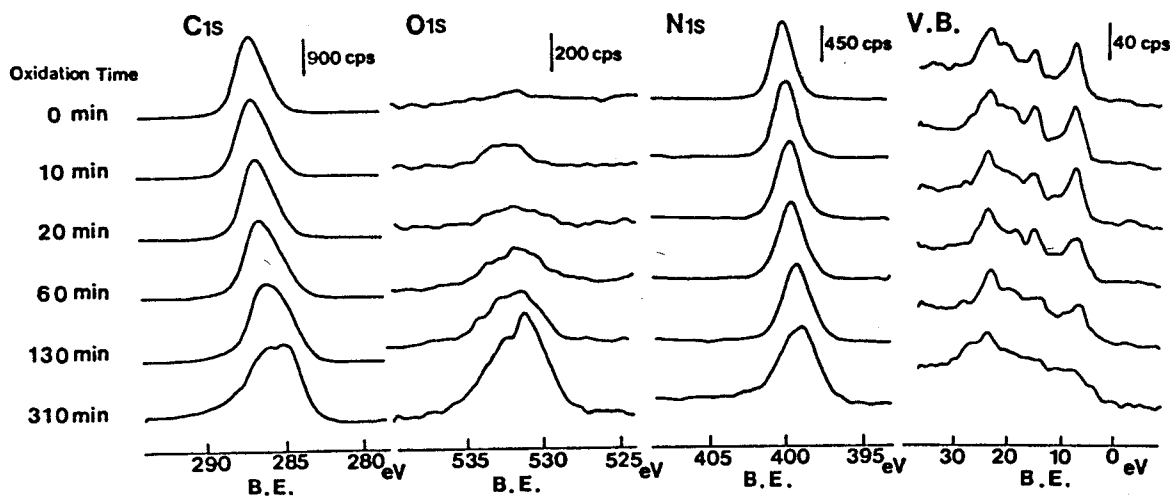


Figure 7.4 XPS spectra of PAN fiber during the stabilization process at 240 C in air.

and 24 eV on B.E. scale. The two peaks at 8 and 15 eV due to cyano groups gradually diminished in the process, and the peak shape of the whole valence band comes to resemble that of graphite.

The O1s, N1s and C1s peaks of stabilized PAN are curve-resolved and assigned in Figure 7.5. The O1s spectrum of stabilized PAN has a main peak at 531.5 eV and a characteristic long tail extending to 539 eV. The O1s spectra of conjugated carbonyl compound such as benzophenone and quinacridone have peaks in the same unusually low energy region between 531.1 eV and 531.8 eV as listed in Table 7.1. They also have a characteristic satellite component on the higher binding energy side due to the π -electron excitation. The lower binding energy component of O1s spectrum of stabilized PAN can be assigned to an oxygen of the acridone ring from a comparison with above model compounds in Table 7.1. The higher binding energy component is ascribed to oxygens of alcohol and unconjugated carbonyl groups.

Curve resolving of the O1s spectrum of the stabilized PAN was carried out using the asymmetric peak shape of O1s spectrum of quinacridone for the lower binding energy component, and Gaussian peak shape for the higher binding energy one. From oxygen taken up into stabilized PAN fiber, 80 % is considered to come from acridone type carbonyl and 20 % from alcohol and unconjugated carbonyl.

Binding energy values of N1s spectra of model compounds and PAN are listed in Table 7.2. Acridine and quinacridone have peaks at 398.6 eV and 399.9 eV and both show satellite components at higher binding energy side of the main peaks arising from conjugated π -electron system. The N1s spectrum of stabilized PAN has a main peak at 399.0 eV and a shoulder around 400 eV and also a long tail at higher binding energy side of the main peak. It was curve-resolved to two components using

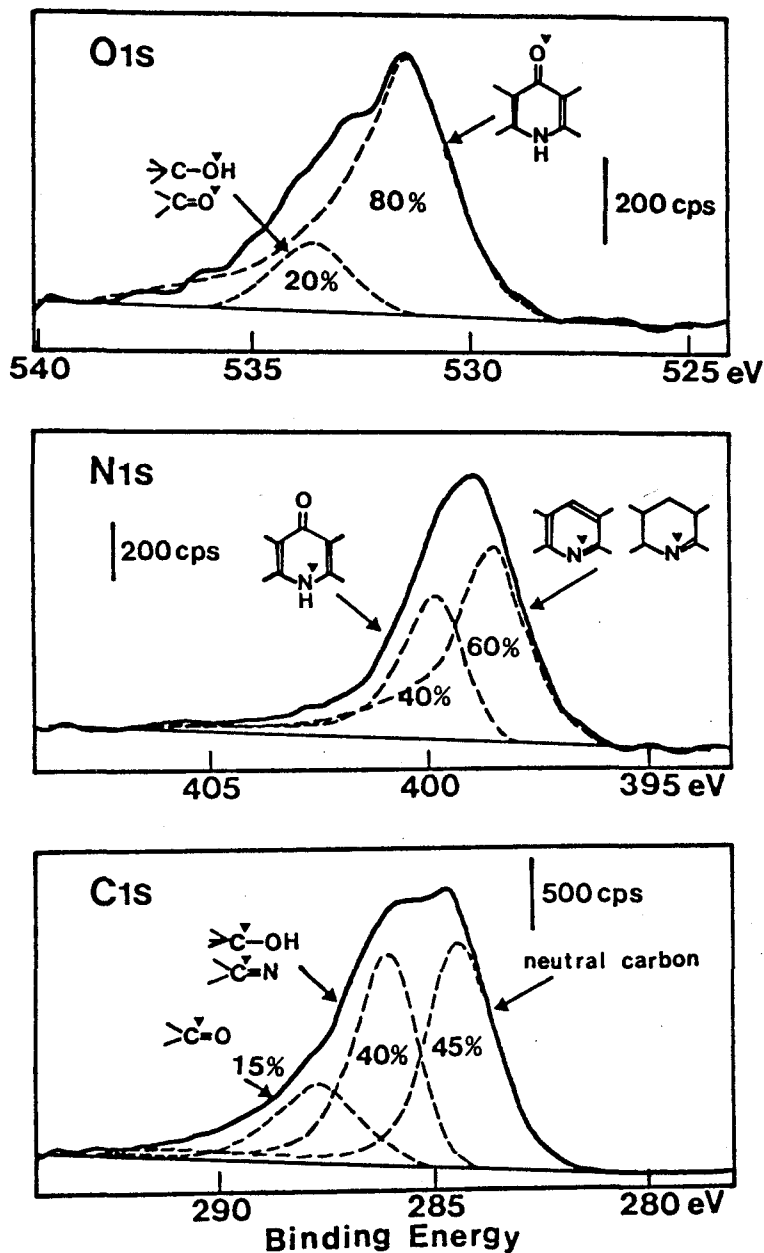


Figure 7.5 Assignment of curve resolved components of the O1s, N1s and C1s spectra of stabilized PAN in air.

Table 7.1 The chemical shifts of O1s of conjugated carbonyl compounds.

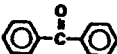
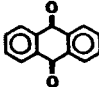
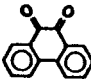
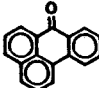
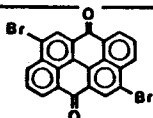
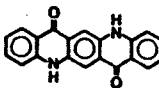

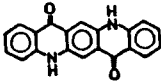
Compound	Chemical structure	Binding energy (eV)
Benzophenone		531.8
Anthraquinone		531.5
Penanthrenequinone		531.9
Benzanthrone		531.0
Anzathrone		531.2
Quinacridone		531.1

Table 7.2 The chemical shifts of N1s of model compounds and PAN.

Compound	Chemical structure	Binding energy (eV)
Acridine		398.6
Quinacridone		399.9
Polyacrylonitrile	$\{ \text{CH}_2 - \underset{\text{CN}}{\text{CH}} \}_n$	399.0

the chemical shifts and the peak shapes of acridine and quinacridone. The higher binding energy component with 40 % intensity is assigned to nitrogen of acridone ring and the other one with 60 % intensity is assigned to nitrogen of naphthyridine and hydronaphthyridine rings. The latter component may be assigned to nitrile groups of PAN because the chemical shift agrees well, but above FT-IR study on the same system indicates that amount of remaining cyano group in stabilized PAN is negligible.

The Cls spectrum of stabilized PAN is curve-resolved to three components which are assigned to 45 % of neutral carbon, 40 % of carbon in C-O and C=N- groups and 15 % of carbonyl carbon. The author confirms the chemical structure shown in Figure 7.6 for stabilized PAN from the results of XPS, FT-IR and elemental analysis and also taking the previous worker's suggestions¹⁻⁸ into account. The ladder structure consists of 40 % of acridone ring, 30 % of naphthyridine ring, 20 % of hydronaphthyridine ring and 10 % of others. The ladder structure is an essential factor for the thermal stabilization and the structure well explains in the succeeding carbonization process on carbon fiber production. The conjugated π -electron system of naphthyridine and acridone rings over the whole polymer chain develop the dimensional stability of the fiber at high temperature. Moreover, hydrogen bonds formation between adjacent ladder molecular chains help to keep the orientation of molecular chains constant in the carbonization stage.

7-3-3 Reaction Mechanism

In order to study the reaction mechanism of the thermal stabilization process, the digital difference FT-IR spectrum method was used. The difference spectra were calculated between two successive spectra in the

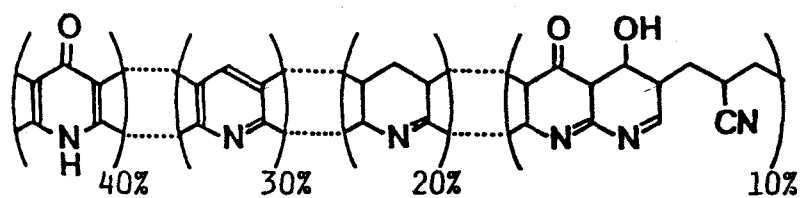


Figure 7.6 The proposed chemical structure of stabilized PAN in air.

process shown in Figure 7.2, and indicated in Figure 7.7. The condition of subtraction is to eliminate the band of nitrile group at 2240 cm^{-1} . The difference spectra obtained may be considered as the IR spectra of product generated between the successive steps. They are similar each other and also to the final product of the stabilization. It indicates that the products in all steps in the stabilization process are same as the final product. It can be concluded that the various reactions expected in the process, such as cyclization, dehydrogenation and oxygen uptake occur almost simultaneously.

The only exceptions are positive and negative intensities observed at 1280 cm^{-1} and 1150 cm^{-1} , respectively in the difference spectrum (A in Figure 7.7). They may correspond to a side reaction taking place only in the beginning of the process. There was no difference observed in this analysis between PAN and the copolymer. A kinetic study was carried out to understand the reaction more in detail, and also to see the difference between PAN and the copolymer. Fibers with different heating time were freeze ground and sieved to prepare fine powders of equal particle size for quantification. An equal amount of powder was formed into a KBr disk to normalize the spectral intensity. The peak area of the CH asymmetric stretch band at 2940 cm^{-1} and two kinds of carbonyl stretch bands at 1725 and 1655 cm^{-1} are used to study the reaction rate.

A plot of 2940 cm^{-1} band intensity as a function of time is indicated in Figure 7.8 for PAN and the copolymer. Decrease of methylene groups is found to proceed as a first-order reaction concerning the concentration of the precursor polymers. The reaction rate of the copolymer is larger than that of the homopolymer, PAN, indicating the effect of the comonomer in accelerating the dehydrogenation reaction.

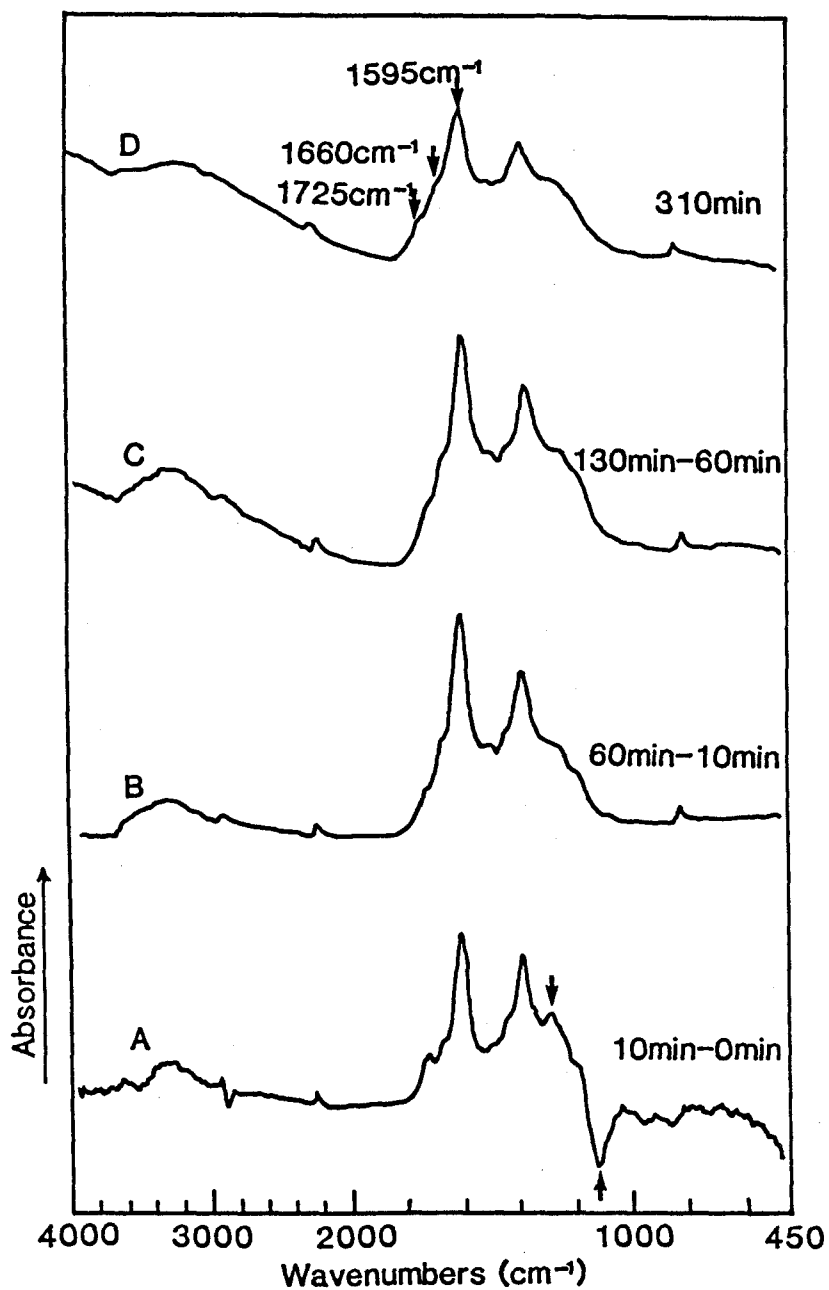


Figure 7.7 Difference spectra obtained by successive subtraction between the spectra of the intermediate products in the stabilization reaction in air. (A) heated for 10 min - PAN, (B) heated for 60 min - heated for 10 min, (C) heated for 130 min - heated for 60 min, (D) stabilized PAN.

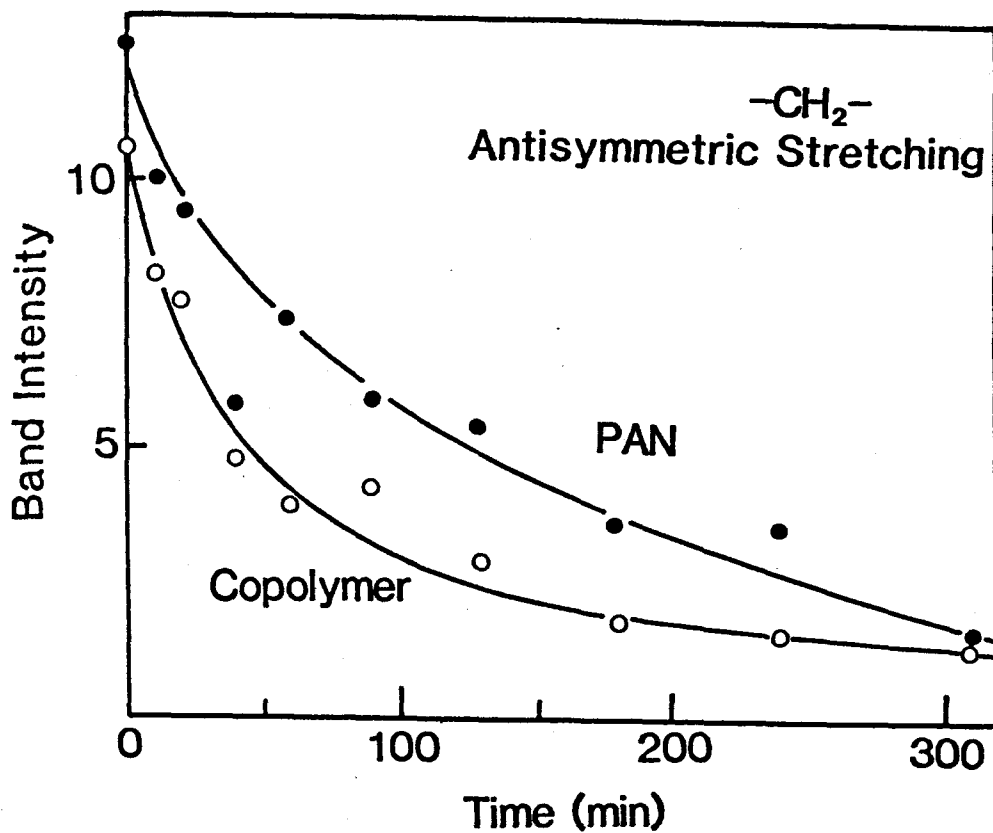


Figure 7.8 Variation of band intensity of methylene band at 2940cm^{-1} in the stabilization process in air for PAN and the copolymer.

Similar plots were carried out for the increase of carbonyl groups in the air stabilization reaction. The bands of the two kinds of carbonyl groups overlap each other and also with the band due to aromatic rings of the ladder structure. Curve resolving of this particular wavelength region was done as shown in Figure 7.9. The base line correction in the figure is to eliminate the contribution from intense neighboring absorption bands in the smaller wave-number region. The obtained peak area is plotted for both of carbonyls. The result is depicted in Figure 7.10.

There is apparent difference in the rate of generation of the carbonyl group of acridone type structure between PAN and the copolymer while there is none for the other carbonyl group. The reaction rate for acridone carbonyl generation in copolymer is estimated to be twice as much as in PAN. This leads us to the idea that the comonomer accelerates the dehydrogenation reaction and also the generation of the acridone ring, although it does not affect the oxidation reaction to produce the unconjugated carbonyl.

References

1. R. C. Houtz, *Textile Res. J.*, 20, 786 (1950).
2. W. J. Burlant and J. L. Parsons, *J. Polym. Sci.*, 22, 249 (1956).
3. L. H. Peebles, Jr. and J. Brandrup, *Macromol. Chem.*, 98, 189 (1966).
4. A. E. Standage and R. Matkowsky, *Nature*, 224, 688 (1969).
5. W. Watt, *Proc. Roy. Soc. Lond., A*, 319, 5 (1970).
6. N. Grassie and R. McGuchan, *Eur. Polym. J.*, 7, 1356 (1971).
7. J. W. Johnson, W. Potter, P. G. Rose and G. Scott, *Br. Polym. J.*, 4, 527 (1972).
8. M. M. Coleman and R. J. Petcavich, *J. Polym. Sci. Polym. Phys. Ed.*,

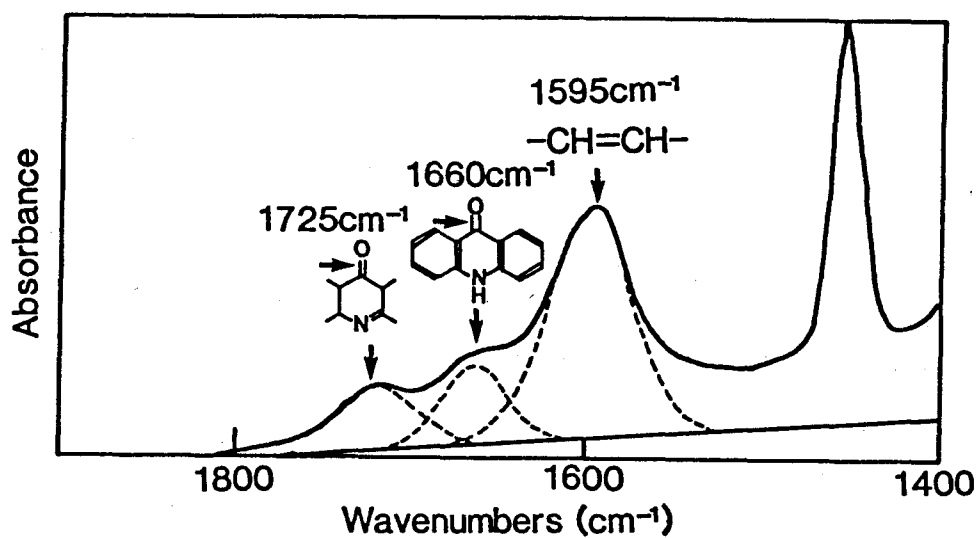


Figure 7.9 Curve resolving of FT-IR spectrum in the carbonyl stretching band region of the stabilized PAN in air.

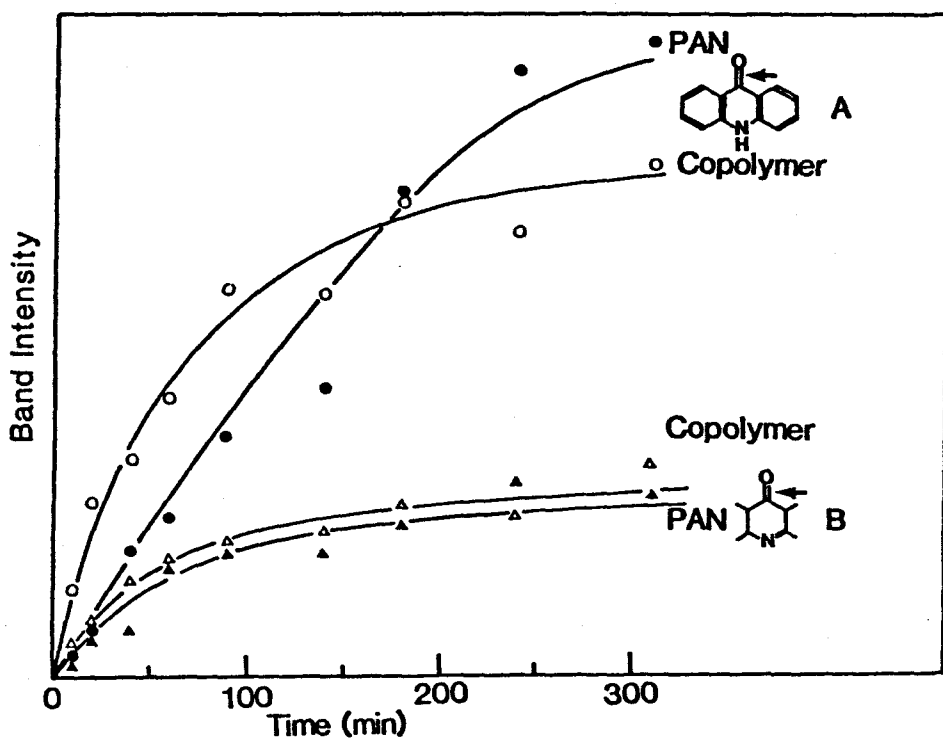


Figure 7.10 Variation of band intensity of two kinds of carbonyl groups in the stabilization process for PAN and the copolymer.

15, 821 (1978).

9. A. Ishitani, Carbon, 19, 269 (1981).
10. M. M. Coleman and G. T. Sivy, Carbon, 19, 123 (1981).
11. G. T. Sivy and M. M. Coleman, Carbon, 19, 127 (1981).
12. H. S. Fochler, J. R. Mooney, L. E. Ball, R. D. Boyer and J. G. Grasselli, Spectrochimica Acta., 41A, 271 (1985).

Chapter 8

Molecular and Crystal Structure of Poly(vinylidene chloride)

8-1 Introduction

Several molecular models of poly(vinylidene chloride) (PVDC) have been proposed in order to account for the fiber period of 4.7 \AA which is appreciably shorter than the repeat distance of two monomeric units in the fully extended zigzag chain, 5.1 \AA . Fuller¹ suggested an alternatively twisted zigzag model, and Reinhardt² proposed a tub-form with an alternate repetition of cis and trans conformations. De Santis³⁻⁵ proposed a (2/1) helical model based upon the conformation energy calculation and the optical transform.

By means of calculation of normal vibration, Miyazawa and Ideguchi⁶ proposed a glide model with $\text{TGT}\overline{\text{G}}$ conformation which was again supported by Hendra and Mackenzie⁷ by Raman study. Employing a combination of FT-IR and Raman studies and geometric consideration, Coleman⁸⁻¹⁰ concluded that a $\text{TXT}\overline{\text{X}}$ ($\text{X} : 32.5^\circ$) chain conformation is favored. The problem of the crystal structure of PVDC has not yet been settled with certainty, though Reinhardt² and Okuda^{11,12} independently proposed different monoclinic lattices. Therefore, in the present work, the author studies the molecular and crystal structure of PVDC in more detail by X-ray diffraction together with conformation energy calculation.

8-2 Experimental

8-2-1 Sample

Since it was rather difficult to prepare a well oriented PVDC homopolymer specimen by drawing, so-called "canal polymerization method"¹³ was employed for single crystals of the vinylidene chloride-thiourea adduct to obtain highly oriented PVDC homopolymer specimens suitable for X-ray diffraction. The canal polymerization of vinylidene chloride-thiourea adduct was carried out by the following procedure.

First, needle-like crystals of the vinylidene chloride-thiourea adduct were obtained from a mixture of methanol solution of thiourea (4 wt%, 10 ml) and vinylidene chloride (4.6 ml) at -20 °C. The monomer-thiourea adduct was converted into the poly(vinylidene chloride)-thiourea adduct by γ -ray irradiation from a cobalt 60 source of the Radiation Laboratory of Osaka university (total dose; 2 Mrad) at -78 °C. A uniaxially oriented PVDC filament was obtained by washing out the thiourea from the irradiated adduct crystal with hot water. The infrared spectrum of this polymer was in accordance with that of PVDC homopolymer obtained by usual way.

8-2-2 X-ray Diffraction

The nickel-filtered $\text{CuK}\alpha$ radiation was used throughout the present study. Specimens with a diameter of 0.15 mm were used. Photographs were taken with a cylindrical camera with a radius of 45 mm or 50 mm. The number of observed reflections was 34. Observed d-spacings were calibrated with reference to those of aluminum powder. The reflection intensities in fiber photographs taken by the multiple-film method were measured by visual comparison with a standard intensity scale. The correction for the single crystal rotation Lorentz-polarization factor was made to the observed intensities.

8-3 Structure Determination

8-3-1 Conformation Energy

In this study, the conformational energy for the PVDC chain with the observed identity period of 4.68 \AA , in which two monomeric units are contained, was evaluated varying the C-CH₂-C and C-CCl₂-C bond angles, and this procedure made it possible to examine the various molecular models proposed so far on one energy contour map as shown in Figure 8.1.

In the energy calculation, besides internal rotation barriers, van der Waals interactions, and electrostatic interactions, bending energies were also taken into account. The constrained conditions in the calculation were as follows; (1) the Cl-C-Cl bond angles as well as the H-C-H bond angles are fixed at the tetrahedral value (109.5°); (2) all the C-C, C-Cl and C-H bond lengths are assumed to be 1.54, 1.78 and 1.09 \AA , respectively; (3) two monomeric units in the identity period are related by the symmetry of either two-fold screw axis or glide plane along the fiber axis.

The function for the internal rotation barriers was the sinusoidal type, and the barrier height V was assumed to be 2.0 kcal/mol .^{14,15} The potential function for the van der Waals interactions between non-bonded atoms was approximated by the Lennard-Jones "6-12" function. The parameters used for the van der Waals interactions are listed in Table 8.1.¹⁶⁻¹⁸

Electrostatic interactions were estimated by the use of the point dipole-dipole interaction equation. The point dipole was assumed to be at the midpoint of the C-Cl bond. The value of C-Cl bond moment was taken as 2.0 D from the data for 2,2-dichloropropane, 2-chloropropane.¹⁹ The value of dielectric constant was assumed to be 4.0 .^{20,21} Summations

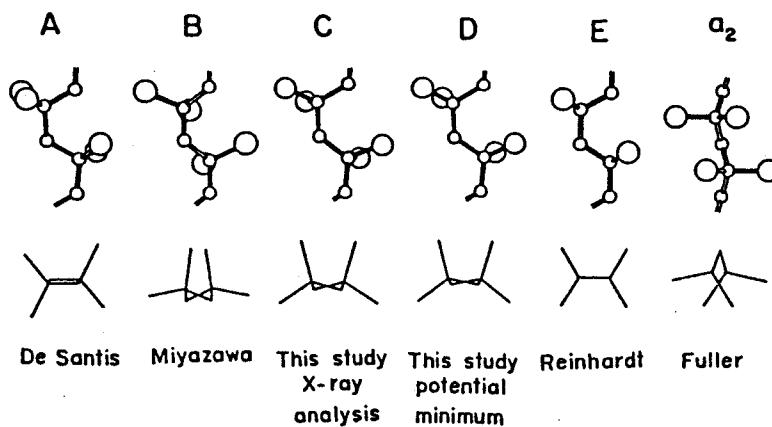
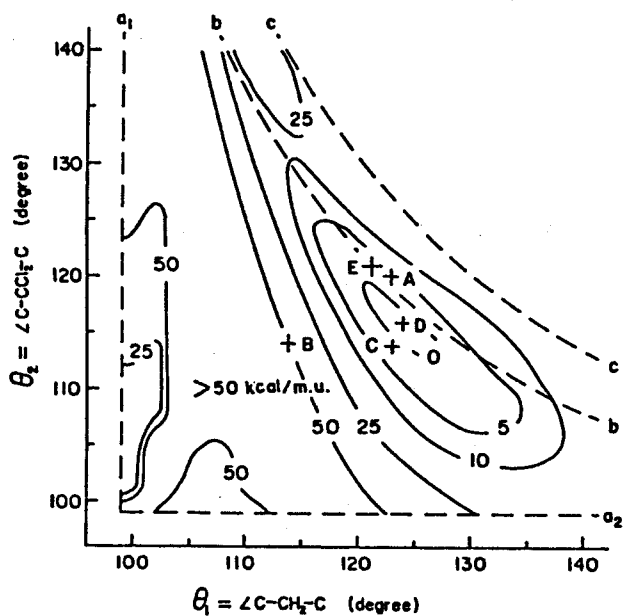


Figure 8.1 Conformational energy contour map against two backbone bond angles, and several molecular models of PVDC. The Fuller's model will be located anywhere on the line a₂.

Table 8.1 Parameters for van der Waals interactions.

Atom pair	ϵ , kcal/mol	r_{\min} , Å
C ... C	0.120	3.40
C ... Cl	0.287	3.45
C ... H	0.108	2.90
Cl... Cl	0.688	3.50
Cl... H	0.250	2.95
H ... H	0.122	2.40

Table 8.2 Parameters for bending energies.

Angle	k , kcal/mol rad ²	θ_0 , degree
θ_1 (C-CH ₂ -C)	107.2	112.0
θ_2 (C-CCl ₂ -C)	144.8	112.0
θ_3 (C-C-H)	92.8	109.5
θ_4 (C-C-Cl)	157.1	109.5

of the van der Waals and electrostatic energies were made in a range of 10 Å and 40 Å, respectively.

The bending energies were estimated by

$$E = (1/2)k(\theta - \theta_0)^2 \quad (1)$$

here θ_0 is the zero strain value of bond angle θ , and k is the force constant for the bending. The constant k and θ_0 have been assumed as listed in Table 8.2.⁶ The total bending energy is the sum of the contributions from the bond angles $\theta_1(\text{C-CH}_2\text{-C})$, $\theta_2(\text{C-CCl}_2\text{-C})$, $\theta_3(\text{C-C-H})$ and $\theta_4(\text{C-C-Cl})$.

Figure 8.1 shows the map of the total energy represented with energy level contour vs. θ_1 and θ_2 . Here the author obtained the following equation

$$(1 - \cos \theta_1)(1 - \cos \theta_2) - I^2/r^2 \gtrless 0 \quad (2)$$

where I is the axial pitch of monomeric unit, i.e., $4.68 \text{ Å} / 2 = 2.34 \text{ Å}$, and r is the C-C bond length, 1.54 Å , respectively. In the region surrounded by the lines a_1 , a_2 and b , the value of equation 2 is negative, and the molecular chain has some glide conformation. In the region surrounded by the lines b and c , the value of equation 2 is positive, and the molecular chain has some (2/1) helical conformation. The value of equation 2 is zero on the border line b . Reinhardt's model shown by the cross E in Figure 8.1 is on this line. Other three border lines are defined as follows.

$$\begin{aligned} a_1; \quad & \cos \theta_1 = 1 - I^2/(2r^2) \\ a_2; \quad & \cos \theta_2 = 1 - I^2/(2r^2) \\ c; \quad & \cos \theta_1 + \cos \theta_2 + I^2/(2r^2) = 0 \end{aligned} \quad (3)$$

No molecular model can exist in outer region of three lines, a_1 , a_2 and c . The Fuller's model will be located anywhere on the line a_2 . The crosses A and B correspond to the (2/1) helical model proposed by De

Santis and the glide model by Miyazawa and Ideguchi, respectively. The position of the conformation energy minimum is shown by the cross D ($\theta_1 = 124^\circ$, $\theta_2 = 116^\circ$). This energy minimum is near the border line b, and its molecular conformation is of glide. The cross C corresponds to the resulting conformation of the X-ray analysis as shown later.

8-3-2 Molecular Transform

The cylindrically averaged X-ray intensities about the chain axis (the chain axis is conventionally taken as the axis instead of the b axis which is the fiber axis in the following crystal structure analysis) scattered by one molecular chain, $|T|^2$, was evaluated from the following equation.

$$\begin{aligned} |T|^2 &= \langle |F(R, 1/c)|^2 \rangle_\phi \\ &= \sum_i \sum_j f_i f_j J_0(2\pi R r_{ij}) \exp(2\pi i l z_{ij}/c) \exp(-2B \sin^2 \theta / \lambda^2) \end{aligned} \quad (4)$$

here $(R, \phi, 1/c)$ are the cylindrical coordinates of a point in the reciprocal space, f_j is the atomic scattering factor, J_0 is the Bessel function of zero order, and r_{ij} and z_{ij} are the radial and axial components of the interatomic distance between i and j th atoms in the fiber period. A thermal parameter B of 5 \AA^2 was assumed.

Figure 8.2 shows the calculated intensities for the four models. The vertical rods in the figure show the observed relative intensities of reflections after correction for the Lorentz-polarization factor. Fuller's model cannot interpret the strongest reflection on the first layer line, while Miyazawa's model cannot interpret the remarkably intense meridional reflection of the second layer line. Both the glide model proposed by the energy calculation and the (2/1) helical model by De Santis give sufficient interpretation for the X-ray fiber diagram.

Accordingly, it was difficult to decide which is the preferable

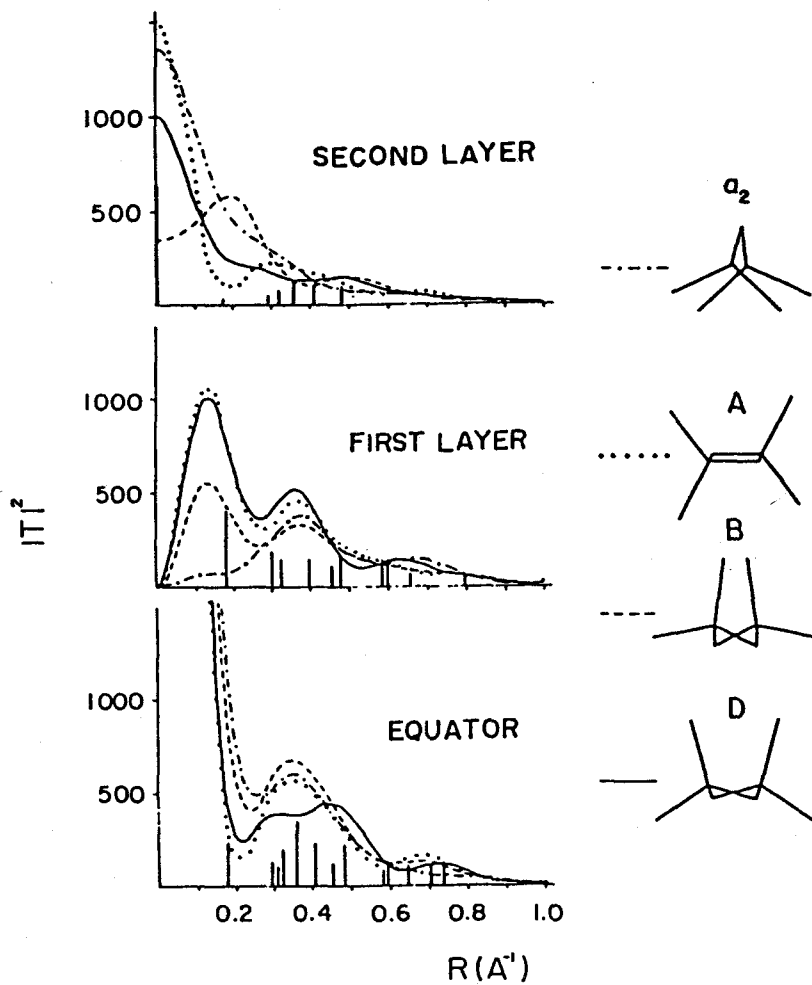


Figure 8.2 Comparison between observed reflection intensities (vertical rods) and the cylindrically averaged intensities $|T|^2$ for several molecular models. Letters, a_2 , A, and so on have the same meaning as in Figure 8.1.

model either the glide or (2/1) helical model from the result of the molecular transform alone; both the models are in accordance with each other when the internal rotation angles are 0° and 180° corresponding to Reinhardt's model.

8-3-3 Unit Cell and Space Group

All reflections observed in the fiber diagram were indexed by a monoclinic cell with cell dimensions of $a = 6.71 \text{ \AA}$, $b(\text{fiber axis}) = 4.68 \text{ \AA}$, $c = 12.51 \text{ \AA}$ and $\beta = 123^\circ$. In the unit cell determination, a doubly oriented specimen of a copolymer with vinyl chloride was also utilized.

From the systematic absence of reflections, $0k0$ when k is odd, the possible space groups are $P2_1$ and $P2_1/m$. The calculated density assuming two polymer chains (four monomeric units) in the unit cell is 1.95 g/cm^3 , which is reasonable comparing with the observed density of 1.859 g/cm^3 for a commercial PVDC.¹¹ The cell dimensions are essentially the same as those reported by Okuda.¹²

8-3-4 Determination of Crystal Structure

The author considered at first possible molecular packing ways in the ac-projection for the glide and (2/1) helical models adopting the plane group $p2$: both space groups of $P2_1$ and $P2_1/m$ possess the plane group $p2$ in the ac-projection. The x and z coordinates of all chlorine atoms were determined unequivocally. Referring these positions of chlorine atoms, two (2/1) helical chains must be situated such that the chain axes coincide with non-equivalent two two-fold screw axes at $(x = 0.5, z = 0.0)$ and $(x = 0.5, z = 0.5)$ (see Figure 8.4). In this case, therefore two chains in the unit cell are crystallographically non-equivalent. On the other hand, two monomeric units in the molecular

chain of glide type are non-equivalent, because the space group $P2_1$ or $P2_1/m$ does not possess the glide symmetry: two chains in the unit cell are related by a two-fold screw axis in the case of glide chain.

Trial and error procedure with the three dimensional reflection data indicated that the agreement between observed and calculated structure factors for the glide structure was more satisfactory than the (2/1) helical structure. However, slight controversy existed between observed and calculated structure factors for weak or non-observed reflections in the case of glide structure with the space group $P2_1$. This problem could be settled up by introducing a statistically disordered structure with respect to the molecular direction. In such a structure, upward and downward molecular chains exist in equal probability. This implies that the space group $P2_1/m$ should be adopted. Further refinement of the glide and also (2/1) helical structures with the space group $P2_1/m$ was carried out. In the case of (2/1) helical structure, there are right-handed and left-handed helices. The combination about the chain direction and the helical sense for two chains in the unit cell makes 12 different structures in the case of $P2_1$ and 6 in $P2_1/m$.

The final discrepancy factors R ($= \sum |\sqrt{I_o} - \sqrt{I_c}| / \sum \sqrt{I_o}$, where $I = mF^2$, m : multiplicity, F : structure factor) for four difference type crystal structures are shown in Table 8.3; the R factors were calculated for observed reflections only. In the table, the data of the most favorable ones for the (2/1) helical structures are listed up. The glide structure in the $P2_1/m$ cell is the most favorable. The atomic coordinates and thermal parameters of the glide structure in the $P2_1/m$ cell are given in Table 8.4. The bond lengths, bond angles and internal rotation angles are shown in Figure 8.3. The crystal structure is shown in Figure 8.4,

Table 8.3 Final discrepancy factors, R.

Molecular conformation	Space group	R, %
Glide	$P2_1/m$	15
	$P2_1$	20
<hr style="border-top: 1px dashed black;"/>		
(2/1) Helix	$P2_1/m$	30
	$P2_1$	31

Table 8.4 Atomic coordinations.

Atom	x/a	y/b	z/c
C ₀	0.415	0.191	0.166
C ₁	0.350	0.373	0.245
C ₂	0.415	0.691	0.273
C ₃	0.350	0.873	0.158
Cl ₀₁	0.244	0.309	0.006
Cl ₀₂	0.717	0.192	0.218
Cl ₂₁	0.244	0.809	0.334
Cl ₂₂	0.717	0.692	0.399

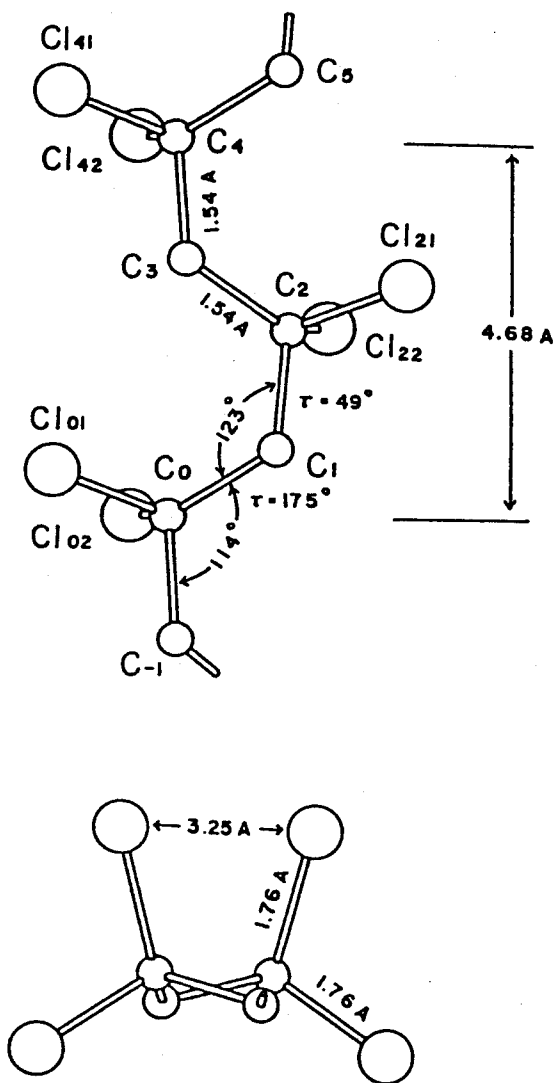


Figure 8.3 Bond lengths, bond angles, and internal rotation angles of the PVDC chain obtained by the present X-ray analysis.

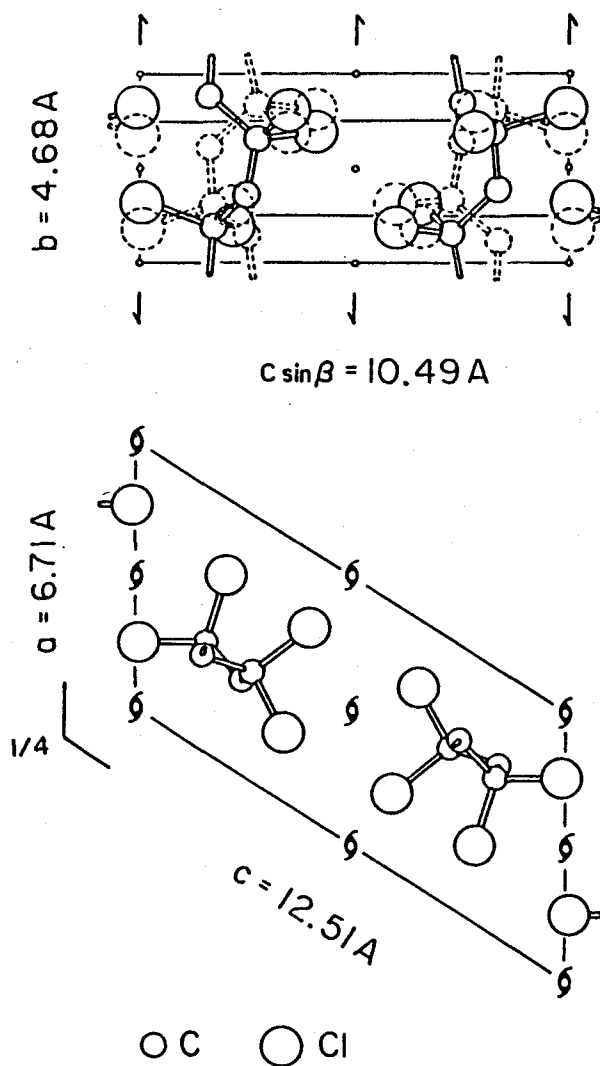


Figure 8.4 Crystal structure of PVDC. Molecular chains shown by solid and broken lines indicate upward and downward chains, respectively.

the molecules shown by solid and broken lines are upward and downward.

8-4 Result and Discussion

8-4-1 Molecular Structure

It was revealed that the molecular chain of PVDC has a glide conformation of $TG'T\bar{G}'$ type in the crystal, although the two successive monomeric units in the chain are not related by a crystallographic glide plane symmetry. The internal rotation angles of the skeletal bonds are 175° (T) and 49° (G'), the latter deviates appreciably from the exact gauche form (60°).

The set of the skeletal bond angles ($\theta_1 = 123^\circ$, $\theta_2 = 114^\circ$) nearly agrees with the set for the glide model with the minimum energy in the conformation energy calculation ($\theta_1 = 124^\circ$, $\theta_2 = 116^\circ$). Although the C-CCl₂-C bond angle of 114° is close to 112° as on the average in linear hydrocarbons, the C-CH₂-C bond angle is 123° . Such large values of C-CH₂-C bond angles have been reported for polyisobuthylene (128°)²³ and 2,2,3,4-tetramethyl adipic acid (122.6°).²⁴ It is therefore obvious that the large C-CH₂-C bond angle is attributed to the steric hindrance between adjacent CCl₂ groups. There is an extremely close intramolecular Cl...Cl contact of 2.35 \AA between adjacent CCl₂ groups in Miyazawa's glide model, which is also an improper model from the consideration of molecular transform. The glide conformation obtained by the X-ray analysis has the Cl...Cl contact of 3.25 \AA , which is near unreasonable as the intramolecular contact. For example, the closest methyl...methyl carbon distance in polyisobuthylene is only 3.02 \AA despite the large C-CH₂-C bond angle, 128° . Therefore, it can be said that the Cl...Cl repulsion is released by the large depending of C-CH₂-C bond angle as

well as the deviation of internal rotation angles of the skeletal bond from the exact gauche form.

The molecular conformation of PVDC is similar to that of poly(vinylidene fluoride) in the form II²⁵: the internal rotation angles of the PVDC chain are very close to those of poly(vinylidene fluoride) chain (179° and 45°). In the poly(vinylidene fluoride) chain, however, the closest intramolecular F...F distance of 2.70 Å, which corresponds to the sum of van der Waals radii, is preserved by a smaller C-CH₂-C bond angle, 116° , as compared with 123° in PVDC.

Poly(vinylidene fluoride) exhibits polymorphism, and several molecular conformation appear by the transformation between trans and gauche forms.²⁶⁻²⁸ On the other hand, the strong repulsion of CCl groups will restrict a variation of the molecular found for PVDC.

8-4-2 Crystal Structure

The copolymer with vinyl chloride (20 mol%), which gives essentially the same X-ray diffraction pattern as that PVDC, could be doubly oriented by rolling: the rolled plane is parallel to the (100) plane. Although the molecular chain of PVDC is not planar, the molecular packing in the crystal lattice may interpret well the feature of the double orientation. That is to say, as shown in the ac-projection of the crystal structure, the crystal is composed of molecular sheets parallel to the (100) plane.

The systematic absence of reflections can not show the space group unequivocally: P2₁ and P2₁/m were retained as the possible space group. Then it was revealed that the space group P2₁/m gives the best explanation of reflection intensities. This structure has the disorder with respect to the molecular chain direction, i.e. either upward chain or downward chain occupies one site in the crystal lattice with equal

probability. Some close intermolecular atomic distances are shown in Table 8.5. This statistical structure is never unreasonable in view of the packing manner of molecular chains.

References

1. C. S. Fuller, Chem. Rev., 26, 143 (1940).
2. R. C. Reinhardt, Ind. Eng. Chem., 35, 422 (1943).
3. P. De Santis, E. Giglio, A. M. Liquori, and A. Ripamonti, J. Polym. Sci., A, 1, 1383 (1963).
4. V. M. Coiro, P. De Santis, A. M. Liquori, and A. Ripamonti, Rec. Sci., 33 (II-A), 1043 (1963).
5. V. M. Coiro, P. De Santis, and A. M. Liquori, J. Polym. Sci., B, 4, 821 (1966).
6. T. Miyazawa and Y. Ideguchi, J. Polym. Sci., B, 3, 541 (1965).
7. P. J. Hendra and J. R. Mackenzie, Spectrochim. Acta, 25A, 1349 (1969).
8. M. M. Coleman, M. S. Wu, I. R. Harrison, and P. C. Painter, J. Macromol. Sci. Phys., B15(3), 463 (1978).
9. M. S. Wu, P. C. Painter, and M. M. Coleman, J. Polym. Sci., Polym. Phys. Ed., 18, 95 (1980).
10. M. S. Wu, P. C. Painter, and M. M. Coleman, J. Polym. Sci., Polym. Phys. Ed., 18, 111 (1980).
11. S. Narita and K. Okuda, J. Polym. Sci., 38, 270 (1959).
12. K. Okuda, J. Polym. Sci., A, 2, 1749 (1964).
13. J. F. Brown, Jr. and D. M. White, J. Amer. Chem. Soc., 82, 5671 (1960).
14. R. A. Scott and H. A. Scheraga, J. Chem. Phys., 42, 2209 (1965).
15. R. A. Scott and H. A. Scheraga, J. Chem. Phys., 44, 3054 (1966).

Table 8.5 Intermolecular atomic distances less than 4.0 Å.

Between molecules of the same direction, Å		Between upward and downward molecules, Å	
C ₃ (A)...Cl ₀₁ (B)	3.36	C ₃ (L)...Cl ₀₁ (B)	3.45
C ₂ (A)...Cl ₀₁ (B)	3.91	C ₁ (K)...Cl ₀₁ (C)	3.79
Cl ₀₁ (A)...Cl ₀₂ (H)	3.46	C ₂ (L)...Cl ₀₁ (B)	3.87
Cl ₂₁ (D)...Cl ₀₂ (F)	3.50	Cl ₂₂ (L)...Cl ₂₂ (I)	3.68
Cl ₂₁ (A)...Cl ₀₁ (B)	3.70	Cl ₂₁ (L)...Cl ₀₁ (B)	3.74
Cl ₀₁ (A)...Cl ₀₁ (B)	3.95	Cl ₀₂ (K)...Cl ₀₁ (H)	3.78
Cl ₂₂ (A)...Cl ₂₂ (G)	3.98	Cl ₂₁ (L)...Cl ₀₂ (J)	3.81
		Cl ₀₂ (K)...Cl ₂₂ (E)	3.86

Symmetry relationship in fractional atomic coordinates

A: x,y,z; B: -x 0.5+y,-z; C: -x,-0.5+y,-z; D: 1-x,-0.5+y,
1-z; E: 1+x,y,z; F: 2-x,0.5+y,1-z; G: 2-x,-0.5+y,1-z; H: 1-x,
0.5+y,y,-z; I: -x,0.5+y,1-z; J: -1+x,y,z; K: x,0.5-y,z; L: x,
1.5-y,z

16. A. Bondi, J. Phys. Chem., 68, 441 (1964).
17. J. Ketelaar, "Chemical constitution", p59, Elsevier Pub. Co., New York, 1959.
18. K. S. Pitzer, Advan. Chem. Phys., 2, 59 (1959).
19. A. L. McClellan, "Tables of Experimental Dipole Moments", Freeman Pub. Co., San Francisco, 1963.
20. D. A. Brant and P. J. Flory, J. Amer. Chem. Soc., 87, 663 (1965).
21. D. A. Brant and P. J. Flory, J. Amer. Chem. Soc., 87, 2791 (1965).
22. Y. Chatani, Y. Okita, H. Tadokoro, and Y. Tamashita, Polymer J., 1, 555 (1970).
23. T. Tanaka, Y. Chatani, and H. Tadokoro, J. Polym. Sci. Polym. Phys. Ed., 12, 515 (1974).
24. E. Benedetti, C. Pedone, and G. Allegra, Macromolecules, 3, 16 (1970).
25. R. Hasegawa, Y. Takahashi, Y. Chatani, and H. Tadokoro, Polymer J., 3, 600 (1972).
26. Y. Takahashi and H. Tadokoro, Macromolecules, 13, 1316 (1980).
27. Y. Takahashi, H. Tadokoro and A. Odajima, Macromolecules, 13, 1318 (1980).
28. Y. Takahashi, Y. Matsubara and H. Tadokoro, Macromolecules, 15, 334 (1980).

Chapter 9

Concluding Remarks

This thesis has dealt with the following subjects :

- (1) the investigation of a unique structural feature of the surface of polymers and the carbon fibers made from PAN by using XPS,
- (2) the application of XPS to examination of bulk chemical structure of polymeric substances. The summary is listed below.

* * *

Chapter 2. Surface Cleaning and Effect of X-ray Flux on XPS Study of Polymers

The surface cleaning and the effect of X-ray flux on the XPS measurement of polymers was examined. Contamination free surfaces of polymer samples for XPS study was found to obtain by using ultrasonic washing in organic solvents. The surface chemical activity of the polymer substances was revealed to be less than that of metal and semiconductor crystals. PET, polyimide and PAN has high stability for X-ray flux. PTFE and Nylon with less resistance to X-ray need attention to the degradation in usual XPS measurement. High X-ray sensitivity of nitrocellulose prevents us to carry out quantitative XPS analysis. The degradation behavior of polymers induced by the X-ray irradiation was clarified to be difference from that in the thermal degradation process.

Chapter 3. A Non-Empirical LCAO MO SCF and Experimental Investigation on the Core-Ionization Process of Poly(vinylidene chloride) and Poly(vinyl chloride)

The study of chemical shift of carbon atoms in PVDC and PVC was

carried out by XPS measurement and a non-empirical LCAO MO SCF calculation on the ground state. The primary and secondary substituent effects on Cls binding energies by replacement of a hydrogen atom with a chlorine atom are respectively 1.8 eV and 0.3 eV, which are less than that with a fluorine atom.

Chapter 4. Monte Carlo Simulation of an Ion Sputtering Process of Fluoro Polymers

The sputtering of Ar ion bombarded PTFE and PVDF was studied by XPS. Monte Carlo simulation of the Ar ion sputtering process of both polymers was performed to understand the variation of XPS spectra during sputtering. In both polymer systems, fluorine atoms are preferentially sputtered away from the polymer chains leaving carbon atoms behind. The damaged layer produced by the process has a homogeneous composition within the sampling depth of XPS. Observed XPS spectra of both polymers were explained by the random elimination of fluorine atoms from a polymer chain, although better fitting was acquired by also taking a double fluorine atom elimination mechanism into account.

Chapter 5. XPS Study by Use of the Digital Difference Spectrum Technique of Functional Groups on the Surface of Carbon Fiber

The digital difference spectrum technique in XPS was proved to be effective for the analysis of the functional groups introduced by surface oxidation treatment of carbon fibers. The major functional groups introduced to the carbon fiber surface by surface oxidation are hydroxyl and carboxyl groups. Disorder of the crystal lattice was also observed together with generation of carboxyl group in the surface oxidation process of graphite fibers.

Chapter 6. XPS Study on the Surface Structure of Carbon Fibers Using Chemical Modification and Cls Line Shape Analysis

The chemical modification technique coupled with XPS was proved to be a useful tool for detailed and quantitative analysis of surface functional groups of carbon fibers. Major functional groups on unoxidized and oxidized carbon fibers surface were found to be carbonyl group, and hydroxyl and carbonyl groups, respectively. Line shape analysis of XPS Cls spectrum was found to provide good parameters to evaluate degree of graphitization on carbon fiber surface. A narrower and more asymmetric Cls spectrum is revealed to correspond to more complete graphite lattice structure. With use of the parameters, crystal lattice on surface of graphite fiber is found to get disordered by surface oxidation.

Chapter 7. XPS and FT-IR Studies on the Chemical Structure of Stabilized Polyacrylonitrile Fiber and the Mechanism of Stabilization Reaction in Carbon Fiber Production Process

In the carbon fiber production process from PAN precursor, the precursor is heated first in air to secure stabilization in the succeeding carbonization process at higher temperature. Mechanism of the stabilization reaction and chemical structure of the stabilized PAN were examined with XPS, FT-IR and elemental analysis. The stabilized PAN was determined to have a ladder-like structure consisting of 40 % acridone ring, 30 % of naphthyridine ring, 20 % of hydronaphthyridine ring, and others. This structure well explains stability of the polymer in the succeeding carbonization process on carbon fiber production with conjugated π -electron systems over the whole polymer chain and inter-

molecular hydrogen bonds. A comonomer addition to the precursor was elucidated to accelerate dehydrogenation reaction in the stabilization process.

Chapter 8. Molecular and Crystal Structure of Poly(vinylidene chloride)

The molecular and crystal structure of PVDC were determined by X-ray structure analysis together with conformational energy calculation. Two molecular chain with glide conformation are packed in the monomeric unit cell. The geometrical data of PVDC molecule obtained in this study was used in the non-empirical LCAO MO SCF calculation to study the chemical shift in XPS above mentioned.

* * *

In the present study, the author mainly discussed characteristic properties and behaviors of the surface of polymeric substances and carbon fibers by using XPS and also applied the technique to examine chemical structure of highly condensed heterocyclic amorphous polymer. XPS was proved to be a very powerful technique for the investigation of the surface structure of polymers and its related materials including carbon fibers. The author hopes more extensive development of the study in this field in the future.

List of Publications

The contents of this thesis have been or will be published in the following papers.

- (1) T. Takahagi, A. Ishitani
"XPS Studies by Use of the Digital Difference Spectrum Technique of Carbon Fibers", Carbon, 22, 43 (1983).
- (2) T. Takahagi, I. Shimada, M. Fukuhara, K. Morita and A. Ishitani
"XPS Studies on the Chemical Structure of Stabilized Fiber of Polyacrylonitrile in the Carbon Fiber Production Process", J. Polym. Sci. Polym. Chem. Ed., 24, 3101 (1986).
- (3) I. Shimada, T. Takahagi, M. Fukuhara, K. Morita and A. Ishitani
"FT-IR Study of the Stabilization Reaction of Polyacrylonitrile in the Production of Carbon Fibers", J. Polym. Sci. Polym. Chem. Ed., 24, 1989 (1986).
- (4) T. Takahagi and A. Ishitani
"XPS Study of an Ion Sputtering Process of Fluoropolymers Using Monte Carlo Simulation", Macromolecules, 20, 404 (1987).
- (5) T. Takahagi and A. Ishitani
"XPS Study on the Surface Analysis of Carbon Fibers Using Chemical Modification and Cls Line Shape Analysis", Carbon, in press.
- (6) T. Takahagi and A. Ishitani
"Surface Cleaning and Effect of X-ray Flux on XPS Study of Polymers", Surf. Interface Anal., to be submitted.
- (7) Y. Chatani, T. Takahagi, T. Kusumoto and H. Tadokoro
"Molecular and Crystal Structure of Poly(vinylidene chloride)", Polym. J., to be submitted.

List of Related Papers

- (1) Y. Nakayama, T. Takahagi, F. Soeda, K. Hatada, S. Nagaoka, J. Suzuki and A. Ishitani
"XPS Analysis of NH_3 Plasma Treated Polystyrene Films Utilizing Gas Phase Chemical Modification", J. Polym. Sci. Polym. Chem. Ed., in press.
- (2) Y. Nakayama, T. Takahagi, F. Soeda, A. Ishitani, N. Higashi, T. Kunitake
"XPS Study of Oriented Organic Molecules. Vesicles of Azobenzene-Containing Alkyl Ammonium Amphiphiles", J. Colloid Interface Sci., in press.
- (3) T. Takahagi and A. Ishitani
"Automation Systems for Chemical Analysis", Koubunshi (High Polymers, Japan), 34, 986 (1985).
- (4) T. Takahagi
"What is ESCA?" and "What is Carbon Fibers?", Polymer Lounge, Edited by H. Tadokoro, Kagaku Doujin, 20 and 35 (1985).
- (5) T. Takahagi and A. Ishitani
"Automation Technique for Physico Chemical Analysis", Koubunshi Data Handbook, Kiso Ed., Baifuukan, 719 (1986).
- (6) T. Takahagi, A. Ishitani
"High Technology and Future Advanced Composite Materials : Surface Analysis of Fillers by ESCA", Gendai Kagaku Zoukan, Tokyo Kagaku Doujin, 158 (1986).
- (7) T. Takahagi
"Analysis of Specialty Materials : Analysis of Polymer Surface and Interface by XPS", Nihon Bunkou Gakkai (Sokuteihou Series), Gakkai

Shuppan Center, in press.